

THÈSE

En vue de l'obtention du

DOCTORAT DE L'UNIVERSITÉ DE TOULOUSE

Délivré par :

Institut National Polytechnique de Toulouse (INP Toulouse)

Discipline ou spécialité :

Réseaux, Télécommunications, Systèmes et Architecture

Présentée et soutenue par :

M. NIL GARCIA GARCIA

le mercredi 29 avril 2015

Titre :

METHODES D'OPTIMISATION POUR LA LOCALISATION ACTIVE ET PASSIVE DES CIBLES

Ecole doctorale :

Mathématiques, Informatique, Télécommunications de Toulouse (MITT)

Unité de recherche :

Institut de Recherche en Informatique de Toulouse (I.R.I.T.)

Directeur(s) de Thèse :

M. MARTIAL COULON

M. MARCO LOPS

Rapporteurs :

M. ALI ABDI, NEW JERSEY INSTITUTE OF TECHNOLOGY

Mme MONICA BUGALLO, STONY BROOK UNIVERSITY ETATS UNIS

M. OSVALDO SIMEONE, NEW JERSEY INSTITUTE OF TECHNOLOGY

M. YEHESKEL BAR-NESS, NEW JERSEY INSTITUTE OF TECHNOLOGY

Membre(s) du jury :

M. ALEXANDER HAIMOVICH, , Président

M. MARTIAL COULON, INP TOULOUSE, Membre

ABSTRACT

OPTIMIZATION METHODS FOR ACTIVE AND PASSIVE LOCALIZATION

by
Nil Garcia

Active and passive localization employing widely distributed sensors is a problem of interest in various fields. In active localization, such as in MIMO radar, transmitters emit signals that are reflected by the targets and collected by the receive sensors, whereas, in passive localization the sensors collect the signals emitted by the sources themselves. This dissertation studies optimization methods for high precision active and passive localization.

In the case of active localization, multiple transmit elements illuminate the targets from different directions. The signals emitted by the transmitters may differ in power and bandwidth. Such resources are often limited and distributed uniformly among the transmitters. However, previous studies based on the well known Crámer-Rao lower bound have shown that the localization accuracy depends on the locations of the transmitters as well as the individual channel gains between different transmitters, targets and receivers. Thus, it is natural to ask whether localization accuracy may be improved by judiciously allocating such limited resources among the transmitters. Using the Crámer-Rao lower bound for target localization of multiple targets as a figure of merit, approximate solutions are proposed to the problems of optimal power, optimal bandwidth and optimal joint power and bandwidth allocation. These solutions are computed by minimizing a sequence of convex problems. The quality of these solutions is assessed through extensive numerical simulations and with the help of a lower-bound that certifies their optimality. Simulation results reveal that bandwidth allocation policies have a stronger impact on performance than power.

Passive localization of radio frequency sources over multipath channels is a difficult problem arising in applications such as outdoor or indoor geolocation. Common approaches that combine ad-hoc methods for multipath mitigation with indirect localization relying on intermediary parameters such as time-of-arrivals, time difference of arrivals or received signal strengths, are unsatisfactory. This dissertation models the localization of known waveforms over unknown multipath channels in a sparse framework, and develops a direct approach in which multiple sources are localized jointly, directly from observations obtained at distributed sources. The proposed approach exploits channel properties that enable to distinguish line-of-sight (LOS) from non-LOS signal paths. Theoretical guarantees are established for correct recovery of the sources' locations by atomic norm minimization. A second-order-cone-based algorithm is developed to produce the optimal atomic decomposition, and it is shown to produce high accuracy location estimates over complex scenes, in which sources are subject to diverse multipath conditions, including lack of LOS.

OPTIMIZATION METHODS FOR ACTIVE AND PASSIVE LOCALIZATION

by
Nil Garcia

A Dissertation
Submitted to the Faculty of
Institut National Polytechnique de Toulouse – Toulouse, France – and
New Jersey Institute of Technology – Newark, USA
in Partial Fulfillment of the Requirements for the Degree of
Doctor of Philosophy in Electrical Engineering

Institut de Recherche en Informatique de Toulouse, INPT
Department of Electrical and Computer Engineering, NJIT

April 2015

Copyright © 2015 by Nil Garcia
ALL RIGHTS RESERVED

APPROVAL PAGE

OPTIMIZATION METHODS
FOR ACTIVE AND PASSIVE LOCALIZATION

Nil Garcia

Dr. Martial Coulon, Dissertation Advisor — Date
Professor, Institut National Polytechnique de Toulouse

Dr. Alexander M. Haimovich, Dissertation Advisor — Date
Distinguished Professor of Electrical and Computer Engineering, New Jersey Institute of Technology

---

Dr. Yeheskel Bar-Ness, Committee Member — Date
Distinguished Emeritus Professor of Electrical and Computer Engineering, New Jersey Institute of Technology

---

Dr. Osvaldo Simeone, Committee Member — Date
Associate Professor of Electrical and Computer Engineering, New Jersey Institute of Technology

---

Dr. Ali Abdi, Committee Member — Date
Associate Professor of Electrical and Computer Engineering, New Jersey Institute of Technology

---

Dr. Mónica F. Bugallo, Committee Member — Date
Associate Professor of Electrical and Computer Engineering, Stony Brook University

BIOGRAPHICAL SKETCH

Author: Nil Garcia

Degree: Doctor of Philosophy

Date: April 2015

Date of Birth: November 15, 1983

Place of Birth: Vilafranca del Penedes, Barcelona, Spain

Undergraduate and Graduate Education:

- Doctor of Philosophy in Electrical Engineering,
  Institut National Polytécnique de Toulouse, Toulouse, France, 2015
- Doctor of Philosophy in Electrical Engineering,
  New Jersey Institute of Technology, Newark, United States of America, 2015
- Master of Science in Telecommunications Engineering,
  Universitat Politècnica de Catalunya, Barcelona, Spain, 2008

Major: Electrical Engineering

Publications:

Nil Garcia, Alexander M. Haimovich, Martial Coulon, and Jason A. Dabin, "High precision TOA-based direct localization of multiple sources in multipath," submitted to the IEEE Transactions on Information Theory.

Nil Garcia, Martial Coulon, Alexander M. Haimovich, Jason A. Dabin, and Marco Lops, "Localisation directe de cibles multiples par un réseau de capteurs distribués en environnement multi-trajet," submitted to *Groupe de Recherche et d'Etudes du Traitement du Signal et des Images (GRETSI 2015)*, September 2015.

Nil Garcia, Alexander M. Haimovich, Jason A. Dabin, Martial Coulon, and Marco Lops, "Direct localization of emitters using widely spaced sensors in multipath environments," in *Signals, Systems and Computers, IEEE Asilomar Conference on*, pp. 695–700, November 2014.

Nil Garcia, Alexander M. Haimovich, Martial Coulon, and Marco Lops, "Resource allocation in MIMO radar with multiple targets for non-coherent localization," *Signal Processing, IEEE Transactions on*, vol. 62, pp. 2656–2666, April 2014.

Nil Garcia, Martial Coulon, Marco Lops, and Alexander M. Haimovich, "Allocation de ressources pour la localisation non-cohérente par radar MIMO," in *Groupe de Recherche et d'Etudes du Traitement du Signal et des Images (GRETSI 2013)*, pp. 1–5, September 2013.

Nil Garcia, Martial Coulon, Marco Lops, and Alexander M. Haimovich, "Resource allocation in radar networks for non-coherent localization," in *IET International Conference on Radar Systems (Radar 2012)*, October 2012.

To my parents and my wife.

You can be creative in anything — in math, science, engineering, philosophy — as much as you can in music or in painting or in dance.

Ken Robinson

ACKNOWLEDGMENT

Foremost, I would like to express my gratitude to Professors Alexander M. Haimovich, Martial Coulon and Marco Lops. Especially, to Alex, my mentor in New Jersey Institute of Technology, for giving me the opportunity to join his lab, funding my research and his valuable guidance. To Martial, my mentor in Institut National Polytechnique de Toulouse, for offering me the chance to become a Doctor, for providing funding while in France, for his advice and support throughout the entire program. To Marco Lops for putting together this double PhD program between Newark and Toulouse and for inspiring me with his strong mathematical expertise.

I would like to express my sincere gratitude to Professors Yeheskel Bar-Ness, Ali Abdi, Mónica F. Bullago and Osvaldo Simeone for serving as committee members. Special thanks go to Osvaldo for his valuable technical advice and also for disseminating his deep knowledge through his advanced-level courses in NJIT.

To my parents, Enric and Anna, thank you for giving me the strength when I got stuck and the happiness to enjoy what I was doing. To my wife, Xie, thanks for all the support you have given me throughout this process. It is wonderful to be on this life-long journey with you, pursuing our dreams as human beings as well as scientists.

I also would like to thank all my colleagues at CWCSPR and TéSA for all the great moments we shared. In particular, I would like to thank Haley, Liu, Pelin, Angela, Wei, Bahar, Fabio, Behzad, Ali, Marco, Jorge, Jean-Phillipe, Florian, Raoul and many others for the many moments we shared talking, climbing, eating and drinking.

Last but not least, special appreciation to Ms. Angela Retino, Ms. Marlene Toeroek, Ms. Clarisa Gonzalez-Lenahan and in general most of the staff in NJIT,

INPT and TéSA for their advice, help and support with administrative matters during my PhD studies.

TABLE OF CONTENTS

Chapter	Page
1 INTRODUCTION	1
1.1 Allocation of Power and Bandwidth in MIMO Radar	4
1.2 Direct Localization for Passive Localization in Multipath Channels	6
1.3 Contributions	8
2 RESOURCES ALLOCATION FOR ACTIVE LOCALIZATION	11
2.1 Signal Model	11
2.2 Resource Allocation	14
2.2.1 Problem Formulation	14
2.2.2 Unified Framework	16
2.3 Proposed Approximate Solution	20
2.4 Lower Bound on the Accuracy of the Optimal Allocations	24
2.5 Numerical Results	28
2.5.1 Resource Allocation for Different SNR Values	29
2.5.2 Number of Active Transmitters	31
2.5.3 Numerical Evaluation of the Approximations	32
3 DIRECT LOCALIZATION FOR PASSIVE LOCALIZATION	34
3.1 Signal model	34
3.2 Proposed Localization Technique	36
3.3 Stage 1: Deconvolution	38
3.4 Stage 2: Localization	40
3.4.1 Guarantee for Correct Recovery of the Sources' Locations	45
3.4.2 Practical Implementation: Discretization of the Atomic Set	50
3.4.3 Estimation of the Number of LOS Sensors	54
3.4.4 Spurious Locations	55
3.4.5 Tuning Parameter ϵ	57

TABLE OF CONTENTS
(Continued)

Chapter **Page**

3.4.6 Grid Refinement 58

3.5 Algorithm 61

3.6 Numerical Results 63

3.6.1 Performance in the Absence of Multipath 67

3.6.2 Performance in Multipath 68

3.6.3 Probability of Correct Recovery vs. Delay Spread 70

3.6.4 Probability of Correct Recovery vs. Number of Grid Refinement Steps 71

3.6.5 Multiple Sources 73

4 CONCLUSIONS AND FUTURE WORK 75

APPENDIX A PROOF OF PROPOSITION 1 78

APPENDIX B PROOF OF PROPOSITION 2 80

APPENDIX C PROOF OF LEMMA 5 81

APPENDIX D PROOF OF LEMMA 6 83

BIBLIOGRAPHY 86

LIST OF FIGURES

Figure		Page
2.1	Square root maximum CRLB vs. SNR after resource allocation.	29
2.2	Square root maximum localization error vs. SNR after resource allocation.	30
2.3	Relative frequencies of the number of active transmitters.	31
2.4	Comparison of the maximum CRLB, the approximate maximum CRLB, and the lower-bounds on the approximate maximum CRLB	33
3.1	Flow diagram of the process for recovering the sources' locations.	45
3.2	Probability of correct recovery in the sense of Definition 1 in the absence of noise.	50
3.3	Illustration of three steps of a grid refinement procedure.	59
3.4	Map with the locations of the sensors and source used in many of the experiments in Section 3.6.	64
3.5	Root mean square error vs. SNR.	67
3.6	Probability of correct recovery vs. SNR.	68
3.7	Root mean square error vs. SNR in a multipath environment.	69
3.8	Probability of correct recovery vs. SNR in a multipath environment.	69
3.9	Probability of correct recovery vs. error.	70
3.10	Probability of correct recovery vs. rms delay spread	71
3.11	Elapsed time and probability of correct recovery vs. the number of grid refinement steps.	72
3.12	Average probability of correct recovery vs. the number of sources.	74
3.13	Probability of correct recovery of all sources vs. the number of sources.	74

CHAPTER 1

INTRODUCTION

Localization (or Geolocation or Positioning) is the determination of the geographic location of an object. There are a wide variety of localization systems, each characterized by its own requirements and different applications. For instance, Global Navigation Satellite Systems (GNSS) [1, 2], such as the Global Positioning System (GPS) [3, 4], are very popular because they provide worldwide autonomous localization to their users. Such systems employ constellations of satellites transmitting highly synchronized signals, allowing a receiver to locate itself by measuring the propagation times. Another example, which has gone through major advancements since its invention, is radar [5, 6]. In its most basic form, an antenna or group of antennas transmit pulses that bounce off any object in their path. By measuring the propagation delays and angles of incidence of the returns, a radar is able to find the positions of those objects.

This thesis focuses on localization with observations obtained by widely distributed sensors. Multiple examples of such systems may be found in civil and military applications. For instance, cellular networks comprise many cells that provide radio coverage over large geographical areas. At the center of each cell lies a base station that can transmit and receive signals to and from user equipments (UE), such as mobile phones. The main purpose of cellular networks is to provide communications to UE's. Nevertheless, cellular networks can also provide additional services, such as localization [7, 8]. In particular, in uplink localization, multiple base stations collect the signals emitted by the user equipments to infer their locations. Multiple-input multiple-output (MIMO) radar is another example [9, 10]. MIMO radar is a new paradigm in radar, where instead of a single antenna with high-directional gain, multiple omni-directional sensors are employed. Every transmit sensor sends a

different waveform, which are then bounced off by the targets and collected by receive sensors. If the transmit and receive sensors are widely distributed, MIMO radar provides advantages over traditional radar, such as higher resolution [11, 12] and higher probability of detection [13, 14].

Localization employing widely distributed sensors falls into two categories: *active* and *passive*. In active localization, transmitters actively illuminate the targets and the reflections are used to infer their locations, such as in MIMO radar. In contrast, in passive localization, sensors collect signals that the sources emit. These signals are processed to infer the sources' location. This is the case of uplink localization in cellular networks.

Whether active or passive, it is possible to localize sources/targets using widely distributed sensors because the received signals carry information from their locations. The strength of the received signals decays, approximately, at a rate that is inversely proportional to the square of the distance travelled, whereas the propagation delays of the received signal are directly proportional to the distance traveled. Once the distances traveled by the received signals are estimated, the locations of the sources/targets can be found by *multilateration* or similar techniques [15, 16]. Several classes of localization methods exist in the literature depending on which signal parameters are exploited. In received signal strength (RSS) [17, 18], as the name points out, the traveled distances of the received signals are estimated from the signal strengths. However, in practice, the function relating signal strengths and distances is known only approximately, thus resulting in coarse location estimates. In time-of-arrival (TOA)-based localization, the traveled distances are found by estimating the propagation delays of the received signals [19, 20]. Such approach requires knowledge of the baseband waveforms and synchronization among transmitters and receivers. Techniques based on time-difference-of-arrivals (TDOA) measure the difference of propagation delays between different sensors. This may

be accomplished by subtracting the estimated TOA's at each sensor with the TOA estimated at a reference sensor [21], or if the baseband waveforms are unknown, by cross-correlating the received signals at all sensors with that of the reference sensor and finding the location of its peak [22]. TDOA techniques overcome some of the requirements of TOA techniques as they require synchronization only at the receivers. In coherent localization [11, 23], the traveled distances of the received signals are estimated from their phases. Since the phase varies much faster than the envelope of the signals, accuracies much higher than in the other techniques may be achieved. However, coherent localization requires phase synchronization of the order of nanoseconds or better. This thesis focus on active and passive localization based on TOA information, i.e., based on the delays of the signal envelope and not on the phase delays of the received signals. TOA and TDOA-based localization techniques are more accurate than RSS-based technique because signal strengths depend on other factors rather than just the signals travelled distances. While employing TOA information requires synchronization between transmitters and receivers, it also results in techniques with better accuracy than those employing TDOA.

The clear distinction between active and passive localization is that in the active case, transmitters are required. While in passive localization, all the processing takes place after receiving the signals, in active localization, the processing takes place also at the transmitting end. In a network of widely distributed sensors, the receivers process the signals and relay them, or a function of them, to a fusion center that combines all the information in order to infer the locations. The transmitters, in the case of active localization, emit some signals that are appropriate for the task of localization. Irrespective of the waveforms of choice, there are two fundamental parameters that need to be selected depending on the requirements of the applications: the transmitting power and the signal bandwidth. Obviously, such resources are not

unlimited. Thus, in the case of multiple transmitters, it is natural to ask what is the *optimal* strategy for allocating such limited resources among the transmitters.

Ideally, analytical solutions to the problem of localizing the sources and allocating resources are preferred because of their simplicity. Nonetheless, analytical solutions are usually very hard, if not impossible, to obtain if the mathematical models are not simplified. Instead, it is possible in many cases to obtain solutions by numerically solving one or multiple optimization problems. The purpose of an optimization problem is to find the best solution which maximizes or minimizes a certain function from a set of feasible solutions. This dissertation proposes some optimization methods for efficient resources allocation in active localization in Chapter 2 and for precise passive localization of sources in Chapter 3. Next, the motivation of the proposed methods is reviewed in more detail.

1.1 Allocation of Power and Bandwidth in MIMO Radar

In a MIMO radar, transmit elements emit their respective signals, which are subsequently scattered by targets in the field of view towards receive elements. If the antenna elements are widely spaced, then they view the targets from different aspect angles, making these (substantially diverse) paths exhibit different amplitudes and phases [9, 10, 13, 24]. The point target model employed in traditional radar, breaks down in favor of an extended target model [25], because targets display different radar cross-sections (RCS) in different directions. In this case, processing is non-coherent and angular diversity becomes an object of interest [10, 26, 27]. In a non-coherent MIMO system where phase is not preserved across the elements, and if the system elements are time-synchronized, targets may be localized by, first, estimating the TOA's of the paths at each sensor, and then performing multilateration [28, 29], or by more computation-intensive techniques such as Direct Position Determination (DPD) [30]. When the target reflections towards different directions are unknown,

performance is enhanced by illuminating the target from different angles, and averaging the target scintillations [13].

Besides high-accuracy localization, resource-aware design is of importance in surveillance radars with mounted mobiles stations powered off-grid, as it can be found in network-centric warfare [31]. Such a configuration with multiple transmitters and receivers is robust to the loss of nodes, e.g., due to hostile action. Furthermore, resource management is an essential part of military operations in hostile environments, where low-probability-of-intercept operation may be required [32]. Another growing field where non-coherent MIMO might be applied, is ultra wide band (UWB) radar sensor networks [33], which usually operate under severe power constraints because they reuse wireless communications equipment or operate in unregulated frequencies. The ability of UWB to perform through-the-wall detection makes it an attractive tool for detecting intruders in buildings [34]. Another example of non-coherent radar localization, very similar to our system as it will become clear in the next paragraphs, is presented in [35], where an air traffic control radar uses multiple transmitters operating at different frequencies, and multilateration techniques are used for tracking.

A criterion for measuring the target location accuracy is necessary for allocating the resources. The Crámer-Rao lower bound (CRLB) for the estimation of a target location in a distributed architecture [36] is picked as cost function. An advantage of this cost function is that it is in closed form, thus making it suitable for algebraic manipulations. Also, the CRLB is known to provide a tight lower bound on the error of an unbiased estimator at high signal-to-noise ratio (SNR) [27, 37], and this is the SNR regime in which we operate. And lastly, another important particularity of this CRLB is that, under the assumption of full orthogonality between transmitted signals, it depends only on the two parameters of interest: power and effective bandwidth (see [38] for the definition of effective bandwidth). It is shown in [39] that this CRLB is

the product of two factors, which capture the nature of the localization error: one is the CRLB of time delay estimation by a single sensor, and the second is a term known as Geometric Dilution of Precision (GDOP), which depends on the number of transmit and receive elements and their locations. Tight bounds are also available for lower SNR, such as the Barankin [40] and Ziv-Zakai [41] bounds, however, they entail more complicated expressions not suitable to serve as cost functions.

Chapter 2 is concerned with improving the accuracy of the localization of multiple detected and stationary targets. The premise of the work is that, judicious allocation of system resources, power and bandwidth, has an impact on the accuracy of localization. To this end, it is proposed a technique for finding the optimal power allocation, bandwidth allocation and joint power bandwidth allocation to minimize the CRLB on the localization of multiple targets. The model assumes that a fusion center performs resource allocations based on past localization estimates.

1.2 Direct Localization for Passive Localization in Multipath Channels

Traditional time-of-arrival (TOA)-based localization is accomplished through a two-step process. In the first step, sensors estimate TOA's from all incoming signals; in the second step, such estimates are transmitted to a central node, that subsequently estimates the location of each source by multilateration [42]. These localization techniques are known as *indirect*. In a multipath environment, each sensor receives, in addition to a line-of-sight (LOS) signal, multiple (possibly overlapping) replicas due to non-line-of-sight (NLOS) paths. Due to these multiple arrivals, it is, in general, more challenging to obtain accurate TOA estimates of the LOS components at the sensors. Matched filtering is a method for time delay estimation. However, its performance degrades greatly in the presence of multipath whose delay is of the same order than the inverse of the bandwidth of the signal. Moreover, in the case of blockage of the LOS path, the TOA of the first arrival does not correspond to a LOS component

anymore, and will corrupt localization. In such a case, it is customary to apply techniques, like the one in [43], to mitigate NLOS channel biasing of the geolocation estimate.

A better approach than indirect localization is to infer the source locations directly from the signal measurements without estimating any parameters such as propagation delays. The concept of direct localization was first introduced by Wax and Kailath [44, 45] in the 70's, however it is in the last decade that Weiss et al. have further investigated and proposed actually efficient techniques [30, 46, 47, 48]. In the absence of multipath, the state-of-the-art is Direct Position Determination (DPD) [46] which outperforms standard indirect localization, particularly at low signal-to-noise ratio (SNR), because it takes into account the fact that signals arriving at different sensors are emitted from the same location. The literature on direct localization in the presence of multipath is scarce. In [49] a maximum likelihood (ML) estimator has been developed for the location of a single source assuming a fixed and known number of multipath, but without providing an efficient way to compute the estimator. In [48], a Direct Positioning Estimation (DPE) technique is proposed for operating in dense multipath environments, but requires knowledge of the power delay profile and is limited to localization of a single source.

A requirement of direct localization is that the signals, or a function of them, are sent to a fusion center which estimates the source's locations. Thus, direct techniques are best suited for centralized networks. An example of this are Cloud Radio Access Networks (C-RAN) [50, 51]. C-RAN is a novel architecture for wireless cellular systems whereby the base stations relay the received signals to a central unit center which does all the baseband processing. Cellular systems are required to be location-aware, that is they must be able to estimate the locations of the user equipments (UE) for applications such as security, disaster response, emergency relief and surveillance in GPS-denied environment [33]. In uplink localization, the

base stations perform time measurements of the received signals emitted by the UE's in order to infer their positions. In addition, in the USA, it is required by the Federal Communications Commission (FCC) that by 2021 the wireless service providers must locate 80% of the UE's initiating an Emergency 911 (E-911) call with an accuracy of 50 meters [52]. Consequently, a high accuracy direct localization technique designed for multipath channels, such as the one proposed in Chapter 3 work, may enhance the localization accuracy of current existing cellular networks by utilizing the C-RAN infrastructure. Moreover, it exists other applications that may benefit from high accuracy TOA-based geolocationm such as in WLAN and WPAN networks. For instance, the setup of [53] uses radios with the IEEE 802.15 (WPAN) standard to localize devices. The setups by [54, 55] employ TOA-based localization for localizing 802.11 devices (WLAN). In [56] it is proposed a hybrid RSS(received signal strength)-TOA based localization algorithm that works with 802.11 and 802.15 technologies. Other TOA-based localization applications are in the radio frequency identification (RFID) field [57].

Chapter 3 presents a TOA-based **d**irect **l**ocalization technique for multiple sources in **m**ultipath environments (DLM) assuming known waveforms and no prior knowledge of the statistics of the NLOS paths. Without some prior knowledge on the multipath, NLOS components carry no information, and the best performance is obtained by using only LOS components [33]. Based on ideas of compressive sensing and atomic norm minimization [58], an innovative approach is proposed for jointly estimating the sources' locations using as inputs the signals received at all sensors.

1.3 Contributions

In summary, the contributions of this dissertation are:

1. Using the CRLB for localization accuracy in MIMO radar as figure of merit, a new unified framework is proposed for formulating three resource allocation problems:

   (a) Optimal power allocation.

   (b) Optimal bandwidth allocation.

   (c) Joint power and bandwidth allocation.

2. Efficient algorithms are developed for power and/or bandwidth allocation in MIMO radar for static targets. The inputs are the initial estimates of the targets locations. The algorithms rely on solving a series of convex optimization problems where the preceding solution is passed as initialization point to the next problem. The algorithms stop when practical convergence is achieved, i.e., two consecutive solutions result in the same localization accuracy.

3. Lower-bounds are obtained on the optimum value of the cost function of the optimization problems. The lower-bounds provide a certificate that can confirm that the allocations resulting from our algorithms are close to the optimal one.

4. A method is proposed for mitigating the non-line-of-sight interference on the received signals at each sensor. The propagation delays of different paths are estimated, and the multipath contributions are removed from the received signals.

5. Developing a framework for passive localization in multipath channels that incorporates contributions to the signals of both LOS and NLOS paths. In this framework, the observations at the sensors are described as a noisy linear combination of atoms. Such atoms are the *building blocks* of the received signals and act as proxies for the locations of the sources. By finding the sparsest linear combination of atoms describing the observations, the locations of the sources are estimated.

6. Developing an algorithm for **d**irect **l**ocalization of sources in **m**ultipath (DLM). In order to find the sparsest linear combination of atoms describing the observations, it is proposed to minimize the atomic norm of the received signals, which is cast as a convex optimization problem. DLM exploits the sparsity of the sources as well as differences in the properties of line of sight versus multipath components of signals received at the sensors. The proposed technique requires no a priori channel state information. The inputs are solely the noise variance and the signal waveforms, whereas the outputs are the sources' location and the number of LOS paths. By design, DLM is robust to multipath and to sensors with block LOS.

7. Establishing theoretical guarantees for correct recovery of the sources' locations. It is shown how the correct recovery depends on a parameter that determines the relative contributions of the LOS and NLOS atoms to the cost function of the DLM's optimization problem.

8. Proposing a grid refinement procedure to reduce the high computational complexity of the DLM's optimization problem.

CHAPTER 2

RESOURCES ALLOCATION FOR ACTIVE LOCALIZATION

Multi-input multi-output (MIMO) radar [10] utilizes multiple transmit and receive antennas. The antennas at each end of the radar system are sufficiently separated such that the target provides uncorrelated reflection coefficients between each transmit/receive pair of antennas. Because the transmit antennas emit orthogonal waveforms for all delays, the receivers can distinguish the received signals from different transmitters. In general, the available power and bandwidth are limited. In this chapter is addressed the problem of finding the optimal power and/or bandwidth allocation among multiple transmitters for best localization of multiple targets. To assess the the optimality of any localization, the well known Crámer-Raw lower bound (CRLB) [36] for target localization is used as a figure of merit.

2.1 Signal Model

Consider a MIMO-radar network consisting of M transmitters, located at $\{(x_m^{\text{tx}}, y_m^{\text{tx}})\}_{m=1}^{M}$, N receivers, located at $\{(x_n^{\text{rx}}, y_n^{\text{rx}})\}_{n=1}^{N}$, and Q stationary targets, located at $\{(x_q^{\text{tar}}, y_q^{\text{tar}})\}_{q=1}^{Q}$. Denote $d_{m,q}^{\text{tx}}$ and $d_{q,n}^{\text{rx}}$ the Euclidean distances from transmitter m to target q and from target q to receiver n, respectively. Let $\{s_m(t)\}_{m=1}^{M}$ be the transmitted pulses, where each pulse $s_m(t)$ has bandwidth w_m, energy E_m and time duration T_m. Assuming a fixed pulse repetition f_r frequency, the pulse energy E_m is connected to the average power p_m through the formula $p_m = E_m f_r$. For later use, the vector of powers $\mathbf{p} = [p_1, \ldots, p_M]^\top$ and the vector of effective bandwidths $\mathbf{w} = [w_1, \ldots, w_M]^\top$ are defined. The transmitted signals are assumed narrowband in the sense that a target's frequency response (for a given transmitter-receiver pair) is represented by a complex-valued scalar. For sufficiently spaced sensors, the target returns vary among pairs of transmitters and receivers, thus each target is modeled

as a collection of MN reflection coefficients. In this work, target returns are assumed deterministic and unknown. The low-pass signal observed at the n-th receiver is written as

$$r_n(t) = \sum_{q=1}^{Q} \sum_{m=1}^{M} \sqrt{\alpha_{mqn} E_m} h_{mqn} s_m(t - \tau_{mqn}) + e_n(t) \tag{2.1}$$

where f_c is the carrier frequency, c the speed of light,

$$\alpha_{mqn} = \frac{1}{4\pi \left(d^{\text{tx}}_{m,q}\right)^2} \frac{1}{4\pi \left(d^{\text{rx}}_{q,n}\right)^2} \frac{1}{4\pi f_c^2} \tag{2.2}$$

models the pathloss in free space along the path transmitter m – target q – receiver n. For simplicity, the pathloss α_{mqn} assumes free space propagation, however any other power-law model may be used for the pathloss without impacting any of the theoretical results. The time delay along the path is τ_{mqn}, and h_{mqn} represents the targets complex gains. The noise $e_n(t)$ is assumed circularly-symmetric complex Gaussian and white (AWGN) with constant power spectral density N_0.

The unknown parameters in (2.1) are the target locations $\{(x_q^{\text{tar}}, y_q^{\text{tar}})\}_{q=1}^{Q}$ and the MQN complex gains h_{mqn}. The goal of the radar system is to estimate the target location, with the complex gains h_{mqn} serving as nuisance parameters. Our objective is to allocate resources (power and/or bandwidth) to system elements, to optimize the target localization performance, using the CRLB as the optimization metric.

In the case of a single target, the CRLB is a 2×2 matrix, obtained by inverting the Fisher information matrix (FIM), whose diagonal elements are the lower-bounds on the variances of respectively the target location estimate along the x-axis ($\text{var}(\hat{x}^{\text{tar}})$) and y-axis ($\text{var}(\hat{y}^{\text{tar}})$). The trace of this matrix represents a lower-bound on the mean square error (MSE) of the target location estimate, i.e. $\text{var}(\hat{x}_q^{\text{tar}}) + \text{var}(\hat{y}_q^{\text{tar}}) \geq \text{tr}\{\mathbf{C}_q\} \triangleq T_q$, where $\mathbf{C}_q$ is the CRLB matrix of a target located at $\{(x_q^{\text{tar}}, y_q^{\text{tar}})\}$. An expression for the trace of the CRLB for localizing a single target using a single

observation is derived in [36]:

$$\mathrm{var}(\hat{x}_q^{\mathrm{tar}}) + \mathrm{var}(\hat{y}_q^{\mathrm{tar}}) \geq T_q \triangleq \frac{(\mathbf{a}_q + \mathbf{b}_q)^\top (\mathrm{diag}\,\mathbf{w})^2 \mathbf{p}}{\mathbf{p}^\top (\mathrm{diag}\,\mathbf{w})^2 \mathbf{H}_q (\mathrm{diag}\,\mathbf{w})^2 \mathbf{p}}. \tag{2.3}$$

The symbol $(\cdot)^\top$ denotes the transpose operator and diag forms a diagonal matrix with the input vector $\mathbf{w}$. $\mathbf{H}_q = (0.5\mathbf{a}_q\mathbf{b}_q^\top + 0.5\mathbf{b}_q\mathbf{a}_q^\top - \mathbf{c}_q\mathbf{c}_q^\top)$, and $\mathbf{a_q}$, $\mathbf{b}_q$ and $\mathbf{c}_q$ are length M vectors defined as follows:

$$\mathbf{a}_q = \eta \begin{bmatrix} \sum_{n=1}^{N} \alpha_{1qn}|h_{1qn}|^2 \left(\frac{x_1^{\mathrm{tx}} - x_q^{\mathrm{tar}}}{d_{1,q}^{\mathrm{tx}}} + \frac{x_n^{\mathrm{rx}} - x_q^{\mathrm{tar}}}{d_{q,n}^{\mathrm{rx}}} \right)^2 \\ \vdots \\ \sum_{n=1}^{N} \alpha_{Mqn}|h_{Mqn}|^2 \left(\frac{x_M^{\mathrm{tx}} - y_q^{\mathrm{tar}}}{d_{M,q}^{\mathrm{tx}}} + \frac{y_n^{\mathrm{rx}} - y_q^{\mathrm{tar}}}{d_{q,n}^{\mathrm{rx}}} \right)^2 \end{bmatrix} \tag{2.4}$$

$$\mathbf{b}_q = \eta \begin{bmatrix} \sum_{n=1}^{N} \alpha_{1qn}|h_{1qn}|^2 \left(\frac{y_1^{\mathrm{tx}} - x_q^{\mathrm{tar}}}{d_{1,q}^{\mathrm{tx}}} + \frac{x_n^{\mathrm{rx}} - x_q^{\mathrm{tar}}}{d_{q,n}^{\mathrm{rx}}} \right)^2 \\ \vdots \\ \sum_{n=1}^{N} \alpha_{Mqn}|h_{Mqn}|^2 \left(\frac{x_M^{\mathrm{tx}} - x_q^{\mathrm{tar}}}{d_{M,q}^{\mathrm{tx}}} + \frac{x_n^{\mathrm{rx}} - x_q^{\mathrm{tar}}}{d_{q,n}^{\mathrm{rx}}} \right)^2 \end{bmatrix} \tag{2.5}$$

$$\mathbf{c}_q = \eta \begin{bmatrix} \sum_{n=1}^{N} \alpha_{1qn}|h_{1qn}|^2 \left(\frac{x_1^{\mathrm{tx}} - x_q^{\mathrm{tar}}}{d_{1,q}^{\mathrm{tx}}} + \frac{x_n^{\mathrm{rx}} - x_q^{\mathrm{tar}}}{d_{q,n}^{\mathrm{rx}}} \right) \left(\frac{y_1^{\mathrm{tx}} - x_q^{\mathrm{tar}}}{d_{1,q}^{\mathrm{tx}}} + \frac{x_n^{\mathrm{rx}} - x_q^{\mathrm{tar}}}{d_{q,n}^{\mathrm{rx}}} \right) \\ \vdots \\ \sum_{n=1}^{N} \alpha_{Mqn}|h_{Mqn}|^2 \left(\frac{x_M^{\mathrm{tx}} - y_q^{\mathrm{tar}}}{d_{M,q}^{\mathrm{tx}}} + \frac{y_n^{\mathrm{rx}} - y_q^{\mathrm{tar}}}{d_{q,n}^{\mathrm{rx}}} \right) \left(\frac{x_M^{\mathrm{tx}} - x_q^{\mathrm{tar}}}{d_{M,q}^{\mathrm{tx}}} + \frac{x_n^{\mathrm{rx}} - x_q^{\mathrm{tar}}}{d_{q,n}^{\mathrm{rx}}} \right) \end{bmatrix}. \tag{2.6}$$

The constant η is given by $\eta = \frac{8\pi^2}{c^2 f_r N_0}$. The vectors (2.5) relate the CRLB parameter T_q to the sensors locations, target location, target gain, and pathloss. Note that the matrix $\mathbf{H}_q$ is symmetric.

Computation of the CRLB for localizing Q targets requires inverting a $2Q \times 2Q$ FIM which is a complicated mathematical operation. To simplify the matrix inversion, we make the following assumption which makes the FIM approximately block diagonal

(see [59]):

$$\frac{1}{\|s_m(t)\|^2}\int_{-\infty}^{\infty} s_m(t-\tau_{mqn})s_m^*(t-\tau_{mq'n})\,dt \approx 0 \tag{2.7}$$

for any pair of targets $q \neq q'$, and for any transmitter m and receiver n. Let $\mathbf{C}$ denote the CRLB matrix for multiple targets, then assuming (2.7), the FIM becomes a block diagonal matrix, that can be easily inversed, and leads to a CRLB matrix for multiple targets $\overline{\mathbf{C}}$ whose main diagonal is

$$\mathrm{dg}\left(\overline{\mathbf{C}}\right) \approx \left[\mathrm{dg}\left(\mathbf{C}_1\right),\ldots,\mathrm{dg}\left(\mathbf{C}_Q\right)\right] \triangleq \mathrm{dg}\left(\mathbf{C}\right). \tag{2.8}$$

where operator dg takes the main diagonal of the matrix between the brackets. The lower bounds on the variances of the targets locations estimates are obtained by taking the sum of the diagonal elements corresponding to the respective target:

$$\mathrm{var}(\hat{x}_q^{\mathrm{tar}}) + \mathrm{var}(\hat{y}_q^{\mathrm{tar}}) \geq \mathrm{dg}\left(\overline{\mathbf{C}}\right)_{2(q-1)+1} + \mathrm{dg}\left(\overline{\mathbf{C}}\right)_{2q} \triangleq \overline{T}_q \tag{2.9}$$

where the subindex selects the components in $\mathrm{dg}\left(\overline{\mathbf{C}}\right)$. Hence, if (2.7) is satisfied, combining (2.8) and (2.9) results in $\overline{T}_q \approx T_q$. In section 2.5, the validity of this approximation will be assessed by evaluating $\overline{T}_q$ and T_q for multiple scenarios and allocations.

2.2 Resource Allocation

2.2.1 Problem Formulation

In this section we formulate several optimization problems that minimize the lower-bounds on the MSE (which are tight under a high-SNR regime) of the targets locations (2.3) given constraints on power and bandwidth. These lower-bounds form a length Q vector function $[\mathrm{C}_1(\mathbf{p},\mathbf{w}),\ldots,\mathrm{C}_Q(\mathbf{p},\mathbf{w})]$, where the dependency on the transmitters powers and bandwidths is made explicit. A standard technique for minimizing a vector function is known as scalarization [60], and it consists in minimizing a scalar

function whose input is the vector function. In this regard a common requirement is ensuring that the localization error of any target is not too large. This can be cast as minimizing the worst CRLB on the variance of all target locations estimates, a criterion known in the literature as minimax. The worst MSE among all targets is written as the scalar function $\max_q \overline{T}_q$. According to this, a possible objective function $\overline{f}$ to minimize is

$$\overline{f}(\mathbf{p}, \mathbf{w}) = \max_{q \in \{1,\ldots,Q\}} \overline{T}_q(\mathbf{p}, \mathbf{w}). \tag{2.10}$$

We refer from now on to this cost function as the "maximum CRLB". However, because $\overline{T}_q$ lacks an easy-manipulable algebraic expression, we rely to its approximation

$$f(\mathbf{p}, \mathbf{w}) = \max_{q \in \{1,\ldots,Q\}} T_q(\mathbf{p}, \mathbf{w}) \tag{2.11}$$

which will be referred to as the "approximate maximum CRLB". Three allocation problems can now be formally stated using this objective function:

Problem 1 (Power allocation): *Given a total power P and a fixed bandwidth w per transmitter, the optimal power allocation is the solution $\mathbf{p}_{opt}$ to*

$$\mathbf{p}_{opt} = \begin{cases} \min\limits_{\mathbf{p}} & f(\mathbf{p}, w\mathbf{1}) \\ \text{s.t.} & \mathbf{1}^\top \mathbf{p} \leq P \\ & \mathbf{p} \succcurlyeq \mathbf{0} \end{cases} \tag{2.12}$$

where $\min_{\mathbf{p}}$ means "minimize with respect to $\mathbf{p}$", s.t. is the abbreviation for "subject to", $\mathbf{1}$ and $\mathbf{0}$ are the all-ones and all-zeros vectors respectively and $\succcurlyeq$ is component-wise "greater or equal than".

Problem 2 (Bandwidth allocation): *Given a uniform power allocation p and a total bandwidth B, the bandwidth allocation is the solution $\mathbf{w}_{opt}$ to*

$$\mathbf{w}_{opt} = \begin{cases} \min\limits_{\mathbf{w}} & f(p\mathbf{1}, \mathbf{w}) \\ \text{s.t.} & \mathbf{1}^\top \mathbf{w} \leq B \\ & \mathbf{w} \succcurlyeq \mathbf{0} \end{cases} . \tag{2.13}$$

Problem 3 (Joint power and bandwidth allocation): *Given a total power P and bandwidth B, the power and bandwidth allocations are the solution $(\mathbf{p}^j_{opt}, \mathbf{w}^j_{opt})$ to*

$$\left(\mathbf{p}^j_{opt}, \mathbf{w}^j_{opt}\right) = \begin{cases} \min\limits_{\mathbf{p},\mathbf{w}} & f(\mathbf{p}, \mathbf{w}) \\ \text{s.t.} & \mathbf{1}^\top \mathbf{p} \leq P \\ & \mathbf{1}^\top \mathbf{w} \leq B \\ & \mathbf{p}, \mathbf{w} \succcurlyeq \mathbf{0} \end{cases} . \tag{2.14}$$

In all of the above problems, the function that is minimized is (2.11), which depends on the targets locations through T_q (2.3). The target locations are not known, otherwise power and/or bandwidth would not be allocated to improve the localization accuracy. Thus from now on it is assumed that the target locations in T_q are coarse estimates obtained in previous cycles and denoted $[\tilde{x}^{\text{tar}}_1, \tilde{y}^{\text{tar}}_1, \ldots, \tilde{x}^{\text{tar}}_Q, \tilde{y}^{\text{tar}}_Q]$.

2.2.2 Unified Framework

Next, the three previous allocation problems are rewritten in a unified form. Such reformulation enables us to find an approximate solution to all three problems using the same mathematical tools. In order to write the allocation problems in this unified form, some algebraic manipulations are performed. First, the following lemma is enunciated.

Lemma 1 (Scaling): *For any constants $\alpha, \beta > 0$, the lower-bound on the MSE of a target location meets the following scaling property*

$$T_q(\alpha \mathbf{p}, \beta \mathbf{w}) = \frac{1}{\alpha \beta^2} T_q(\mathbf{p}, \mathbf{w}). \tag{2.15}$$

Proof. It suffices to expand $T_q(\alpha \mathbf{p}, \beta \mathbf{w})$ using (2.3). □

Applying Lemma 1 to Problems 1 and 2, simplifies the respective objective functions by moving from scaling the argument to scaling the full function. The following proposition will be applied to simplify Problem 3:

Proposition 1 : *The power $\mathbf{p}_{opt}^j$ and bandwidth $\mathbf{w}_{opt}^j$ solutions to Problem 3 are related through*

$$\mathbf{w}_{opt}^j = \frac{B}{P} \mathbf{p}_{opt}^j. \tag{2.16}$$

Proof. See Appendix A. □

By knowing beforehand how the power ($\mathbf{p}_{opt}^j$) and bandwidth ($\mathbf{w}_{opt}^j$) solutions relate to each other for Problem 3, the feasible set of Problem 3 can be restricted to points satisfying $\mathbf{w} = \frac{B}{P}\mathbf{p}$. Performing such substitution for vector $\mathbf{w}$ in Problem 3, transforms it into an optimization problem with only one vector variable $\mathbf{p}$ instead of two,

$$\mathbf{p}_{opt}^j = \begin{cases} \min\limits_{\mathbf{p}} & f(\mathbf{p}, \mathbf{p}) \\ \text{s.t.} & \mathbf{1}^\top \mathbf{p} \leq P \\ & \mathbf{p} \succcurlyeq \mathbf{0} \end{cases} \tag{2.17}$$

where $\mathbf{w}_{opt}^j$ is recovered by applying Proposition 1.

At this point, it has been shown that the specific values of bandwidth per user (w) and power per user (p) in Problems 1 and 2, do not change the solutions, and consequently Problems 1 and 2 can be solved with $w = p = 1$. Additionally thanks

to Proposition 1, Problem 3 has been rewritten in a more compact form (2.17). Notice that except for the problem specific constants P and B, Problems 1, 2 and 3 (expressed as (2.17)) have similar objective functions and constraints. In fact, upon introducing the function

$$g_q(\mathbf{y}, k) = \frac{(\mathbf{a}_q + \mathbf{b}_q)^\top (\operatorname{diag} \mathbf{y})^k \mathbf{y}}{\mathbf{y}^\top (\operatorname{diag} \mathbf{y})^k \mathbf{H}_q (\operatorname{diag} \mathbf{y})^k \mathbf{y}} \tag{2.18}$$

that closely resembles that of T_q in (2.3), the three problems can be dealt with in a unified manner through

$$\begin{aligned} \min_{\mathbf{y}} \quad & \max_{q \in \{1,\ldots,Q\}} g_q(\mathbf{y}, k) \\ \text{s.t.} \quad & \mathbf{1}^\top \mathbf{y} \leq D \\ & \mathbf{y} \succcurlyeq \mathbf{0} \end{aligned} \tag{2.19}$$

Denoting the optimal solution $\mathbf{y}_{opt}$, it is easily verified that if

$$\mathbf{y} = \mathbf{p} \qquad D = P \qquad k = 0 \tag{2.20a}$$

then $\mathbf{p}_{opt} = \mathbf{y}_{opt}$, if

$$\mathbf{y} = \mathbf{w} \qquad D = B \qquad k = 1 \tag{2.20b}$$

then $\mathbf{w}_{opt} = \mathbf{y}_{opt}$, and lastly if

$$\mathbf{y} = \mathbf{p} \qquad D = P \qquad k = 2 \tag{2.20c}$$

then $(\mathbf{p}^j_{opt}, \mathbf{w}^j_{opt}) = (\mathbf{y}_{opt}, \frac{B}{P}\mathbf{y}_{opt})$.

An optimization problem where the max operator appears in the constraints, instead of being in the objective function like in problem (2.19), is in general easier to solve. If a problem had constraint $\max_{q \in \{1,\ldots,Q\}} g_q(\mathbf{y}, k) \leq E$ where E is just a constant, then the max operator may be avoided by expressing the constraint

$$g_q(\mathbf{y}, k) \leq E \qquad \text{for all } q = 1, \ldots, Q. \tag{2.21}$$

It turns out that the solution to the optimization problem,

$$\begin{aligned} \min_{\mathbf{y}} \quad & \mathbf{1}^\top \mathbf{y} \\ \text{s.t.} \quad & \max_{q\in\{1,\dots,Q\}} g_q(\mathbf{y},k) \leq E \\ & \mathbf{y} \succcurlyeq \mathbf{0} \end{aligned} \tag{2.22}$$

which has no max operator in the objective function, can be closely related to that of problem (2.19) as established by the following proposition:

Proposition 2 : *For any value of constant E, the solution to problem* (2.19) *is the same than for problem* (2.22) *up to a scaling factor.*

Proof. See Appendix B. □

We impose $E = 1$ because it leads to the same solution than any other E up to a scaling factor. Therefore, the solution to (2.19) can be recovered through problem (2.22) with $E = 1$, and later according to Lemma 2, the solution can be normalized by the correct factor. Writing the constraints of problem (2.22) in the form of (2.21), and expressing $g_q(\mathbf{y}, k)$ using (2.18), problem (2.22) is rewritten as

Problem 4 (Canonical problem):

$$\min_{\mathbf{y}} \quad \mathbf{1}^\top \mathbf{y} \tag{2.23}$$

$$\text{s.t.} \quad (\mathbf{a}_q + \mathbf{b}_q)^\top (\operatorname{diag}\mathbf{y})^k \mathbf{y} \leq \mathbf{y}^\top (\operatorname{diag}\mathbf{y})^k \mathbf{H}_q (\operatorname{diag}\mathbf{y})^k \mathbf{y} \tag{2.24}$$

$$\text{for all } q = 1, \dots, Q$$

$$\mathbf{y} \succcurlyeq \mathbf{0} \tag{2.25}$$

The goal of this section was to attain Problem 4, however, the scaling constant relating its solution to the solution of problem (2.19) is still unknown. To this end the following lemma is enunciated

Lemma 2 : *Constraint $\mathbf{1}^\top \mathbf{y} \leq D$ in problem* (2.19) *is active at the solution $\mathbf{y}_{opt}$.*

Proof. The proof is done by contradiction. Assume there exists a minimum point $\mathbf{y}'$ such that $\mathbf{1}^\top \mathbf{y}' < D$, i.e., constraint is not active. Define $\mathbf{y}^* = \frac{D}{\mathbf{1}^\top \mathbf{y}'} \mathbf{y}'$. From the definition of $g_q(\mathbf{y}, k)$ in (2.18)

$$\max_{q \in \{1,\ldots,Q\}} g_q(\mathbf{y}^*, k) = \left[\left(\frac{\mathbf{1}^\top \mathbf{y}'}{D} \right)^{k+1} \max_{q \in \{1,\ldots,Q\}} g_q(\mathbf{y}', k) \right] < \max_{q \in \{1,\ldots,Q\}} g_q(\mathbf{y}', k). \tag{2.26}$$

This contradicts the assumption that the CRLB achieves its minimum at $\mathbf{y}'$. It follows that the power constraint evaluated at the optimal point must be active. □

By Lemma 2, the solution $\mathbf{y}_{\text{opt}}$ to (2.19) satisfies $\mathbf{1}^\top \mathbf{y}_{\text{opt}} = D$; and by Proposition 2, the solution $\mathbf{y}'$ to Problem 4 satisfies $\mathbf{y}' \propto \mathbf{y}_{\text{opt}}$. Thus it is trivial that

$$\mathbf{y}_{\text{opt}} = \frac{D}{\mathbf{1}^\top \mathbf{y}'} \mathbf{y}'. \tag{2.27}$$

Using this result, the solution to Problem 4 can now be related to the solution of problem (2.19), which is related in turn, to the original Problems 1-3 via (2.20). Putting it all together, the direct link between Problem 4, which we plan to solve, and the original Problems 1-3 is obtained. Given the solution to Problem 4, $\mathbf{y}'$, the solutions to Problems 1, 2 or 3, depending on the value of k, can be obtained as follows:

$$\begin{array}{cc} \text{Problem 1} & \text{Problem 2} \\ \mathbf{p}_{opt} = \left. \frac{P}{\mathbf{1}^\top \mathbf{y}'} \mathbf{y}' \right|_{k=0} & \mathbf{w}_{opt} = \left. \frac{B}{\mathbf{1}^\top \mathbf{y}'} \mathbf{y}' \right|_{k=1} \\ & \text{Problem 3} \\ \mathbf{p}_{opt}^j = \left. \frac{P}{\mathbf{1}^\top \mathbf{y}'} \mathbf{y}' \right|_{k=2} & \mathbf{w}_{opt}^j = \left. \frac{B}{\mathbf{1}^\top \mathbf{y}'} \mathbf{y}' \right|_{k=2} \end{array} \tag{2.28}$$

2.3 Proposed Approximate Solution

Currently, the goal is to find an approximate solution to Problem 4 for any $k \in \{0, 1, 2\}$. It is not difficult to see that for Problem 4, the objective function is linear,

constraints (2.24) are polynomials of 2nd (case $k = 0$), 4th ($k = 1$) or 6th ($k = 2$) order, and the last constraint is linear. The problem would fit in the framework of convex optimization, for which very efficient techniques exist [60], if (2.24) were convex. However, this is true only for some very particular cases of $\mathbf{H}_q$. Therefore, we have to rely on techniques designed for nonconvex optimization. In most cases such techniques do not lead to the global minimum. Moreover, the computational cost of such techniques grows exponentially with the dimension of the problem.

An alternative approach is to approximate the original problem with a sequence of convex problems, firstly proposed in [61], and later referred to as Sequential Parametric Convex Approximation (SPCA) [62]. To explain SPCA, observe that any constraint in Problem 4 may be written as $h(\mathbf{y}) \leq 0$, where h will be called the constraint function. If h is a convex function, then $h(\mathbf{y}) \leq 0$ is a convex constraint. The main idea of SPCA is that at each iteration, each of the nonconvex constraints functions in Problem 4 is replaced by a convex approximation. To construct such approximation, the nonconvex function is decomposed into a sum of a convex and a concave function. The concave function is linearized around a point as proposed in [63]. At each iteration, the algorithm solves the approximate convex problem. It stops when there is no further improvement in the objective function. The solution at each iteration is passed to the next iteration as the linearization point. Convergence of this algorithm is ensured at least to a local minimum [61].

As mentioned previously, the first step is to decompose the nonconvex constraints functions in Problem 4 into a sum of a convex and a concave function. Accomplishing this for (2.24) is not straightforward. First, let $\mathbf{z} = [z_1, \ldots, z_M]^\top$ be a vector of slack

variables linked to the components of $\mathbf{y}$ by $z_m = y_m^{k+1}$. Problem 4 is recast as

$$\min_{\mathbf{y},\mathbf{z}} \mathbf{1}^\top \mathbf{y} \tag{2.29a}$$

$$\text{s.t. } (\mathbf{a}_q + \mathbf{b}_q)^\top \mathbf{z} - \mathbf{z}^\top \mathbf{H}_q \mathbf{z} \leq 0 \quad \text{for } q = 1, \ldots, Q \tag{2.29b}$$

$$z_m - y_m^{k+1} = 0 \qquad \text{for } m = 1, \ldots, M \tag{2.29c}$$

$$\mathbf{y}, \mathbf{z} \succcurlyeq \mathbf{0} \quad . \tag{2.29d}$$

The advantage of this new problem over Problem 4 is that (2.29b) is now in a quadratic form, and a simple way to decompose a quadratic function into a convex plus concave function is to separate matrix $\mathbf{H}_q$ into a sum of a nonnegative-definite ($\mathbf{H}_q^+$) and a nonpositive-definite ($\mathbf{H}_q^-$) matrix. Notice that if the newly introduced constraint (2.29c) is relaxed by putting $z_m - y_m^{k+1} \leq 0$ instead, then it is also a sum of a convex (z_m) and a concave ($-y_m^{k+1}$) function:

$$\min_{\mathbf{y},\mathbf{z}} \quad \mathbf{1}^\top \mathbf{y} \tag{2.30a}$$

$$\text{s.t.} \quad (\mathbf{a}_q + \mathbf{b}_q)^\top \mathbf{z} - \mathbf{z}^\top \mathbf{H}_q^- \mathbf{z} - \mathbf{z}^\top \mathbf{H}_q^+ \mathbf{z} \leq 0 \tag{2.30b}$$

$$\text{for } q = 1, \ldots, Q$$

$$z_m - y_m^{k+1} \leq 0 \qquad \text{for } m = 1, \ldots, M \tag{2.30c}$$

$$\mathbf{y}, \mathbf{z} \succcurlyeq \mathbf{0}. \tag{2.30d}$$

Lemma 3 : *The optimal solution to problem* (2.30) *always satisfies* (2.30c) *with equality, and therefore, it is also the optimal solution to problem* (2.29).

Proof. Assume that is a solution $(\mathbf{y}^{opt}, \mathbf{z}^{opt})$ such that for some component m satisfies $z_m^{opt} < (y_m^{opt})^{k+1}$. Then another point $(\mathbf{y}', \mathbf{z}^{opt})$ can be defined such that the mth component of $\mathbf{y}'$ is $y'_m = (z_m^{opt})^{\frac{1}{k+1}} < y_m^{opt}$ and the remaining components are $y'_m = y_m^{opt}$. This point satisfies $z_m - y_m^{k+1} \leq 0$ with equality and gives a smaller value for the objective function, contradicting the fact that $(\mathbf{y}^{opt}, \mathbf{z}^{opt})$ is a solution. □

Given that problem (2.30)'s constraints are separated into convex and concave functions, problem (2.30) may be convexified by linearizing the concave parts, $-\mathbf{z}^\top \mathbf{H}_q^+ \mathbf{z}$ in (2.30b) and $-y_m^{k+1}$ in (2.30c) around a point $(\mathbf{y}_{(n)}, \mathbf{z}_{(n)})$. Linearization may be implemented by a first order Taylor expansion, where n indexes the iteration. Then the optimization problem becomes

$$\min_{\mathbf{y},\mathbf{z}} \quad \mathbf{1}^\top \mathbf{y} \tag{2.31a}$$

$$\text{s.t.} \quad \left(\mathbf{a}_q + \mathbf{b}_q\right)^\top \mathbf{z} - \mathbf{z}^\top \mathbf{H}_q^- \mathbf{z} - \mathbf{z}_{(n)}^\top \mathbf{H}_q^+ (2\mathbf{z} - \mathbf{z}_{(n)}) \leq 0 \tag{2.31b}$$

$$\text{for } q = 1, \ldots, Q$$

$$z_m + k y_{(n),m}^{k+1} - (k+1) y_{(n),m}^k x_m \leq 0 \tag{2.31c}$$

$$\text{for } m = 1, \ldots, M$$

$$\mathbf{y}, \mathbf{z} \succcurlyeq \mathbf{0} \quad . \tag{2.31d}$$

The feasible set of problem (2.31) is convex, and in addition, it is a subset of the feasible set of problem (2.30). To confirm this point, notice the constraint function in (2.31c) is equal or larger than the constraint function in (2.30c) for all $(\mathbf{y}, \mathbf{z})$, and therefore, the set of points satisfying constraint (2.31c) is a subset of the one defined by (2.30c). The set of points defined by (2.31c) is also a subset of (2.30b). Therefore, any solution resulting from solving the approximate problem (2.31b) is in the feasible set of problem (2.30b), and consequently of Problem 4.

Algorithm : First, parameter k in (2.31) is set to 0, 1 or 2, depending on if power (Problem 1), bandwidth (Problem 2) or joint power-bandwidth (Problem 3) are being allocated, respectively. The algorithm consists in solving a series of convex problems (2.31). The solution $(\mathbf{y}_{(n)}, \mathbf{z}_{(n)})$ to (2.31) at each iteration n is passed to the next iteration $n+1$ and used as a linearization point for (2.31). In the initial step, the uniform allocation $\mathbf{y}_{(0)}, \mathbf{z}_{(0)} \propto \mathbf{1}$ is used as the linearization point because it treats all transmitters equally. The algorithm stops when the value in the cost function (2.31a)

does not change substantially. After denoting $\mathbf{y}'$ the solution to (2.31) in the last iteration, the allocation vector is recovered via (2.28).

At each iteration, the above algorithm first proposed in [62], uses the previous solution as the next linearization point of the new convexified optimization problem. Since the linearization point lies within the feasible set of the new problem, the global minimum of the new problem is equal or smaller than the previous one. If the previous solution is not improved, then the algorithm stops, otherwise the algorithm keeps iterating. Therefore, the final solution is ensured to be equal or better than the uniform allocation, which is used as initialization point. Moreover, since the objective function (2.31a) is bounded below by zero and it decreases at each iteration, by the monotone convergence theorem [64], the algorithm is ensured to converge irrespective of the parameters.

2.4 Lower Bound on the Accuracy of the Optimal Allocations

The previous section provided an algorithm that finds approximate solutions to Problems 1 to 3. In this section, we provide a method for assessing their quality. Let $\mathbf{p}_{opt}$, $\mathbf{w}_{opt}$ and $(\mathbf{p}^j_{opt}, \mathbf{w}^j_{opt})$, be the actual solutions to Problems 1, 2 and 3, respectively, and let $\tilde{\mathbf{p}}_{opt}$, $\tilde{\mathbf{w}}_{opt}$ and $(\tilde{\mathbf{p}}^j_{opt}, \tilde{\mathbf{w}}^j_{opt})$ be the approximate solutions to Problems 1, 2 and 3 obtained by the algorithm in the previous section. Obviously, the objective function of Problems 1, 2 and 3 evaluated at the approximate solutions, are equal or larger than if it they were evaluated at the optimal points:

$$\max_q T_q(\tilde{\mathbf{p}}_{opt}, w\mathbf{1}) \geq \max_q T_q(\mathbf{p}_{opt}, w\mathbf{1}) \geq \mathrm{L}_p \tag{2.32}$$

$$\max_q T_q(p\mathbf{1}, \tilde{\mathbf{w}}_{opt}) \geq \max_q T_q(p\mathbf{1}, \mathbf{w}_{opt}) \geq \mathrm{L}_b \tag{2.33}$$

$$\max_q T_q(\tilde{\mathbf{p}}^j_{opt}, \tilde{\mathbf{w}}^j_{opt}) \geq \max_q T_q(\mathbf{p}^j_{opt}, \mathbf{w}^j_{opt}) \geq \mathrm{L}_j \tag{2.34}$$

where L_p, L_b and L_j are some lower-bounds on the unknown global minimums. This section is devoted to developing these lower-bounds, and their usefulness is

explained in the following example. Assume that for Problem 1 (power allocation) the lower-bound is tight to our approximate minimum $\max_q T_q(\tilde{\mathbf{p}}_{opt}, w\mathbf{1}) \approx \mathrm{L}_p$. Then by (2.32) it follows that the approximate minimum is very close to the global minimum $\max_q T_q(\tilde{\mathbf{p}}_{opt}, w\mathbf{1}) \approx \max_q T_q(\mathbf{p}_{opt}, w\mathbf{1}) \approx \mathrm{L}_p$. However, nothing can be asserted if $\max_q T_q(\tilde{\mathbf{p}}_{opt}, w\mathbf{1}) \gg \mathrm{L}_p$.

The process of finding lower-bounds for the global minimums of Problems 1, 2 and 3 is simplified by the following proposition:

Proposition 3 : *Let L_c denote a lower-bound to the global minimum of Problem 4. Then lower-bounds, L_p, L_b and L_j, to the global minimums of Problems 1, 2 and 3 can be obtained through the following equations*

$$L_p = \left.\frac{L_c}{Pw^2}\right|_{k=0}, \qquad L_b = \left.\frac{L_c^2}{pB^2}\right|_{k=1} \text{ and } \qquad L_j = \left.\frac{L_c^3}{PB^2}\right|_{k=2}. \tag{2.35}$$

Therefore, it suffices to find a lower-bound (L_c) for Problem 4. The following lemma is needed for the proof of Proposition 3.

Lemma 4 : *Constraint* (2.24) *in Problem 4 must be active when evaluated at the solution.*

Proof of Lemma 4. Assume there exists a minimum point $\mathbf{y}'$ such that $\max_q g_q(\mathbf{y}', k) < 1$. Define $\mathbf{y}^* = [\max_q g_q(\mathbf{y}', k)]^{\frac{1}{k+1}} \mathbf{y}'$. From (2.18) it follows that $\max_q g_q(\mathbf{y}^*, k) = 1$, thus it satisfies the constraints of the optimization problem (2.22). Next

$$\mathbf{1}^\top \mathbf{y}^* = \left[\max_{q\in\{1,\ldots,Q\}} g_q(\mathbf{y}', k)\right]^{\frac{1}{k+1}} \mathbf{1}^\top \mathbf{y}' < \mathbf{1}^\top \mathbf{y}' \tag{2.36}$$

This contradicts the assumption that the problem achieves its minimum at $\mathbf{y}'$. It follows that (2.22) evaluated at the optimal point must be active. □

Proof of Proposition 3. The proof is done, only, for Problem 1's lower-bound L_p. For Problems 2 and 3, the proof follows the same steps with very minor differences and are

omitted here for brevity. Recall that, according to (2.28), the solution of Problem 1 is directly related to the solution of Problem 4 by $\mathbf{p}_{opt} = \frac{P}{\mathbf{1}^\top \mathbf{y}'}\mathbf{y}'|_{k=0}$. Substituting $\mathbf{p}_{opt}$ in the global minimum (2.32) of Problem 1 results in

$$\max_q T_q(\mathbf{p}_{opt}, w\mathbf{1}) = \frac{\mathbf{1}^\top \mathbf{y}'}{Pw^2} \max_q T_q(\mathbf{y}', \mathbf{1})\Big|_{k=0} \tag{2.37}$$

where we made use of Lemma 1 to simplify it. By Lemma 4, it can be further reduced to $\max_q T_q(\mathbf{p}_{opt}, w\mathbf{1}) = \frac{\mathbf{1}^\top \mathbf{y}'}{Pw^2}|_{k=0}$. By definition L_c is a lower-bound of the global minimum of Problem 4, so it must satisfy $L_c \leq \mathbf{1}^\top \mathbf{y}'$, which leads to

$$\max_q T_q(\mathbf{p}_{opt}, w\mathbf{1}) \geq \frac{L_c}{Pw^2}\Big|_{k=0} \tag{2.38}$$

The right side is obviously a lower-bound to global minimum of Problem 1 and proves the first equality in Proposition 3. □

To get a lower-bound L_c, several relaxations are applied to the feasible set of Problem 4 in order to obtain another optimization problem whose solution can be computed, and whose global minimum is equal or smaller than that of Problem 4. This global minimum then constitutes a lower bound to the minimum of Problem 4, which will be denoted by L_c. To that end, the first step consists in making a variable vector substitution $z_m = y_m^{k+1}$ for all $m = 1, \ldots, M$ in Problem 4. Such operation does not change the global minimum of the problem.

$$\min_{\mathbf{z}} \quad \sum_{m=1}^{M} \sqrt[k+1]{z_m} \tag{2.39}$$

$$\text{s.t.} \quad (\mathbf{a}_q + \mathbf{b}_q)^\top \mathbf{z} \leq \mathbf{z}^\top \mathbf{H}_q \mathbf{z} \quad \text{for } q = 1, \ldots, Q \tag{2.40}$$

$$\mathbf{z} \geq \mathbf{0} \tag{2.41}$$

Where $\mathbf{z} = [z_1, \ldots, z_M]^\top$. It is easy to verify that an equal or smaller objective function to that of (2.39) for all values of z_m is

$$\sqrt[k+1]{\mathbf{1}^\top \mathbf{z}} \tag{2.42}$$

Let $\mathbf{z}'$ denote the solution to problem (2.40) with the new objective function (2.42) instead of (2.39). The minimum will be equal or smaller than that of Problem 4, i.e. $\sqrt[k+1]{\mathbf{1}^\top \mathbf{z}'} \leq \mathbf{1}^\top \mathbf{y}'$. As the root is a monotonically increasing function, suppressing it from the objective function (2.42) still leads to the same solution $\mathbf{z}'$, and therefore, Problems (2.39)-(2.40) can be simplified to

$$\min_{\mathbf{z}} \quad \mathbf{1}^\top \mathbf{z} \tag{2.43}$$

$$\text{s.t.} \quad (\mathbf{a}_q + \mathbf{b}_q)^\top \mathbf{z} \leq \mathbf{z}^\top \mathbf{H}_q \mathbf{z} \quad \text{for } q = 1, \ldots, Q \tag{2.44}$$

$$\mathbf{z} \geq \mathbf{0} \tag{2.45}$$

The feasible set of problem (2.44) is now relaxed by removing $Q-1$ constraints from (2.44):

$$\begin{aligned} \min_{\mathbf{z}} \quad & \mathbf{1}^\top \mathbf{z} \\ \text{s.t.} \quad & (\mathbf{a}_q + \mathbf{b}_q)^\top \mathbf{z} \leq \mathbf{z}^\top \mathbf{H}_q \mathbf{z} \\ & \mathbf{z} \geq \mathbf{0} \end{aligned} \tag{2.46}$$

Here q takes only one value between 1 and Q. Call $\mathbf{z}'_q$ the solution to problem (2.46). Because problem (2.46) is a relaxation of problem (2.44), its minimum satisfies $\mathbf{1}^\top \mathbf{z}'_q \leq \mathbf{1}^\top \mathbf{z}'$. It turns out that this problem has the same algebraic form as the power allocation problem in [65] (Section III.A.2), where an exact solution is provided by solving the Karush-Kuhn-Tucker conditions [66]. By solving (2.46) for all possible values of $q \in \{1, \ldots, Q\}$, a tighter inequality $\max_q(\mathbf{1}^\top \mathbf{z}'_q) \leq \mathbf{1}^\top \mathbf{z}'$ is obtained. Putting this together with the fact that $\sqrt[k+1]{\mathbf{1}^\top \mathbf{z}'} \leq \mathbf{1}^\top \mathbf{y}'$, we obtain the desired computable lower-bound for Problem 4's global minimum:

$$L_c = \sqrt[k+1]{\max_{q \in \{1,\ldots,Q\}} \mathbf{1}^\top \mathbf{z}'_q} \leq \mathbf{1}^\top \mathbf{y}' \tag{2.47}$$

Combining (2.47) with (2.35), the final expressions for the lower-bounds of Problems 1, 2 and 3 are

$$L_p = \frac{\max_q \mathbf{1}^\top \mathbf{z}'_q}{Pw^2}, \qquad L_b = \frac{\max_q \mathbf{1}^\top \mathbf{z}'_q}{pB^2}, \qquad L_j = \frac{\max_q \mathbf{1}^\top \mathbf{z}'_q}{PB^2} \tag{2.48}$$

Quite relevant is that if these lower-bounds are tight to the minimums of Problems 1, 2 and 3, it suggests that bandwidth has a bigger impact than power because the bandwidth variables w and B appear as quadratic terms in comparison to p and P.

2.5 Numerical Results

The numerical examples presented in this section were obtained with five transmitters, five receivers and four targets. The choice of the number of elements enables sufficient choice for resource allocation, while not making the system overly complex. The total bandwidth available to the network is set to 3 MHz. The average power available for the network is an adjustable parameter. The pulse repetition frequency is set to 5 kHz, which is sufficient for unambiguous range estimation in our setup. The targets are static. The pulse integration time is 10 ms.

The proposed allocation algorithms assign power and/or bandwidth depending on the specific locations of the elements and the reflection coefficients of the targets. To avoid obtaining results that are specific to a particular layout, each point in the figures that are to follow is formed as averaging results of 1000 simulations. For each simulation, the transmitters, receivers and targets are positioned randomly in a 20 km $\times$ 20 km area, according to a uniform distribution. The reflection coefficients of the targets are set to a fixed value of 10 m^2. Performance was evaluated from the average of 1000 values of the cost function (2.10). Each value represents an optimal allocation of power, bandwidth, or joint power-bandwidth for an instantiation of targets locations, reflection coefficients and noise.

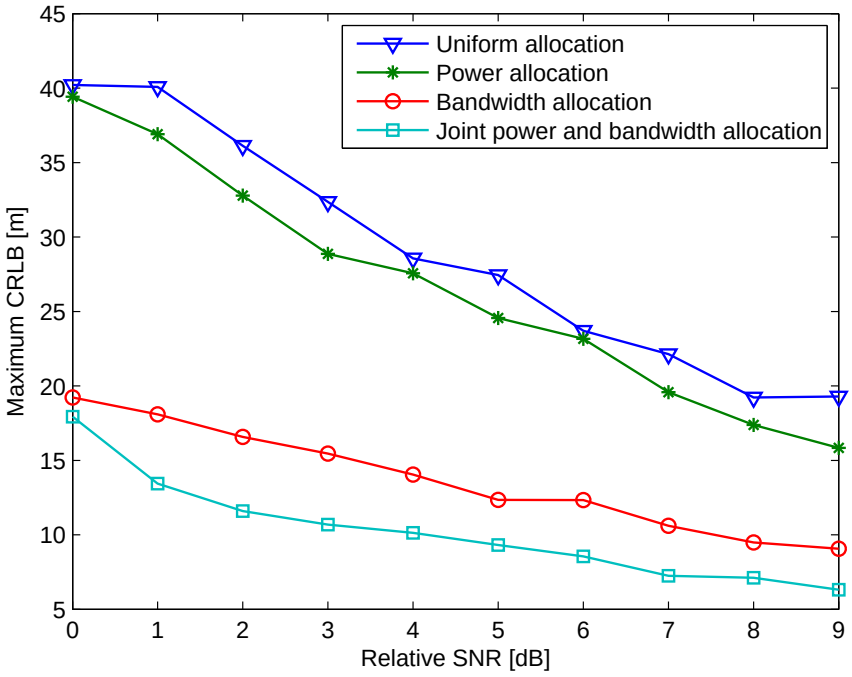

Figure 2.1 Square root maximum CRLB vs. SNR after resource allocation.

2.5.1 Resource Allocation for Different SNR Values

Figure 2.1 presents the square root of the max CRLB as a function of the relative SNR for four different case studies: power and bandwidth evenly distributed among transmitters, power allocation, bandwidth allocation, and joint power-bandwidth allocation. As expected, the joint allocation performs the best decreasing the cost function by 70% compared to uniform allocation, which has the worst performance. Bandwidth allocation is second best and power allocation is just slightly better than uniform allocation, with decreases in the cost of 50% and 10%, respectively. Increasing the SNR improves the localization accuracy for all methods.

To validate the results based on the CRLB, localization errors are computed also for a multilateration algorithm implemented to estimate the target locations. Multilateration is comprised of three steps. In the first step, the time of arrivals (TOA's) of the transmitted pulses are estimated at all the receivers by the WRELAX algorithm [67]. The TOA information is then transmitted to a fusion center, where an

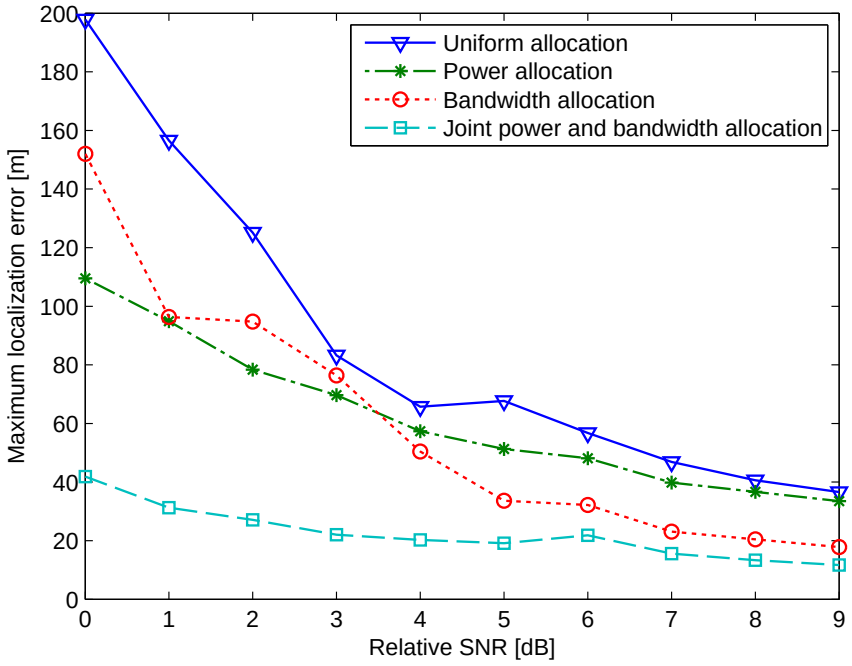

Figure 2.2 Square root maximum localization error vs. SNR after resource allocation.

algorithm associates TOA's to targets. Finally, using the TOA's, the target locations are estimated using the BLUE method in [39]. For the simulation, we choose the square root of the Hamming window [68] as pulse shape in the frequency domain, which can be shown to have a good mainlobe to secondary lobe ratio necessary for TOA estimation. For a given simulation, all elements are positioned randomly in the area. After positioning the elements, resources are allocated among the transmitters and, then the signals at the receivers are simulated and we perform localization by multilateration. To compare it with the cost function (2.10), the maximum localization error among all targets is averaged for all 1000 instantiations.

Figure 2.2 plots the square root of the maximum localization error versus SNR. Here an increase of 1 dB is simply used to denote an increase of 1 dB in total power. Obviously, the localization error decreases with the increase in SNR. A threshold effect is observed approximately at around 4 dB of relative SNR with slight variations for the different allocation algorithms. On the right of this threshold the maximum

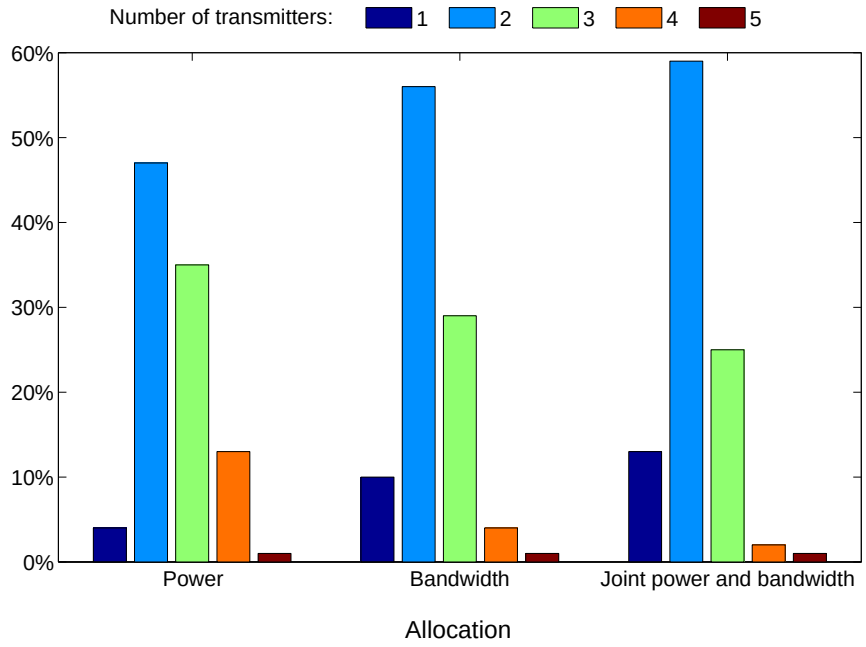

Figure 2.3 Relative frequencies of the number of active transmitters.

localization error tightens over the maximum CRLB in Figure 2.1, even though it still maintains a gap for all SNR values. The reason for this gap is, to the best knowledge of the authors, because there do not exist multilateration techniques that converge to the CRLB in the presence of multiple targets.

2.5.2 Number of Active Transmitters

The resource allocation algorithms distribute among the transmitters power, bandwidth, or both. Figure 2.3 plots the relative frequency of the number of active transmitters (transmitters whose assigned power and bandwidth is different than zero) for the three types of resource allocation. The SNR is not specified because, for all allocations the SNR simply scales the amount of resources to be assigned, but does not change which transmitters are selected.

2.5.3 Numerical Evaluation of the Approximations

The purpose of this section is to validate two approximations used in this chapter. The first one is due to the fact that the resource allocation algorithms employ an approximate closed-form formula for the CRLB of multiple targets (2.8) as explained in section 2.1. The second approximation was to consider that the solutions of our algorithms are almost as good as the optimal (but unknown) solutions. For this purpose were developed the lower-bounds in Section 2.4.

Simulations for all three types of resource allocations are performed, and plot in Figure 2.4, the maximum CRLB (2.10), the approximate maximum CRLB (2.11), and the lower-bound on the optimal CRLB for a prescribed total power. The figure shows how the approximate maximum CRLB and the true maximum CRLB do not vary more than 10%. It also shows how the lower-bound is tight to the approximate maximum CRLB for the case of power allocation, thus in this case the algorithm is performing optimally. For the bandwidth and joint allocation cases, the lower-bound is not as tight, being the separation greater for the joint case, meaning another joint power-bandwidth allocation algorithm could perhaps perform slightly better.

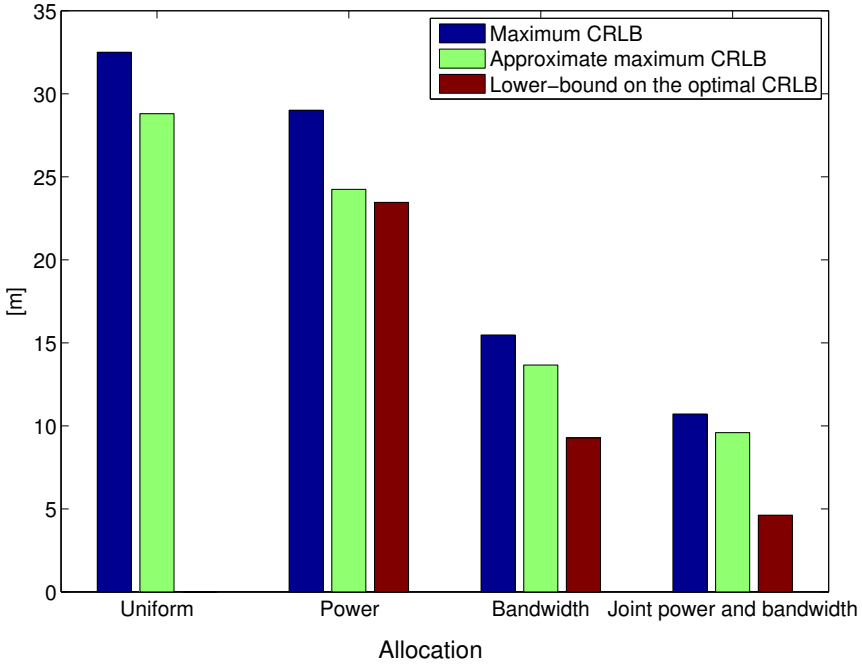

Figure 2.4 Comparison of the maximum CRLB, the approximate maximum CRLB, and the lower-bounds on the approximate maximum CRLB

CHAPTER 3

DIRECT LOCALIZATION FOR PASSIVE LOCALIZATION

Traditional time-of-arrival (TOA)-based localization is accomplished through a two-step process. In the first step, sensors estimate TOAs from all incoming signals; in the second step, such estimates are transmitted to a central node, which subsequently estimates the location of each source by multilateration. We refer to these localization techniques as indirect localization. A better approach than indirect localization is to infer the source locations directly from the signal measurements, without estimating any intermediary parameters such as propagation delays. In the absence of multipath, a method known as Direct Position Determination (DPD) [46] outperforms standard indirect localization, particularly at low signal-to-noise ratio (SNR), because it takes into account the fact that signals arriving at different sensors are emitted from the same location. In a multipath environment, each sensor receives, in addition to a line-of-sight (LOS) signal, multiple (possibly overlapping) replicas due to non-line-of-sight (NLOS) paths. Due to these multiple arrivals, it is, in general, more challenging to obtain accurate TOA estimates of the LOS components at the sensors. This chapter presents a passive direct localization technique for frequency-selective channels based on TOA information.

3.1 Signal model

Consider a network composed of L sensors and Q sources located in a plane. The location of the q-th source is defined by two coordinates stacked in a vector $\mathbf{p}_q$. All sources share the same bandwidth B, and transmit their own signals $\{s_q(t)\}_{q=1}^{Q}$. The number of sources Q and their waveforms are known. The observation time is T, assumed to be shorter than the time coherence of the channel, therefore, the channel

is time-invariant. The complex-valued baseband signal at the l-th sensor is

$$r_l(t) = r_l^{\mathrm{LOS}}(t) + r_l^{\mathrm{NLOS}}(t) + w_l(t) \qquad 0 \le t \le T, \tag{3.1}$$

where $w_l(t)$ is circular symmetric complex white Gaussian noise with known variance $\mathrm{E}\,|w_l(t)|^2 = \sigma_w^2$. The term $r_l^{\mathrm{LOS}}(t)$ is the sum of all LOS components:

$$r_l^{\mathrm{LOS}}(t) = \sum_{q=1}^{Q} a_{ql} s_q \left(t - \tau_l(\mathbf{p}_q)\right), \tag{3.2}$$

where a_{ql} is an unknown complex scalar representing the signal strength and phase of the LOS path between the q-th source and l-th sensor, and $\tau_l(\mathbf{p})$ is the delay of a signal originating at $\mathbf{p}$ and reaching the l-th sensor:

$$\tau_l(\mathbf{p}) = \left\|\mathbf{p} - \mathbf{p}_l'\right\|_2 / c. \tag{3.3}$$

In (3.3), $\mathbf{p}_l'$ is the location of the l-th sensor, c is the speed of light and $\|\cdot\|_2$ denotes the standard Euclidean norm. The term $r_l^{\mathrm{NLOS}}(t)$ in (3.1) aggregates all NLOS arrivals:

$$r_l^{\mathrm{NLOS}}(t) = \sum_{q=1}^{Q} \sum_{m=1}^{M_{ql}} a_{ql}^{(m)} s_q \left(t - \tau_{ql}^{(m)}\right), \tag{3.4}$$

where M_{ql} denotes the unknown number of NLOS paths between the q-th source and the l-th sensor, $a_{ql}^{(m)}$ is an unknown complex scalar representing the amplitude of the m-th NLOS path between the q-th source and l-th sensor, and $\tau_{ql}^{(m)}$ is the delay of the NLOS component. The received signal (3.1) is sampled at a frequency f_s satisfying the Nyquist sampling criterion: $f_s \ge 2B$, where B is the bandwidth of $r(t)$. Each sensors collects N time samples at each observation time. By stacking the N acquired samples, the received signal $\mathbf{r}_l = [r_l(0), \ldots, r_l((N-1)/f_s)]^T$ at the l-th sensor can be written in the following vector form

$$\mathbf{r}_l = \sum_{q=1}^{Q} \alpha_{ql} \mathbf{s}_q \left(\tau_l(\mathbf{p}_q)\right) + \sum_{q=1}^{Q} \sum_{m=1}^{M_{ql}} \alpha_{ql}^{(m)} \mathbf{s}_q \left(\tau_{ql}^{(m)}\right) + \mathbf{w}_l, \tag{3.5}$$

where $\mathbf{s}_q(\tau)$ is the vector of the N received samples from the q-th source waveform with delay τ:

$$\mathbf{s}_q(\tau) = \begin{bmatrix} s_q\left(0-\tau\right) & \cdots & s_q\left((N-1)/f_s-\tau\right) \end{bmatrix}^T. \tag{3.6}$$

Since all sensors acquire the same number of samples, the samples may be stacked in an $N \times L$ matrix

$$\begin{aligned} \mathbf{R} &= \begin{bmatrix} \mathbf{r}_1 & \cdots & \mathbf{r}_L \end{bmatrix} = \\ &= \sum_{q=1}^{Q} \begin{bmatrix} \alpha_{q1}\mathbf{s}_q\left(\tau_1(\mathbf{p}_q)\right) & \cdots & \alpha_{qL}\mathbf{s}_q\left(\tau_L(\mathbf{p}_q)\right) \end{bmatrix} + \sum_{q=1}^{Q}\sum_{l=1}^{L}\sum_{m=1}^{M_{ql}} \alpha_{ql}^{(m)}\mathbf{s}_q\left(\tau_{ql}^{(m)}\right)\mathbf{v}_l^T + \mathbf{W}, \end{aligned} \tag{3.7}$$

where the rows and columns index time instants and sensors, respectively, and $\mathbf{v}_l$ is an all-zeros vector except for the l-th entry which is one. The LOS and NLOS components are parametrized by the first and second summands in (3.7), respectively. From now on, we will switch between the notations in (3.5) and (3.7) depending on whether we are interested in the signal of one sensor only or of all sensors.

3.2 Proposed Localization Technique

In order to develop a localization technique, it is first necessary to understand what parameters of the received signals depend on the sources locations. In the signal model introduced in the previous section, the propagation delays of the NLOS components (3.4) were assumed to be unknown and arbitrary, because of the lack of prior statistical knowledge of the channel. Thus information on the sources locations is carried only by the LOS components (3.2). This claim is supported by the analysis in [33], which showed that the CRB increases when NLOS components are present. Consequently, without a priori knowledge, the optimal strategy is to reject NLOS components as much as possible, and rely on the LOS components to infer the sources' locations.

With indirect techniques, first, the TOA's of the LOS components are estimated, and then used to localize the sources by multilateration. However, indirect techniques are suboptimal because they estimate the TOA of the first path at each sensor independently, instead of taking into account that all LOS components originate from a single source location. In this section, we propose a direct localization technique that relies on the fact that all LOS components associated with a source must originate from the same location. Under the Gaussian assumption, the maximum likelihood estimator (MLE) is the solution to the following fitting problem

$$\min_{\substack{\mathbf{p}_1,\ldots,\mathbf{p}_Q \\ a_{11},\ldots,a_{LQ} \\ M_{11},\ldots,M_{LQ} \\ \tau_{11}^{(1)},\ldots,\tau_{LQ}^{(M_{LQ})} \\ a_{11}^{1},\ldots,a_{LQ}^{M_{LQ}}}} \sum_{l=1}^{L} \left\| \mathbf{r}_l - \sum_{q=1}^{Q} a_{ql}\mathbf{s}_q\left(\tau_l(\mathbf{p}_q)\right) - \sum_{q=1}^{Q}\sum_{m=1}^{M_{ql}} a_{ql}^{(m)}\mathbf{s}_q\left(\tau_{ql}^{(m)}\right) \right\|_2^2 \tag{3.8}$$

subject to $\tau_{ql}^{(m)} > \tau_l(\mathbf{p}_q)$, for all q, l and m. The parameters of interest are the source locations $\{\mathbf{p}_q\}_{q=1}^{Q}$, while the rest act as nuisance parameters. Besides the fact that it is an enormous challenge to find an efficient technique for minimizing this objective function, the ML criterion does not even lead to a satisfactory solution. The reason is that M_{ql}, for all l and q, are hyperparameters that control the number of NLOS paths in our model. It is known that increasing the values of hyperparameters always leads to a better fitting error [69], and in our case, it would lead to the erroneous conclusion that there is a very large number of NLOS arrivals. Instead, we assume that the number of NLOS arrivals and the number of sources is low with respect to the number of observations. This assumption enables the formulation of a feasible solution to the ML multipath estimation problem by means of a sparse recovery technique.

In order to obtain a high-precision localization technique, there are two properties of the signal paths that need to be exploited. These properties allow to distinguish LOS from NLOS components. The first one is that NLOS components

arrive with a longer delay than LOS components, and the second property is that all LOS paths originate from the same location. Our technique is divided in two stages, which are explained in the following two sections. In the first stage, NLOS components are canceled out from the received signals by exploiting the fact that LOS components must arrive first. This processing can be done locally at each sensor. In the second stage, the cleaned version of the received signals are sent to a fusion center that finds the sources' location. It is in this stage that the source locations are estimated by exploiting the fact that LOS components must originate from the same location, whereas NLOS components may be local to the sensors.

3.3 Stage 1: Deconvolution

In this stage, the multipath channel is deconvolved, or equivalently, the propagation delays of different paths are estimated, and the multipath contributions are removed from the received signals. Our technique of choice for deconvolution is the sparsity-based delay estimation technique proposed by Fuchs [70] because of its high accuracy and because it uses only a single snapshot of data as in our case. Other high accuracy time delay estimation methods, like MUSIC [19], are not applicable here because they require multiple uncorrelated data snapshots. Let $\tau_{\max}$ be the largest possible propagation delay, then in the Fuchs' technique, the continuous set of all possible propagation delays $[0, \tau_{\max}]$ is discretized forming a grid of delays

$$\mathcal{D} = \{0, \tau_{\text{res}}, \ldots, \tau_{\max}\}, \tag{3.9}$$

where parameter τ_{res} denotes the finesse of the grid. Define the dictionary matrix stacking the received signal waveforms for all possible (discrete) delays (3.9):

$$\mathbf{A} = \begin{bmatrix} \mathbf{s}(0) & \cdots & \mathbf{s}(\tau_{\max}) \end{bmatrix}. \tag{3.10}$$

Then, the propagation delays of all paths from a single source reaching the l-th sensor are estimated by solving the following Lasso problem of the form

$$\min_{\mathbf{x}} \lambda \left\|\mathbf{x}\right\|_1 + \left\|\mathbf{r}_l - \mathbf{A}\mathbf{x}\right\|_2^2, \tag{3.11}$$

where λ is a regularization parameter, $\|\cdot\|_1$ is the ℓ_1-norm of a vector, and $\mathbf{r}_l$ is the received signal defined in (3.5). Solving this convex optimization problems, results in a sparse vector $\hat{\mathbf{x}}$ whose non-zero entries indicate the estimated delays. More precisely, if the d-th entry of $\hat{\mathbf{x}}$ is different than zero, then a path has been detected with propagation delay $(d-1)\tau_{\text{res}}$. After estimating the propagation delays, Fuchs uses a maximum description length (MDL) criterion to filter out false detections. For more details on this technique see [70], and for a better understanding on the mathematics behind the Lasso problem see [71]. In [70], the time delay estimation technique was designed for real-valued signals, and assuming only a single emitting source. Here, we generalize such approach to complex valued signals by simply allowing the variables and parameters in (3.11) to be complex. We also generalize it to multiple sources by expanding the columns of the dictionary (3.10) to the waveforms of all sources:

$$\mathbf{A} = \begin{bmatrix} \mathbf{s}_1(0) & \cdots & \mathbf{s}_1(\tau_{\max}) & \bullet\bullet\bullet & \mathbf{s}_Q(0) & \cdots & \mathbf{s}_Q(\tau_{\max}) \end{bmatrix}. \tag{3.12}$$

It is possible to use other delay estimation techniques. Obviously, the more accurate the delay estimation technique, the better performance would be expected from this NLOS interference mitigation. Contrary to indirect localization techniques, the goal here is not to precisely estimate the propagation delays of the first paths, but rather to estimate the propagation delays of all subsequent arrivals, and cancel them out.

Let $\tilde{\tau}_{ql}^1, \ldots, \tilde{\tau}_{ql}^{P_{ql}}$ be the estimated propagation delays from source q to sensor l, then their amplitudes may be estimated by solving a linear least squares fit

$$\left\{\tilde{a}_{ql}^p\right\} = \underset{\left\{a_{ql}^p\right\}}{\arg\min} \left\| \mathbf{r}_l - \sum_{q=1}^{Q} \sum_{p=1}^{P_{ql}} a_{ql}^p \mathbf{s}_q\left(\tilde{\tau}_{ql}^p\right) \right\|_2^2. \tag{3.13}$$

Assuming the estimated propagation delays are ordered in ascending order $\tilde{\tau}_{ql}^{1} < \ldots < \tilde{\tau}_{ql}^{|\mathcal{O}_{ql}|}$, then all arrivals, except the first, can be canceled out from the received signals

$$\tilde{\mathbf{r}}_l = \mathbf{r}_l - \sum_{q=1}^{Q} \sum_{p=2}^{P_{ql}} \tilde{a}_{ql}^{p} \mathbf{s}_q \left(\tilde{\tau}_{ql}^{p} \right). \tag{3.14}$$

Ideally, all NLOS arrivals would be perfectly detected and their propagation delays estimated, in which case we could continue with a direct localization technique designed for absent multipath. However, (3.14) is not guaranteed to cancel all NLOS components for two reasons. First, if the LOS path between a source and sensor is blocked, then the first arrival corresponds to a NLOS paths, in which case it is not removed. Also, it is possible that the chosen delay estimation technique misses some arrivals or detects some false ones, thus failing to remove some NLOS components or adding some extra components, respectively. In short, this stage is essential as it reduces the multipath, but does not necessarily remove it completely. In the next section, we present a localization technique designed to work in the presence of the residual multipath as well as blocked paths.

3.4 Stage 2: Localization

This stage seeks to estimate the sources locations using the signals $\{\tilde{\mathbf{r}}_l\}_{l=1}^{L}$ output by Stage 1. As explained in the preceding section, such signals include LOS and also NLOS components, therefore, the signal model introduced in (3.5) for $\mathbf{r}_l$ is also valid for $\tilde{\mathbf{r}}_l$. Obviously, since $\tilde{\mathbf{r}}_l$ and $\mathbf{r}_l$ are different, so are the values of the parameters appearing in (3.5) that characterize them. From here on, to keep the notation in check, we abuse the notation by writing $\mathbf{r}_l$ instead of $\tilde{\mathbf{r}}_l$. However, always bear in mind that the observations in this stage are the signals output by Stage 1.

To compute the MLE (3.8), it is required that the number of LOS and NLOS paths be known, otherwise the minimization (3.8) tends towards a nonsensical solution with an infinite number of paths. In this section, it is assumed that the number of

sensors that receive a LOS path from the q-th source, say S_q, is known, even though it will be shown later in Section 3.4.3 that such information is not really needed. Nevertheless, even if $\{S_q\}_{q=1}^{Q}$ are known, but since the number of NLOS paths is not, a pure MLE approach is still not feasible. To bypass this issue, we will rely on the fact that the number of sources and NLOS paths is relatively small.

Define a *LOS atom* as the $N \times L$ matrix of measurements of LOS paths of a signal $s_q(t)$ emitted from location $\mathbf{p}$ and received at the L sensors

$$\mathbf{L}_q(\mathbf{b}, \mathbf{p}) = \begin{bmatrix} b(1)\mathbf{s}_q(\tau_1(\mathbf{p})) & \cdots & b(L)\mathbf{s}_q(\tau_L(\mathbf{p})) \end{bmatrix} \tag{3.15}$$

where $\mathbf{b} = [b(1) \cdots b(L)]^T$ are the complex amplitudes of the LOS components. It is important to normalize $\mathbf{b}$ as it will be discussed shortly. Hence, $\|\mathbf{b}\|_2$ is constrained to a given value that we will denote u_q, i.e., $\|\mathbf{b}\|_2 = u_q$. Define a *NLOS atom* as the $N \times L$ matrix of measurements due to a single NLOS path from the q-th source to the l-th sensor

$$\mathbf{N}_{ql}(\phi, \tau) = e^{i\phi}\mathbf{s}_q(\tau)\mathbf{v}_l^T \tag{3.16}$$

where the phase and delay are ϕ and τ, respectively, and $\mathbf{v}_l$ is a unit vector, with the unit entry indexed by l. Let $\hat{\mathbf{R}}$ denote the matrix of received signals (3.7) in the absence of noise. Then, $\hat{\mathbf{R}}$ may be expressed as a positive linear combination of given atoms

$$\hat{\mathbf{R}} = \sum_k c^{(k)}\mathbf{A}^{(k)}, \quad \mathbf{A}^{(k)} \in \mathcal{A} \tag{3.17}$$

where $c^{(k)} > 0$ for all k, and $\mathcal{A}$ is the set of all atoms (or atomic set). The atomic set includes all different LOS and NLOS atoms,

$$\mathcal{A} = \mathcal{A}_{\text{LOS}} \cup \mathcal{A}_{\text{NLOS}} \tag{3.18}$$

where $\mathcal{A}_{\text{LOS}}$

$$\mathcal{A}_{\text{LOS}} = \bigcup_{q=1}^{Q} \left\{ \mathbf{L}_q \left(\mathbf{b}, \mathbf{p} \right) : \mathbf{b} \in \mathbb{C}^L, \mathbf{p} \in \mathcal{S} \subset \mathbb{R}^2, \left\| \mathbf{b} \right\|_2 = u_q \right\} \tag{3.19}$$

and $\mathcal{A}_{\text{NLOS}}$

$$\mathcal{A}_{\text{NLOS}} = \bigcup_{q=1}^{Q} \bigcup_{l=1}^{L} \left\{ \mathbf{N}_{ql} \left(\phi, \tau \right) : 0 \leq \phi < 2\pi, \tau \in [0, \tau_{\max}] \right\}. \tag{3.20}$$

Here, $\mathcal{S}$ denotes the search area of the sources and $\tau_{\max}$ the maximum possible delay in the system. Notice, that set of LOS atoms and the set of NLOS atoms are infinite in the sense that $\mathbf{p}$ and τ are continuous variables within their domain. Thus, this framework is inherently different in comparison to the finite sets of atoms in traditional compressive sensing.

Since the atomic sets are infinite, determining the coefficients $c^{(k)}$ from measurements $\hat{\mathbf{R}}$ is a highly undetermined problem. This problem is resolved by seeking a sparse solution to the coefficients $c^{(k)}$. As motivated in [58], this can be accomplished through the *atomic norm*. Precisely, the atomic norm $\| \cdot \|_{\mathcal{A}}$ induced by $\mathcal{A}$ is defined as

$$\left\| \hat{\mathbf{R}} \right\|_{\mathcal{A}} = \inf_{c^{(k)} > 0} \left\{ \sum_k c^{(k)} : \hat{\mathbf{R}} = \sum_k c^{(k)} \mathbf{A}^{(k)}, \mathbf{A}^{(k)} \in \mathcal{A} \right\}. \tag{3.21}$$

An *atomic decomposition of* $\hat{\mathbf{R}}$ is any set of coefficients $\{c^{(k)}\}$ for given atoms $\{\mathbf{A}^{(k)}\}$ such that $\hat{\mathbf{R}} = \sum_k c^{(k)} \mathbf{A}^{(k)}$. The *cost* of an atomic decomposition is defined as the sum of its positive coefficients: $\sum_k c^{(k)}$. An atomic decomposition is *optimal* if its cost achieves $\| \hat{\mathbf{R}} \|_{\mathcal{A}}$, or equivalently, if its cost is the smallest among all atomic decompositions. Sparsity is imposed here in the sense that we assume that the coefficients $c^{(k)}$ for which the atomic decomposition is optimal are associated with the true solution in terms of locations and time delays. This sparsity condition resolves the undetermined nature of (3.17). In practice, in the presence of noise, we seek

the optimal atomic decomposition that *approximately* matches the received signals. Precisely, in [58] it is suggested that the noiseless signals $\hat{\mathbf{R}}$ may be estimated by minimizing

$$\min_{\hat{\mathbf{R}}} \quad \left\|\hat{\mathbf{R}}\right\|_{\mathcal{A}} \tag{3.22a}$$

$$\text{s.t.} \quad \left\|\mathbf{R}-\hat{\mathbf{R}}\right\|_F^2 \leq \epsilon, \tag{3.22b}$$

where $\|\cdot\|_F$ is the Frobenius norm. Recall that the Frobenius norm is defined as the square root of the sum of the absolute squares of its elements. Roughly speaking, minimizing the atomic norm (3.22a) enforces sparsity, while constraint (3.22b) sets a bound on the mismatch between the noisy signals and the estimated signals. In fact, the left hand side of (3.22b) is the cost function of the MLE (3.8); hence, parameter ϵ may be regarded as an educated guess of the ML cost. The optimum solution to problem (3.22), say $\hat{\mathbf{R}}^\star$, may be regarded as an estimate of the received signals in the absence of noise. However, notice that solving such problem only produces $\hat{\mathbf{R}}^\star$ and not its optimal atomic decomposition, which is the primary goal because the LOS atoms are a proxy for the sources' locations. Thus, in general, in order to recover the optimal atomic decomposition, first, the optimum $\hat{\mathbf{R}}^\star$ to problem (3.22) is computed, and second, the optimal atomic decomposition of $\hat{\mathbf{R}}^\star$ is found.

The atomic decomposition of $\hat{\mathbf{R}}^\star$ may be expressed

$$\hat{\mathbf{R}}^\star = \sum_{q=1}^{Q}\sum_{k=1}^{K_q} c_q^{(k)}\mathbf{L}_q\left(\mathbf{b}_q^{(k)},\mathbf{p}_q^{(k)}\right) + \sum_{q=1}^{Q}\sum_{l=1}^{L}\sum_{k=1}^{K_{ql}} c_{ql}^{(k)}\mathbf{N}_{ql}\left(\phi_{ql}^{(k)},\tau_{ql}^{(k)}\right) \tag{3.23}$$

where $\{c_q^{(k)}\}_{k=1}^{K_q}$ are the positive coefficients associated to the K_q *non-zero* LOS atoms from the q-th source, and $\{c_{ql}^{(k)}\}_{k=1}^{K_{ql}}$ are the positive coefficients associated to the K_{ql} *non-zero* NLOS atoms between the source-sensor pair (q,l). Given $\hat{\mathbf{R}}^\star$ is expressed as in (3.23) and given that (3.23) is an optimal atomic decomposition, i.e., its cost

$$C = \sum_{q=1}^{Q}\sum_{k=1}^{K_q} c_q^{(k)} + \sum_{q=1}^{Q}\sum_{l=1}^{L}\sum_{k=1}^{K_{ql}} c_{ql}^{(k)} \tag{3.24}$$

is the smallest, then the set of locations for the q-th source associated with the optimal atomic decomposition are

$$\left\{\mathbf{p}_q^{(k)} \text{ for all } k = 1, \ldots, K_q\right\}, \tag{3.25}$$

the set of LOS propagation delays between source q and sensor l are

$$\left\{\tau_l\left(\mathbf{p}_q^{(k)}\right) : b_q^{(k)}(l) \neq 0, \text{ for all } k = 1, \ldots, K_q\right\}, \tag{3.26}$$

and the set of NLOS propagation delays between source q and sensor l are

$$\left\{\tau_{ql}^{(k)} \text{ for all } k = 1, \ldots, K_{ql}\right\}. \tag{3.27}$$

Next, a definition of correct recovery is provided.

Definition 1 : *Given* $\hat{\mathbf{R}}^\star$ *is expressed as in* (3.23) *and given that* (3.23) *is an optimal atomic decomposition, then the sources locations are correctly recovered if*

$$K_q = 1 \tag{3.28}$$

$$\mathbf{p}_q^{(1)} = \mathbf{p}_q, \tag{3.29}$$

for $q = 1, \ldots, Q$.

Condition $K_q = 1$ is required for all q because, obviously, it exists only one valid location for each source, and in such case $\mathbf{p}_q^{(1)}$ must match the true location of the q-th source.

In Table 3.1, the procedure for recovering the sources' locations from the received signals is summarized. In some specific cases, such as estimating frequencies from a mixture of complex sinusoids [72], some sophisticated techniques have been devised for minimizing the atomic norm, and then recover the optimal atomic decomposition of $\hat{\mathbf{R}}^\star$, thanks to the particular structure of the atomic set. However,

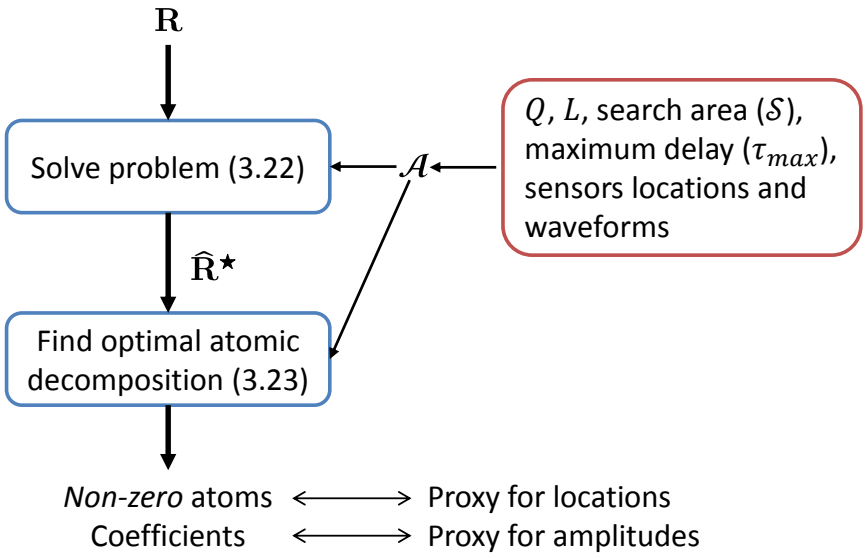

Figure 3.1 Flow diagram of the process for recovering the sources' locations.

in general, it is challenging to solve (3.22), because computing the atomic norm is not always straightforward. In Section 3.4.2, an approximate method based on discretizing the atomic set is proposed for simultaneously solving the atomic norm minimization problem (3.22) and recovering the optimal atomic decomposition (3.23). Before delving into the details on how to actually solve problem (3.22) and find the optimal atomic decomposition as expressed in (3.23), in the next section, it is shown that tuning the parameters $\{u_q\}_{q=1}^{Q}$ appropriately is critical to the correct recovery of the sources' locations.

3.4.1 Guarantee for Correct Recovery of the Sources' Locations

In this part are developed guarantees for correct recovery of the sources' location in the sense of Definition 1. To ensure and identifiable signal model, we make the following assumption

Assumption 1 : *For each sensor, signal model* (3.5) *is identifiable in the sense that the observed data is explained by a unique set of delays,* $\tau_l(\mathbf{p})$ *for* $q = 1, \ldots, Q$, *and* $\tau_{ql}^{(m)}$ *for* $q = 1, \ldots, Q$ *and* $m = 1, \ldots, M_{ql}$.

A justification of Assumption 1 is given based on the identifiability analysis in [73] for the problem of delay estimation in the presence of multipath. In [73], it was shown that if the waveforms are *unambiguous*, then Assumption 1 is true if the number of propagation delays is known to be below a certain threshold. Given that each propagation delay corresponds to a path, in our case, the number of propagation delays at each sensor is *sparse* by assumption, while the optimal atomic decomposition will include a low number of atoms, which in turn means a low number of propagation delays.

Further, to develop correct recovery guarantees, we assume noiseless observations, in which case the solution to (3.22) is trivially $\hat{\mathbf{R}}^{\star} = \mathbf{R}$. However, as shown in the numerical section, the theoretical results obtained in this section are also meaningful in the presence of noise. The key properties that are exploited to obtain guarantees are:

1. LOS signal paths associated with a source have a common location (see (3.2)).

2. NLOS signal paths are local to sensors (see (3.4)).

To formalize the notion that LOS path emitted by a source have a common location, we introduce the notion of location consistency:

Definition 2 : *A location* $\mathbf{p}$ *is said to be consistent with* X *paths (LOS or NLOS), or vice-versa, if the propagation delays of such paths, say* $\tau_1, \ldots, \tau_X$*, satisfy*

$$\tau_x = \tau_{l_x}(\mathbf{p}) \quad \textit{for } x = 1, \ldots, X, \tag{3.30}$$

where $\{l_1, \ldots, l_X\} \subseteq \{1, \ldots, L\}$ *are the indexes of the destination sensors of the* X *paths, and* $\tau_{l_x}(\mathbf{p})$ *is the delay of the direct path between location* $\mathbf{p}$ *and sensor* l_x*.*

In order to find the sources' locations exploiting the notion of consistency in Definition 2, the following assumptions are made.

Assumption 2 : *The number of LOS paths from source q, S_q, is known.*

By its very nature, a source location cannot be consistent with any NLOS, thus the location of the q-th source is consistent with exactly S_q paths.

Assumption 3 : *Only the true location of the q-th source is consistent with S_q paths emitted by the q-th source.*

By Assumptions 2 and 3, given a source with a known emitted waveform and a known number S of LOS paths, its location is the one consistent with S paths. No other location is consistent with S paths with the same waveform.

From (3.23) and Definition 1, the solution containing the true locations of the sources is associated with the optimal atomic decomposition. However, from (3.18) and the definition of atoms, namely, LOS atoms (3.15) and NLOS atoms (3.16), the optimal atomic decomposition is parameterized by the norm of the amplitudes in the LOS atoms u_q (3.15). For given data $\hat{\mathbf{R}}^\star$, decreasing u_q has to be counteracted by an increase in the coefficients of the LOS atoms, thus raising their contribution to the cost C (3.24). Put another way, different values of u_q lead to different explanations of the data $\hat{\mathbf{R}}^\star$ manifested as different optimal atomic decompositions, and thus corresponding to different solutions of the source localization problem. We seek to determine which values of parameters u_q ensure that the corresponding optimal atomic decomposition results in locations that are consistent with the number of paths indicated by Assumption 2. This in turn guarantees that these are the true sources' locations. The next lemma establishes the condition on u_q under which a location associated with the optimal atomic decomposition is also consistent with the number of LOS paths.

Lemma 5 : *Given a known number of LOS paths S_q of the q-th source, if parameter u_q satisfies*

$$u_q < \frac{1}{\sqrt{S_q - 1}}, \tag{3.31}$$

then any location (for the q-th source) associated to the optimal atomic decomposition (3.25) *is consistent with* S_q *or more paths in the sense of Definition 2.*

For the proof of Lemma 5, see Appendix C. The interpretation of this lemma is that given a solution that produces a location with less than S_q paths, and if condition (3.31) is met, there exists another lower cost solution, implying that a solution with fewer than S_q paths cannot be optimal.

The previous lemma guaranteed that any location associated with the optimal atomic decomposition is consistent with S_q paths. The next lemma establishes the condition on u_q which ensures that at least one location is associated with the optimal atomic decomposition.

Lemma 6 : *Given a known number of LOS paths* S_q *of the q-th source, if parameter* u_q *satisfies*

$$u_q > \frac{1}{\sqrt{S_q}}, \tag{3.32}$$

then at least one location (for the q-th source) is associated to the optimal atomic decomposition.

For the proof of Lemma 6, see Appendix D. The interpretation of this lemma is that given a solution that does not produce a location for the q-th source, and if condition (3.32) is met, there exists another lower cost solution that produces a location for the q-th source.

The two lemmas lead directly to the following theorem establishing the guarantee for correct recover of the sources' locations.

Theorem 1 : *The sources' locations are correctly recovered according to Definition 1 if* u_q *is chosen within the interval*

$$\frac{1}{\sqrt{S_q}} < u_q < \frac{1}{\sqrt{S_q - 1}} \tag{3.33}$$

for all q.

Proof. If $u_q > 1/\sqrt{S_q}$ for all q, by Lemma 6, at least one location is associated to the optimal atomic decomposition for each source. By Assumption 2, the number of LOS paths S_q is known for each source q. Therefore, if u_q is chosen such that $u_q < 1/\sqrt{S_q - 1}$ for all q, then by Lemma 5, the locations associated to the optimal atomic decomposition for the source q are consistent with S_q or more paths. However, according to Assumption 3, only the location of the source is consistent with S_q or more paths, thus finishing our proof. □

A numerical examples illustrates Theorem 1. Let the search area be of size 200 m × 200 m and centered around the origin of the coordinate system. A single source is positioned at (20 m, 30 m) and 5 sensors are positioned at coordinates (40 m, −40 m), (−40 m, −40 m), (−40 m, 40 m), (40 m, 40 m) and (0 m, 0 m). All sensors receive a LOS path except for the sensor located (40 m, −40 m). Therefore, the number of LOS paths is $S_1 = 4$. In addition, the sensor at the origin receives a NLOS path whose path length is 91 m. The goal is to compute the probability of correct recovery in the sense of Definition 1 as a function of u_1 and under the conditions of Theorem 1, i.e., the noiseless case. The implementation of the procedure leading to Figure 3.2 is discussed in Section 3.4.2. To estimate the probability of correct recovery, the experiment is repeated 1000 times, and in each experiment the emitted waveform as well as the amplitudes of the LOS and NLOS paths are chosen randomly. The exact model for generating the waveforms, as well as other parameters is the same as the one detailed in Section 3.6. Figure 3.2 plots the probability of correct recovery versus parameter v which is defined as $v = (1/u_1)^2$. Theorem 1 guarantees a correct solution if

$$S_1 - 1 < v < S_1. \tag{3.34}$$

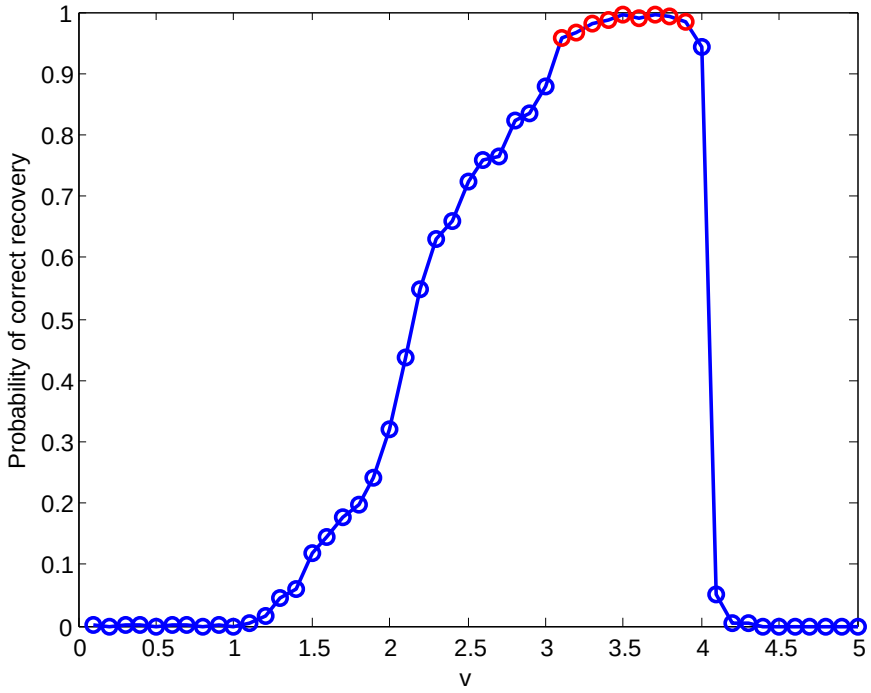

Figure 3.2 Probability of correct recovery in the sense of Definition 1 in the absence of noise.

As it can be seen in Figure 3.2, for values of v within the interval $[3, 4]$, the probability of correct recovery is close to one, whereas it is smaller for other values.

3.4.2 Practical Implementation: Discretization of the Atomic Set

Remind the reader that in general, when noise is present the process for recovering the sources locations follows Figure 3.1. The most straightforward method for solving problem (3.22) and obtain its optimal atomic decomposition (3.23) is to substitute the atomic norm in the objective function (3.22a) by its definition (3.21), and optimize over the set of positive coefficients $\{c^{(k)}\}$. However, such approach yields an infinite-dimensional problem because the number of atoms is infinite. Except for some particular cases, like recovering frequencies of mixtures of sinusoids [72, 74], in general, it is very challenging to optimize infinite-dimensional convex problems. In [75], it is advocated that dictionaries whose atoms depend on continuous parameters are discretized. For instance, the NLOS atoms (3.16) depend on a delay, which is by

definition within the interval $[0, \tau_{\max}]$, and can be discretized into a grid of discrete delays such as (3.9). In [75], it is proven that the optimization problem based on the discretized atomic set converges to the original problem (3.22) as the grid finesse increases. Indeed, grid refinement approaches can be found in some signal processing applications such as delay estimation [70], direction-of-arrival estimation [76, 77, 78] or direct localization of sources [47].

The atomic set is composed of LOS (3.15) and NLOS atoms (3.16). The LOS atoms are parametrized by the location of the source whereas the NLOS atoms are parametrized by their propagation delays. Therefore, two different type of grids need to be created: one grid of locations and one grid of delays. The propagation delays of the NLOS paths vary between 0 and $\tau_{\max}$. Upon discretizing the interval of delays with a resolution of τ_{res}

$$\mathcal{D} = \left\{0, \tau_{\text{res}}, \ldots, \left\lfloor \frac{\tau_{\max}}{\tau_{\text{res}}} \right\rfloor \tau_{\text{res}} \right\}, \tag{3.35}$$

a new set of NLOS atoms is obtained

$$\tilde{\mathcal{A}}_{\text{NLOS}} = \bigcup_{q=1}^{Q} \bigcup_{l=1}^{L} \Big\{ \mathbf{N}_{ql}\left(\phi, \tau\right) : 0 \leq \phi < 2\pi, \tau \in \mathcal{D} \Big\}. \tag{3.36}$$

Similarly, upon discretizing the search area $\mathcal{S}$ into a uniform grid of squared cells whose center points are

$$\mathcal{G} = \{\boldsymbol{\theta}_1, \ldots, \boldsymbol{\theta}_{|\mathcal{G}|}\}, \tag{3.37}$$

where the grid resolution is defined as $d_{\text{res}} = \min_{i \neq j} \|\boldsymbol{\theta}_i - \boldsymbol{\theta}_j\|_2$, a new set of LOS atoms is obtained

$$\tilde{\mathcal{A}}_{\text{LOS}} = \bigcup_{q=1}^{Q} \Big\{ \mathbf{L}_q\left(\mathbf{b}, \mathbf{p}\right) : \mathbf{b} \in \mathbb{C}^L, \mathbf{p} \in \mathcal{G} \subset \mathbb{R}^2, \|\mathbf{b}\|_2 = u_q \Big\}. \tag{3.38}$$

The discrete atomic set including the LOS and NLOS atoms is

$$\widetilde{\mathcal{A}} = \widetilde{\mathcal{A}}_{\text{LOS}} \cup \widetilde{\mathcal{A}}_{\text{NLOS}}, \tag{3.39}$$

and the atomic norm induced by $\widetilde{\mathcal{A}}$ has the same expression than in (3.21)

$$\left\|\hat{\mathbf{R}}\right\|_{\widetilde{\mathcal{A}}} = \inf_{c^{(k)}>0} \left\{ \sum_k c^{(k)} : \hat{\mathbf{R}} = \sum_k c^{(k)} \mathbf{A}^{(k)}, \mathbf{A}^{(k)} \in \tilde{\mathcal{A}} \right\}, \tag{3.40}$$

except for the fact that $\mathcal{A}$ has been replaced by $\tilde{\mathcal{A}}$. By expressing the generic atoms $\mathbf{A}^{(k)}$ in (3.40) as LOS or NLOS atoms, the new atomic norm $\|\cdot\|_{\tilde{\mathcal{A}}}$ may be cast similarly to (3.21) as

$$\left\|\hat{\mathbf{R}}\right\|_{\widetilde{\mathcal{A}}} = \inf_{c_q^{(g)}, c_{ql}^{(d)} \geq 0} \left\{ \sum_{q=1}^{Q} \sum_{k=1}^{|\mathcal{G}|} c_q^{(g)} + \sum_{q=1}^{Q} \sum_{l=1}^{L} \sum_{g=1}^{|\mathcal{D}|} c_{ql}^{(d)} : \right. \tag{3.41a}$$

$$\left. : \hat{\mathbf{R}} = \sum_{q=1}^{Q} \sum_{g=1}^{|\mathcal{G}|} c_q^{(g)} \mathbf{L}_q \left(\mathbf{b}_q^{(g)}, \boldsymbol{\theta}_g\right) + \sum_{q=1}^{Q} \sum_{l=1}^{L} \sum_{d=1}^{|\mathcal{D}|} c_{ql}^{(d)} \mathbf{N}_{ql} \left(\phi_{ql}^{(d)}, (d-1)\tau_{\text{res}}\right) \right\}, \tag{3.41b}$$

and $\mathbf{b}_q^{(g)}$ may be any vector such that $\|\mathbf{b}_q^{(g)}\|_2 = u_q$ for all q and g. By introducing the finite grids of delays and locations, the new atomic norm (3.40) has been expressed as the infimum of a finite sum of coefficients. By replacing the LOS and NLOS atoms in (3.41b) by their definitions (3.15)-(3.16), constraint (3.41b) becomes

$$\hat{\mathbf{r}}_l = \sum_{q=1}^{Q} \sum_{g=1}^{|\mathcal{G}|} c_q^{(g)} b_q^{(g)}(l) \mathbf{s}_q \left(\tau_l \left(\boldsymbol{\theta}_g\right)\right) + \sum_{q=1}^{Q} \sum_{l=1}^{L} \sum_{d=1}^{|\mathcal{D}|} c_{ql}^{(d)} e^{i\phi_{ql}^{(d)}} \mathbf{s}_q \left((d-1)\tau_{\text{res}}\right) \tag{3.42}$$

$$\text{for } l = 1, \ldots, L$$

where $\hat{\mathbf{R}} = [\hat{\mathbf{r}}_1 \cdots \hat{\mathbf{r}}_L]$ and $\mathbf{b}_q^{(g)} = [b_q^{(g)}(1) \cdots b_q^{(g)}(l)]^T$. Next, substituting the atomic norm $\|\cdot\|_{\tilde{\mathcal{A}}}$ instead of $\|\cdot\|_{\mathcal{A}}$ in problem (3.22) with (3.41a) and (3.42) yields

$$\min_{\substack{c_q^{(g)}, c_{ql}^{(d)} \geq 0 \\ \|\mathbf{b}_q^{(g)}\|_2 = u_q \\ 0 \leq \phi_{ql}^{(d)} < 2\pi}} \quad \sum_{q=1}^{Q} \sum_{k=1}^{|\mathcal{G}|} c_q^{(g)} + \sum_{q=1}^{Q} \sum_{l=1}^{L} \sum_{g=1}^{|\mathcal{D}|} c_{ql}^{(d)} \tag{3.43a}$$

$$\text{s.t.} \quad \sum_{l=1}^{L} \|\mathbf{r}_l - \hat{\mathbf{r}}_l\|_2^2 \leq \epsilon \tag{3.43b}$$

$$\hat{\mathbf{r}}_l = \sum_{q=1}^{Q} \sum_{g=1}^{|\mathcal{G}|} c_q^{(g)} b_q^{(g)}(l) \mathbf{s}_q\left(\tau_l\left(\boldsymbol{\theta}_g\right)\right) + \sum_{q=1}^{Q} \sum_{l=1}^{L} \sum_{d=1}^{|\mathcal{D}|} c_{ql}^{(d)} e^{i\phi_{ql}^{(d)}} \mathbf{s}_q\left((d-1)\tau_{\text{res}}\right)$$

$$\text{for } l = 1, \ldots, L. \tag{3.43c}$$

Problem (3.43) is not convex because of the bilinear forms, $c_q^{(g)} b_q^{(g)}(l)$ and $c_{ql}^{(d)} e^{i\phi_{ql}^{(d)}}$, appearing in constraint (3.43c). This can be easily remedied by the following variable changes

$$c_q^{(g)} \mathbf{b}_q^{(g)} = \mathbf{y}_q^{(g)} \tag{3.44a}$$

$$c_{ql}^{(d)} e^{i\phi_{ql}^{(d)}} = z_q^{(d)}(l), \tag{3.44b}$$

from which it follows that

$$\left\|c_q^{(g)} \mathbf{b}_q^{(g)}\right\|_2 = c_q^{(g)} u_q = \left\|\mathbf{y}_q^{(g)}\right\|_2 \tag{3.45a}$$

$$\left|c_{ql}^{(d)} e^{i\phi_{ql}^{(d)}}\right| = c_{ql}^{(d)} = \left|z_q^{(d)}(l)\right|. \tag{3.45b}$$

Combining (3.44) and (3.45) with (3.43c) and (3.43a), respectively, results in the following optimization problem

$$\min_{\substack{\mathbf{y}_q^{(g)} \\ z_q^{(d)}(l)}} \quad \sum_{q=1}^{Q}\sum_{g=1}^{|\mathcal{G}|} \frac{\left\|\mathbf{y}_q^{(g)}\right\|_2}{u_q} + \sum_{q=1}^{Q}\sum_{l=1}^{L}\sum_{d=1}^{|\mathcal{D}|} \left|z_q^{(d)}(l)\right| \tag{3.46a}$$

$$\text{s.t.} \quad \sum_{l=1}^{L} \|\mathbf{r}_l - \hat{\mathbf{r}}_l\|_2^2 \leq \epsilon \tag{3.46b}$$

$$\hat{\mathbf{r}}_l = \sum_{q=1}^{Q}\sum_{g=1}^{|\mathcal{G}|} y_q^{(g)}(l)\mathbf{s}_q\left(\tau_l(\boldsymbol{\theta}_g)\right) + \sum_{q=1}^{Q}\sum_{d=1}^{|\mathcal{D}|} z_q^{(d)}(l)\mathbf{s}_q\left((d-1)\tau_{\text{res}}\right) \tag{3.46c}$$

$$\text{for } l = 1, \ldots, L,$$

which is convex and finite-dimensional. Problem (3.46) is equivalent to the latent group Lasso problem [79], and specific algorithms for solving (3.46) exist in the literature [80]. Moreover, the problem also falls into the class of second-order cone programs (SOCP), a subfamily of convex problems, for which efficient algorithms are available [81]. In our case, the SOCP type of algorithms resulted in the fastest computational times. The variable $y_q^{(g)}(l)$ represents the amplitude of a LOS paths from source q to sensor l with delay $\tau_l(\boldsymbol{\theta}_g)$, whereas the variable $z_q^{(d)}(l)$ represents the amplitude of a NLOS path from source q to sensor l with delay $(d-1)\tau_{\text{res}}$. Let $\{\hat{\mathbf{y}}_q^{(g)}\}$ and $\{\hat{z}_q^{(g)}(l)\}$ be the solutions to problem (3.46). Then, the location of the q-th source is the grid location $\boldsymbol{\theta}_g$ for which $\|\hat{\mathbf{y}}_q^{(g)}\|_2$ is larger than zero. Intuitively speaking, minimizing the term $\sum_{q=1}^{Q}\sum_{l=1}^{L}\sum_{d=1}^{|\mathcal{D}|}|z_q^{(d)}(l)|$ in the objective function (3.46a) induces a sparse number of NLOS paths, whereas minimizing $\sum_{q=1}^{Q}\sum_{g=1}^{|\mathcal{G}|}\|\mathbf{y}_q^{(g)}\|_2$ induces a sparse number of sources' locations.

3.4.3 Estimation of the Number of LOS Sensors

According to Theorem 1, we must fix u_q to a value that satisfies $1/\sqrt{S_q} < u_q < 1/\sqrt{S_q - 1}$ for each source q, where S_q is the number of sensors receiving a LOS component from

the q-th source. Hence, u_q must be set to $u_q = 1/\sqrt{S_q - \mu}$ for a parameter $\mu \in]0, 1[$. For instance, it has been observed that a satisfactory choice was $\mu = 0.2$ as it led to a the best probability of correct recovery for all experiments in Section 3.6. In this section, we propose a method for estimating the sources locations that not only does not require a priori knowledge on the number of LOS sensors S_q, but in fact estimates them. The method works as follows. We start by assuming that all sensors receive a LOS component from all sources, $\hat{S}_q = L$ for all q, and set u_q such that it satisfies (3.33). Then problem (3.46) is solved. According to Lemma 5, the sources' locations associated to the optimal atomic decomposition for the q-th source are consistent with at least $\hat{S}_q$ paths. However, by Assumption 3, no location is consistent with more than S_q paths. Therefore, if the number of LOS sensors ($\hat{S}_q > S_q$) had been overestimated, no location would be obtained for source q. In the next step, $\hat{S}_q$ is decreased by one for all those sources without a location estimate, and problem (3.46b) is solved again. These steps are repeated until a location is obtained for each source. The last value of $\hat{S}_q$ is the estimated number LOS sensors for the q-th source. This method corresponds to steps 10, 11, 20–28 of DLM's algorithm described in Section 3.5.

3.4.4 Spurious Locations

It is observed in numerical simulations that when the sources are off-grid ($\mathbf{p}_q \notin \mathcal{G}$ for any q) and/or when the propagation delays of the paths are off-grid ($\tau_{ql}^{(m)}, \tau_l(\mathbf{p}_q) \notin \mathcal{D}$ for any q, l, m), then some spurious locations may be obtained from problem (3.46). This phenomenon is not new and it was studied in [82] in the case of delay estimation using the ℓ_1-norm (3.11). It was shown that if the propagation delay of a path is off-grid, a peak appears around such propagation delay but also secondary peaks of much weaker strength appear further apart.

To eliminate spurious locations, we set a simple threshold criterion. Let $\hat{\mathbf{y}}_q^{(g)}$ be, for all q and g, the solution to problem (3.46), and denote $\hat{\mathbf{y}}_q^{(g)\downarrow}$ the vector with the

same components, but sorted in descending order, i.e., $|\hat{y}_q^{(g)\downarrow}(1)| \geq \cdots \geq |\hat{y}_q^{(g)\downarrow}(L)|$. The components of $\hat{\mathbf{y}}_q^{(g)}$ are the estimated signal strengths of the LOS paths of source q positioned at $\boldsymbol{\theta}_g$. We propose that for each source q, the locations $\{\boldsymbol{\theta}_g\}_{g=1}^{|\mathcal{G}|}$, whose $\hat{S}_q$ strongest components do not satisfy

$$\left|\hat{y}_q^{(g)\downarrow}\left(\hat{S}_q\right)\right| > A\,T \tag{3.47}$$

are dismissed. Here, $\hat{S}_q$ is the number of guessed LOS paths for source q as explained in Section 3.4.3, parameter A is the strongest (LOS or NLOS) estimated path strength

$$A = \max\left(\max_{g,q,l}\left|\hat{y}_q^{(g)}(l)\right|, \max_{d,q,l}\left|\hat{z}_q^{(d)}(l)\right|\right). \tag{3.48}$$

and T is a value smaller than 1. For instance, in the simulations it was used $T = 1/30$, so that all locations whose signal strengths are $20\log_{10}(30) \approx 30\,\text{dB}$ weaker than the strongest path are discarded. The intuition behind this heuristic approach is that, if $\boldsymbol{\theta}_g$ is the correct location of source q, then the $\hat{S}_q$ largest entries in vector $\hat{\mathbf{y}}_q^{(g)}$ are the more likely to be signal strengths of the LOS paths and they will pass the test (3.47). Instead, if the spurious locations occurred due to off-the-grid noise, some of their entries may be close to zero and not meet (3.47). If after the threshold criterion (3.47) one or more locations still remain for the q-th source, then the one with the largest strength is picked

$$\hat{\mathbf{p}}_q = \boldsymbol{\theta}_{\hat{g}} : \hat{g} = \arg\max_{g}\left|\hat{y}_q^{(g)\downarrow}\left(\hat{S}_q\right)\right|. \tag{3.49}$$

It is important to not skip (3.47), and apply (3.49) directly. As explained in Section 3.4.3, the proposed technique works by initially assuming that the number of LOS paths for the q-th source is $\hat{S}_q = L$, and if no location is obtained, then successively decreasing $\hat{S}_q$ until it matches the true number of LOS paths $\hat{S}_q = S_q$. However, if the threshold criterion (3.47) is skipped and $\hat{S}_q > S_q$, a spurious location

may be erroneously selected as the correct source location instead of concluding that there is no location and that $\hat{S}_q$ needs to be decreased.

3.4.5 Tuning Parameter ϵ

Parameter ϵ in optimization problem (3.46) constraints the fitting error between the received signals and the estimated signals. Such a parameter is set so that the received signals without noise are a feasible solution. Let $\hat{\mathbf{r}}_l$ be the noiseless received signal at sensor l, then we require that

$$\sum_{l=1}^{L} \|\mathbf{r}_l - \hat{\mathbf{r}}_l\|_2^2 = \sum_{l=1}^{L} \|\mathbf{w}_l\|_2^2 \leq \epsilon. \tag{3.50}$$

If ϵ is chosen too small, then it can happen that $\sum_{l=1}^{L} \|\mathbf{w}_l\|_2^2 \not\leq \epsilon$, thus excluding the noiseless signals from the set of possible solutions. Because the noise $\{\mathbf{w}_l\}_{l=1}^{L}$ are random independent complex Gaussian vectors of length N, it follows that the error normalized by the noise variance $2\sigma_n^{-2} \sum_{l=1}^{L} \|\mathbf{w}_l\|_2^2$ is a Chi-square random variable with $2NL$ degrees of freedom. Thus, parameter ϵ must be set to a large enough value so that $\sum_{l=1}^{L} \|\mathbf{w}_l\|_2^2 \leq \epsilon$ is satisfied with high probability, e.g.,

$$\Pr\left(\sum_{l=1}^{L} \|\mathbf{w}_l\|_2^2 \leq \epsilon\right) = 0.99. \tag{3.51}$$

Let $\mathrm{F}(x, k)$ be the cumulative distribution function of the chi-squared distribution with k degrees of freedom evaluated at x, then

$$\epsilon = \frac{\sigma_w^2}{2} \mathrm{F}^{-1}\left(0.99, 2NL\right). \tag{3.52}$$

At low signal-to-noise ratio (SNR), it is possible that the energy of the received signals is too low compared to the energy of the noise causing that $\sum_{l=1}^{L} \|\mathbf{r}_l\|_2^2 \leq \epsilon$. In such case problem (3.46) has the trivial solution $y_q^{(g)}(l) = z_q^{(g)}(l) = 0$ for all q, l, g and d, and it will not output any locations. If $\sum_{l=1}^{L} \|\mathbf{r}_l\|_2^2 \leq \epsilon$, we propose to estimate

the locations by finding the LOS signals which correlate the most with the received signals:

$$\hat{\mathbf{p}}_q = \arg\max_{\mathbf{p}\in\mathcal{G}} \sum_{l=1}^{L} \left| \mathbf{s}_q^H \left(\tau_l \left(\mathbf{p} \right) \right) \mathbf{r}_l \right|^2 . \tag{3.53}$$

This is in fact the ML estimate of the sources' locations in absence of multipath [46] and can result on the correct locations when multipath is scarce.

3.4.6 Grid Refinement

The computational complexity of minimizing the second-order cone problem (3.46) is $O((Q|\mathcal{G}| + QL|\mathcal{D}|)^{3.5})$ [83]. To lower it we propose a recursive grid refinement procedure inspired by the ones in [76, 77, 78]. The optimization problem (3.46) employs a grid of delays in order to estimate the NLOS paths between every source-sensor pair, and a grid of locations in order to estimate the location of every source. In total QL grids of delays and Q grids of locations. In comparison to previous grid refinement approaches, ours is a more complex due to the two different type of grids used to explain the observed data. The idea behind a grid refinement procedure is to start with a coarse grid(s) and refine each grid only around the active points. Let τ_{res} and d_{res} be the grid resolutions we wish to achieve in the grids of delays and locations, respectively, and suppose that in order to lower the computational complexity, the grids are refined R times. If the resolution of the grids is increased by a factor of two at every step, then the grids resolutions at each step are

$$\tau_{\text{res},r} = 2^{R-r}\tau_{\text{res}} \quad \text{for } r = 1, \ldots, R \tag{3.54}$$

$$d_{\text{res},r} = 2^{R-r} d_{\text{res}} \quad \text{for } r = 1, \ldots, R. \tag{3.55}$$

Let $\mathcal{D}_{ql,r}$ be the grid of delays for the source-sensor pair (q, l) at step r, and $\mathcal{G}_{q,r}$ the grid of locations for source q. At the first step ($r = 1$), the continuous set of delays

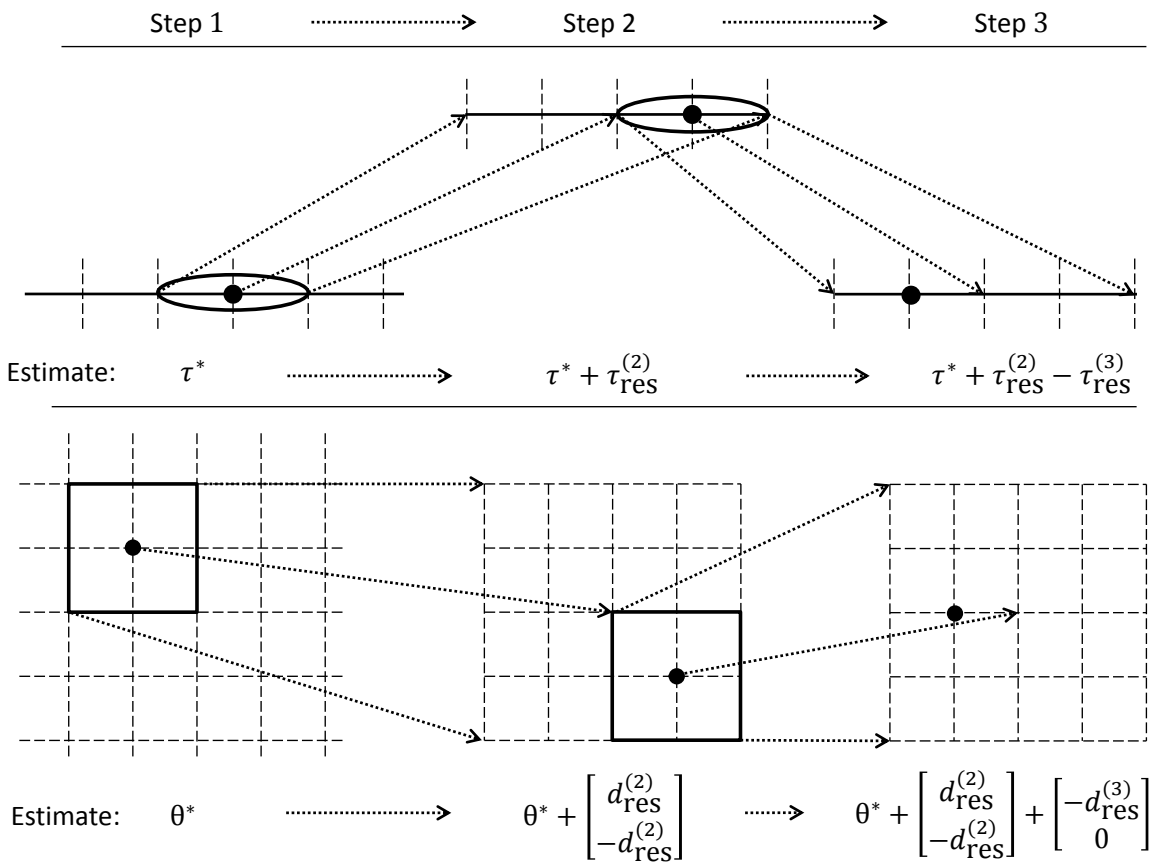

Figure 3.3 Illustration of three steps of a grid refinement procedure. The top image shows the grid refinement for the delays between a hypothetical source and sensor, and the bottom image shows the grid refinement for the locations of some hypothetical source, for $r = 1, 2, 3$. The dots point out the position of a non-zero delay and location as a result of optimizing problem (3.58). The positions of such non-zeros are progressively refined at each step.

$[0, \tau_{\max}]$ is discretized with resolution $\tau_{\text{res},1}$

$$\mathcal{D}_{ql,1} = \{ i\,\tau_{\text{res},1} \in [0, \tau_{\max}] : i \in \mathbb{Z} \}\,, \tag{3.56a}$$

and the search area $\mathcal{S}$ is discretized uniformly with resolution $d_{\text{res},1}$

$$\mathcal{G}_{q,1} = \left\{ d_{\text{res},1} \begin{pmatrix} i \\ j \end{pmatrix} \in \mathcal{S} : i, j \in \mathbb{Z} \right\}, \tag{3.56b}$$

where $\mathbb{Z}$ is the set of integers. Consider step r, and let the active propagation delays between the source-sensor pair (q, l) be $\{\hat{\tau}_{ql,r}^{(m)} : m = 1, \ldots, \hat{M}_{ql,r}\}$, and the active locations for source q be $\{\hat{\mathbf{p}}_{q,r}^{(m)} : m = 1, \ldots, \hat{K}_{q,r}\}$. Then, the grids at step $r+1$ include the previous active delays and locations plus some neighbor points. For instance, in addition to the active delays and locations, we include two points at the left and right of the active delays

$$\mathcal{D}_{ql,r+1} = \bigcup_{m=1}^{\hat{M}_{ql,r}} \left\{ \hat{\tau}_{ql,r}^{(m)} + i\,\tau_{\text{res},r+1} : i = -2, -1, 0, 1, 2 \right\}, \tag{3.57a}$$

and all points within distance $2d_{\text{res},r+1}$ in the x- or y-axis of the active locations

$$\mathcal{G}_{q,r+1} = \bigcup_{m=1}^{\hat{K}_{q,r}} \left\{ \hat{\mathbf{p}}_{q,r}^{(m)} + d_{\text{res},r+1} \begin{pmatrix} i \\ j \end{pmatrix} : i, j = -2, -1, 0, 1, 2. \right\}. \tag{3.57b}$$

Next, problem (3.46) is solved again but only for the new grid points:

$$\min_{\substack{\left\{\mathbf{y}_q^{(g)}\right\},\\ \left\{\mathbf{z}_q^{(d)}\right\}}} \sum_{q=1}^{Q} \sum_{\substack{g:\\ \boldsymbol{\theta}_g \in \mathcal{G}_{q,r+1}}} \frac{\left\|\mathbf{y}_q^{(g)}\right\|_2}{u_q} + \sum_{q=1}^{Q}\sum_{l=1}^{L} \sum_{\substack{d:\\ (d-1)\tau_{\text{res}}\\ \in \mathcal{D}_{ql,r+1}}} \left|z_q^{(d)}(l)\right| \tag{3.58a}$$

$$\text{s.t.} \quad \sum_{l=1}^{L} \left\|\mathbf{r}_l - \hat{\mathbf{r}}_l\right\|_2^2 \leq \epsilon \tag{3.58b}$$

$$\hat{\mathbf{r}}_l = \sum_{q=1}^{Q} \sum_{\substack{g:\\ \boldsymbol{\theta}_g \in \mathcal{G}_{q,r+1}}} y_q^{(g)}(l)\mathbf{s}_q\left(\tau_l(\boldsymbol{\theta}_g)\right) + \sum_{q=1}^{Q} \sum_{\substack{d:\\ (d-1)\tau_{\text{res}}\\ \in \mathcal{D}_{ql,r+1}}} z_q^{(d)}(l)\mathbf{s}_q\left((d-1)\tau_{\text{res}}\right)$$

$$\text{for } l = 1, \ldots, L. \tag{3.58c}$$

The process of refining the grids and solving problem (3.58) is repeated for the R steps. For a more intuitive picture on the grid refinement procedure see the examples in Figure 3.3 with three steps. The proposed grid refinement procedure corresponds to steps 12–18 in DLM's algorithm described in Section 3.5.

In regards to the resolutions of the grids, instead of choosing the resolution of both types of grids completely independently, they are set according to

$$c\,\tau_{\text{res},r} = d_{\text{res},r} \quad \text{for any } r, \tag{3.59}$$

where c is the speed of light.

3.5 Algorithm

In this section, it is presented the proposed DLM algorithm for source localization in multipath. The inputs to the DLM algorithm are the received signals $\{\mathbf{r}_l\}_{l=1}^{L}$ and the noise variance σ_w^2. The number of sensors L, sources Q and samples per sensor N are assumed known. The outputs of the algorithm are the source locations estimates

$\{\hat{\mathbf{p}}_q\}_{q=1}^{Q}$. The summary of the proposed algorithm for direct localization of RF sources in the presence of multipath is as follows:

Input: L, Q, N, $\{\mathbf{r}_l\}_{l=1}^{L}$ and σ_w^2.

Parameters that need to be selected: $\mathcal{S}$, $\tau_{\max}$, d_{res}, T.

Output: The source locations estimates $\{\hat{\mathbf{p}}_q\}_{q=1}^{Q}$

Procedure:

for sensor l where $l = 1, \ldots, L$ **do**
    Estimate multipath TOA's $\{\tilde{\tau}_{ql}^{p}\}$ using [70] or any other delay estimation technique of choice.
    Estimate multipath amplitudes $\{\tilde{a}_{ql}^{p}\}$ through (3.13).
    Reduce NLOS interference on the received signal $\mathbf{r}_l$ through (3.14).
end for
Compute parameter ϵ through (3.52).
if $\sum_{l-1}^{L} \|\mathbf{r}_l\|_2 > \epsilon$ **then**
    Compute the initial coarse grids with (3.56) and (3.59).
    Initialize $\hat{S}_q = L$ for $q = 1, \ldots, Q$
    while $\hat{\mathbf{p}}_q = \emptyset$ for any $q \in \{1, \ldots, Q\}$ **do**
        $u_q = \frac{1}{\sqrt{\hat{S}_q - 0.2}}$ for $q = 1, \ldots, Q$
        for $r = 1, \ldots, R$ **do**
            Optimize problem (3.58). Output: $\{\hat{\mathbf{y}}_{q,r}^{(g)}\}$ and $\{\hat{z}_{q,r}^{(d)}(l)\}$.
            Find the active delays locations $\{\hat{\mathbf{p}}_{q,r}^{(m)}\}$ and $\{\hat{\tau}_{ql,r}^{(m)}\}$.
            if $r \neq 1$ **then**
                Refine the grid with (3.57) and (3.59).
            end if
        end for
        Compute A through (3.48).
        for $q = 1, \ldots, Q$ **do**

21: **if** any locations are active for the q-th source and such locations satisfy (3.47) **then**

22: Estimate the location of the q-th source through (3.49).

23: **else if** $\hat{S}_q > 1$ **then**

24: $\hat{S}_q \leftarrow \hat{S}_q - 1$

25: **else**

26: Estimate the location of the q-th source through (3.53).

27: **end if**

28: **end for**

29: **end while**

30: **else**

31: Recover sources' locations through (3.53).

32: **end if**

3.6 Numerical Results

In this section, we illustrate the performance of the localization method by numerical examples, and compare it to other existing techniques via Monte Carlo simulations. In all examples, the sources and sensors are positioned within a square area of $200\,\mathrm{m} \times 200\,\mathrm{m}$, which is divided into a grid of $1\,\mathrm{m} \times 1\,\mathrm{m}$ cells, thus resulting in 40,000 cells. Unless stated otherwise, we simulate a scenario containing one source positioned at coordinates (20 m,30 m) and 5 sensors positioned at coordinates (40 m, −55 m), (−45 m, −40 m), (−50 m, 55 m), (60 m, 60 m) and (5 m, 0 m) as pictured in Figure 3.4. The signals emitted by the sources are drawn from a white Gaussian process and filtered so that their passband bandwidth is 10 MHz. If multiple sources, such as in the experiment of Section 3.6.5, the waveforms are generated independently, thus the cross-correlation between signals from different sources is low but not necessarily zero. All sensors are time-synchronized and sample the received signals at a 20 MHz

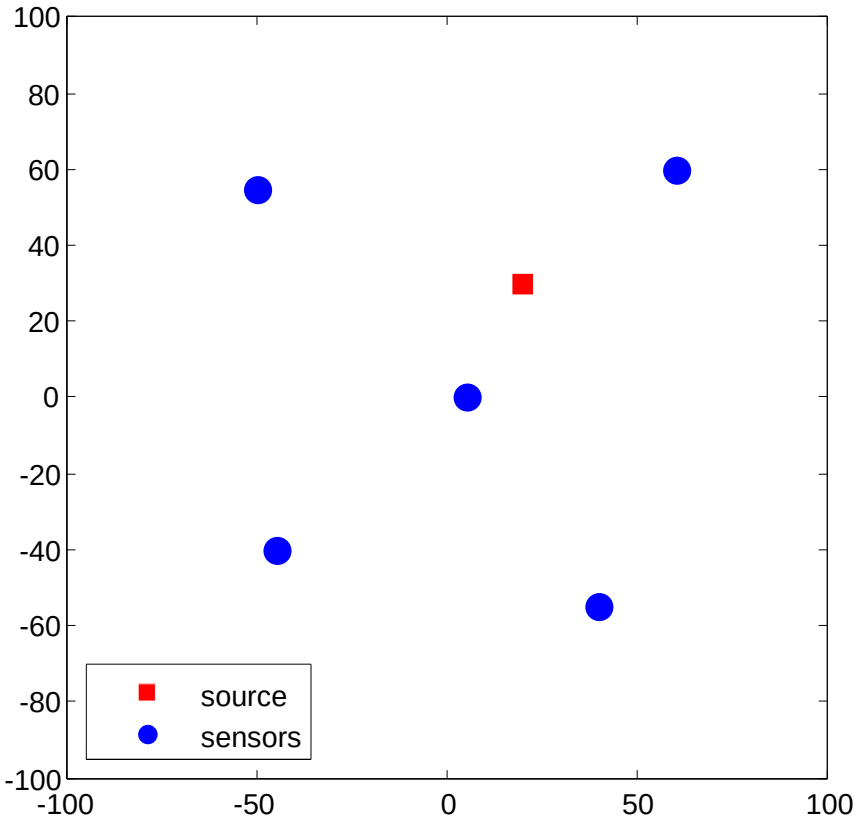

Figure 3.4 Map with the locations of the sensors and source used in many of the experiments in Section 3.6.

frequency for a total time of 5 µs, consequently each sensor observes 100 samples. For each source, we define the SNR per observation time as

$$\mathrm{SNR} = 10 \log_{10} \left(\frac{N \sum_{l=1}^{L} P_l}{\sigma_w^2} \right), \tag{3.60}$$

where N is the number of observations per sensor, P_l is the power of the LOS component between the source and sensor l, and σ_w^2 is the variance of the sampled noise. According to [84], in urban and suburban areas, the signal strengths of LOS and NLOS paths may be modeled as random variables with log-normal distribution. It follows that the channel tap powers expressed in dB are random variables with normal distribution. For our simulations, we set the standard deviation of the tap powers to 10 dB. All multipath experiments simulate Turin's urban channel model [84]. The arrival times of NLOS components at all sensors are modelled by a Poisson process. The mean inter-arrival time is set to 0.2 µs, and the average power $\bar{P}$ of a NLOS arrival at sensor l is governed by the power delay profile (PDP)

$$\bar{P}_l(t) = \exp \left(-\frac{t - t_l^{(0)}}{t_{rms}} \right) \tag{3.61}$$

where t is the arrival time of the NLOS component, $t_l^{(0)}$ is the arrival time of the LOS path and t_{rms} is the root mean square (rms) delay spread. An exponential PDP assigns smaller power to later arrivals. Unless otherwise stated, all LOS paths have normalized unit power. In multipath environments, it is possible that some sensors have their LOS blocked, thus at each Monte Carlo repetition one randomly selected sensor among the five receives no LOS component.

The figures compare the performance of the following two direct localization techniques:

1. **DLM** — The proposed technique.

2. **DPD** — Direct Position Determination as originally propose in [46] for AWGN channels.
3. **DPD with NLOS mitigation** — In this variation, DPD is preceded by the NLOS mitigation method introduced in Section 3.3. The goal is to show that DLM outperforms this variation of DPD, to demonstrate that DLM's high accuracy is not due only to such NLOS interference mitigation method.
4. **Indirect, CS TOA** — Indirect localization comprises a two-step process. In a first step, TOA's at each sensor are estimated by a delay estimation method based on compressive sensing (CS) [70]; in a second step, multilateration is performed using the well-known method developed by Chen [43] to mitigate the problem of potential LOS blockage on sensors.
5. **Indirect, matched filter TOA** — Same as previous indirect technique, except that TOA's are estimated by matched filter.

To solve the conic problem in DLM (step 13 of DLM's algorithm described in Section 13) and in CS TOA, we utilize the Mosek solver [85]. The bandwidth of the emitted signals limits the localization accuracy, and it is known that the ranging resolution is approximately

$$r = \frac{c}{B} \tag{3.62}$$

where c is the speed of light and B is the signal bandwidth. For the particular case of a 10 MHz bandwidth, the waveform ranging resolution is then 30 m. Also, we define the probability of correct recovery for the case of a single source as

$$P_c = \frac{1}{Z}\sum_{z=1}^{Z} \mathbb{1}\left(|\mathbf{p} - \hat{\mathbf{p}}^{(z)}| < \varepsilon\right), \tag{3.63}$$

where $\mathbf{p}$ is the true source's location, Z is the number of times that the experiment is repeated, $\hat{\mathbf{p}}^{(z)}$ is the source's location estimate for the z-th repetition, and $\mathbb{1}(\cdot)$ is the indicator function. Unless otherwise stated, the error is set to $\varepsilon = r/3$, which is a value smaller than the ranging resolution r. In some of the tests, it is plotted the normalized root mean square error

$$\text{rMSE} = \frac{1}{r}\sqrt{\frac{1}{Z}\sum_{z=1}^{Z}\left(\mathbf{p} - \hat{\mathbf{p}}^{(z)}\right)^2}. \tag{3.64}$$

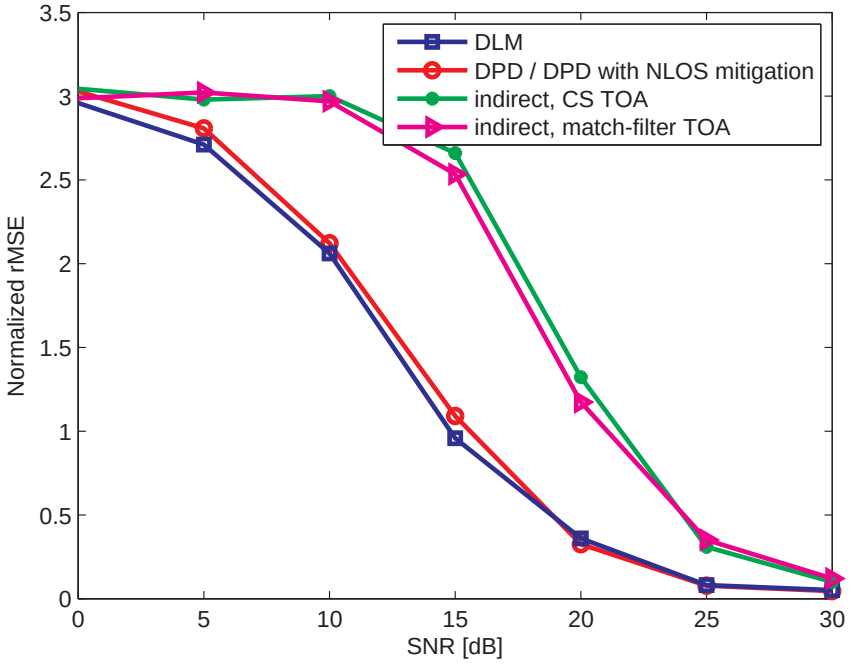

Figure 3.5 Root mean square error vs. SNR for the scenario in Figure 3.4 when no multipath is present.

All experiments are repeated 1000 times, i.e., $Z = 1000$.

3.6.1 Performance in the Absence of Multipath

This experiment's purpose is to validate that DLM performs optimally in the absence of multipath, i.e., its accuracy matches that of the DPD, which was shown to be optimal (see [46]). All five sensors receive LOS components, and Turin's channel model does not apply here, since there are no NLOS paths. Figures 3.5 and 3.6 plot the rMSE and the probability of correct recovery, respectively. DPD and DPD with NLOS mitigation are plotted together because their performance is exactly the same in the absence of multipath. As it can be observed, DPD and DLM perfom equally in terms of rMSE and probability of recovery because essentially both techniques, in the absence of multipath, look up for the location whose LOS signals correlate the most with the received signals. DPD and DLM perform substantially better in comparison to indirect techniques as it is expected from the theory.

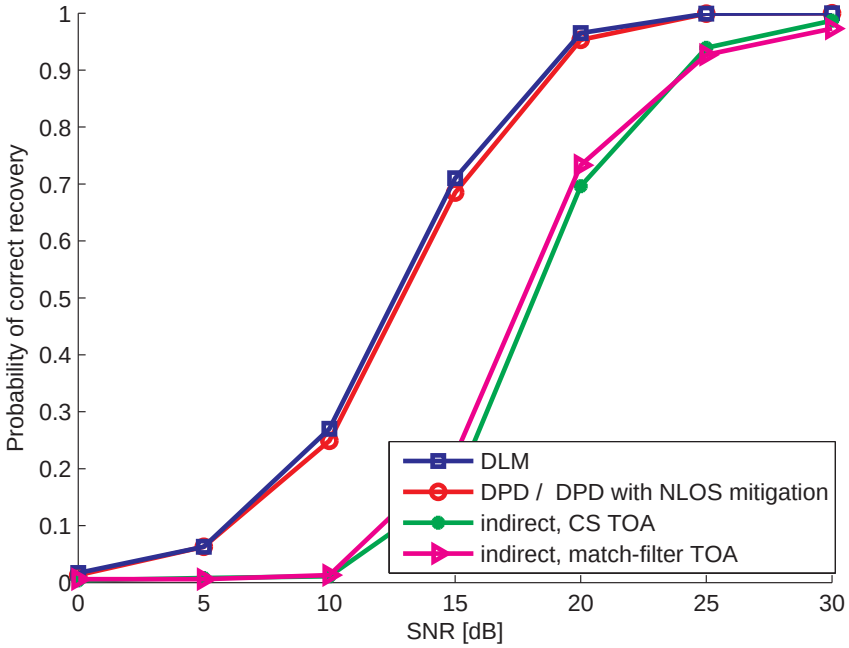

Figure 3.6 Probability of correct recovery vs. SNR for the scenario in Figure 3.4 when no multipath is present.

3.6.2 Performance in Multipath

In this example is simulated the multipath channel model described at the top of this section. The rMSE and the probability of correct recovery vs. SNR are plotted in Figures 3.7 and 3.8, respectively. Observe in Figures 3.7 and 3.8 that DPD fails to localize the sources irrespective of the SNR due to the fact that it is not designed for multipath. Also, the indirect technique relying on estimating by matched filter the TOA of the first arrival, does not perform much better than DPD because matched filter suffers from severe bias when multiple arrivals overlap in time. Interestingly, it seems as if DLM does not perform better, in terms of rMSE, than the indirect technique employing CS TOA estimates. In Figure 3.9, the probability of correct recovery (3.63) is plotted for different errors ranging from 0 to $2r$ for an SNR value of 30 dB. DLM achieves a high probability of correct recovery for much smaller errors than the other methods. For instance, DLM's probability of correct recovery is 0.9 for an error smaller than $0.4r$, whereas for the indirect technique with CS

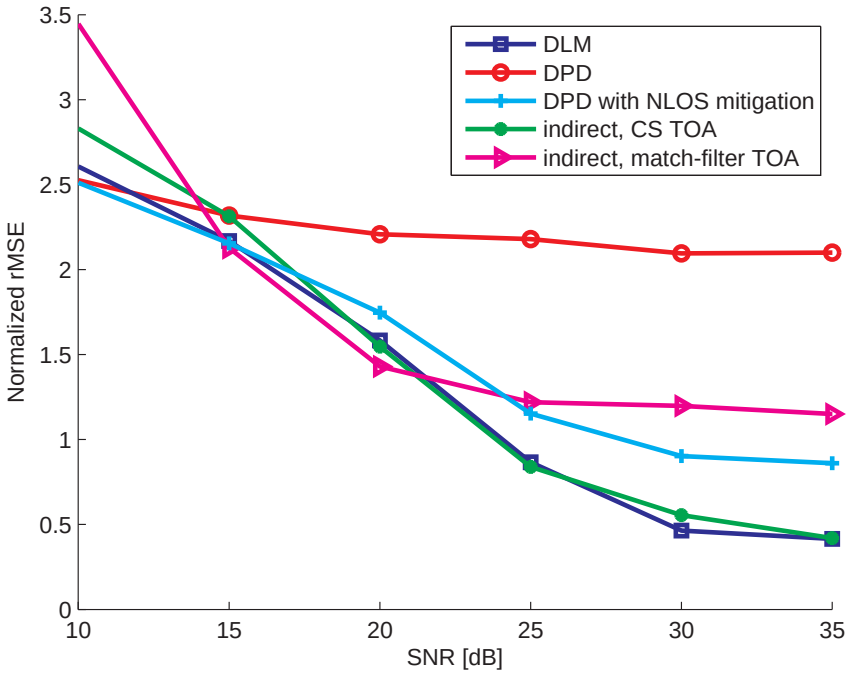

Figure 3.7 Root mean square error vs. SNR for the scenario in Figure 3.4 in a multipath environment.

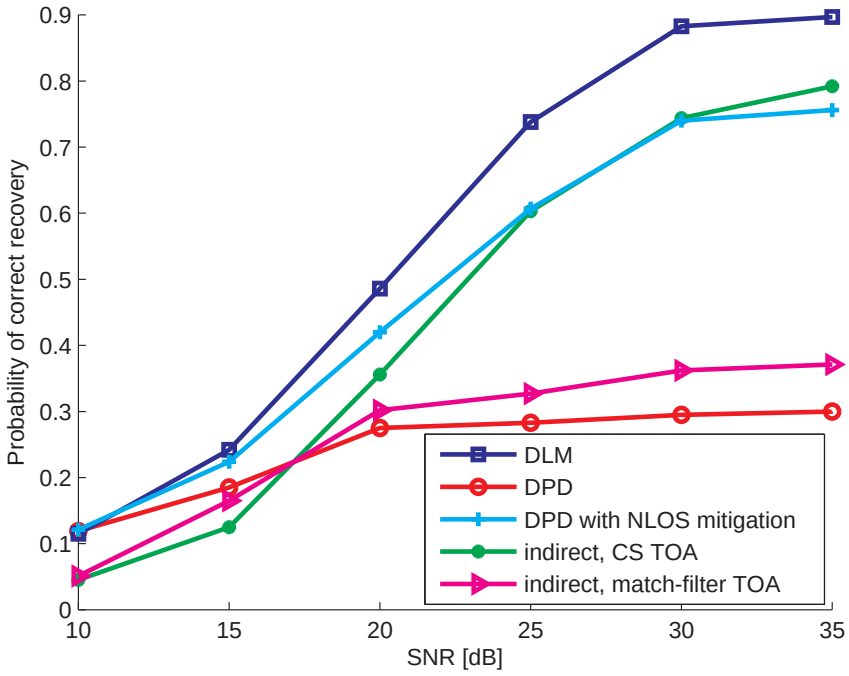

Figure 3.8 Probability of correct recovery vs. SNR for the scenario in Figure 3.4 in a multipath environment.

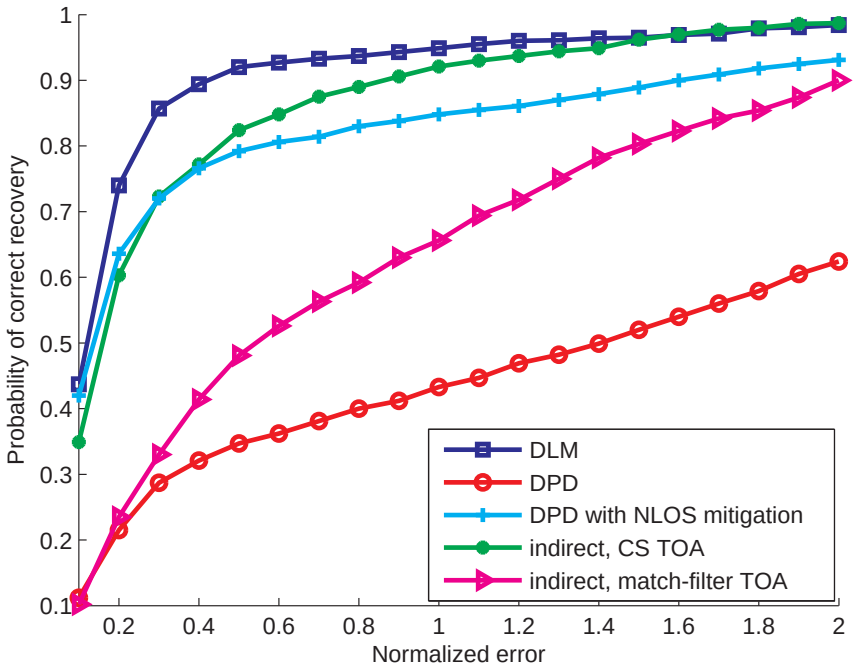

Figure 3.9 Probability of correct recovery vs. error for the scenario in Figure 3.4 for a 30 dB SNR.

TOA, such probability is only achieved when the error is $0.9r$. The other techniques perform substantially worse than DLM, and in fact, they never achieve a probability of recovery close to one even when very large errors are allowed. In summary, DLM can achieve a high probability of recovery for very small errors. In terms of rMSE, DLM and the indirect technique employing CS TOA estimates perform similarly, because in the rMSE metric small errors have a much smaller impact compared to the large errors. Hence, in the next experiments, we focus only on the probability of correct recovery.

3.6.3 Probability of Correct Recovery vs. Delay Spread

The channel model employed depends on the rms delay spread, which determines the interval between the LOS component and the last arriving NLOS component. In general, larger delay spreads imply more multipath that make the localization more challenging. In Figure 3.10, the probability of correct recovery is plotted for an rms

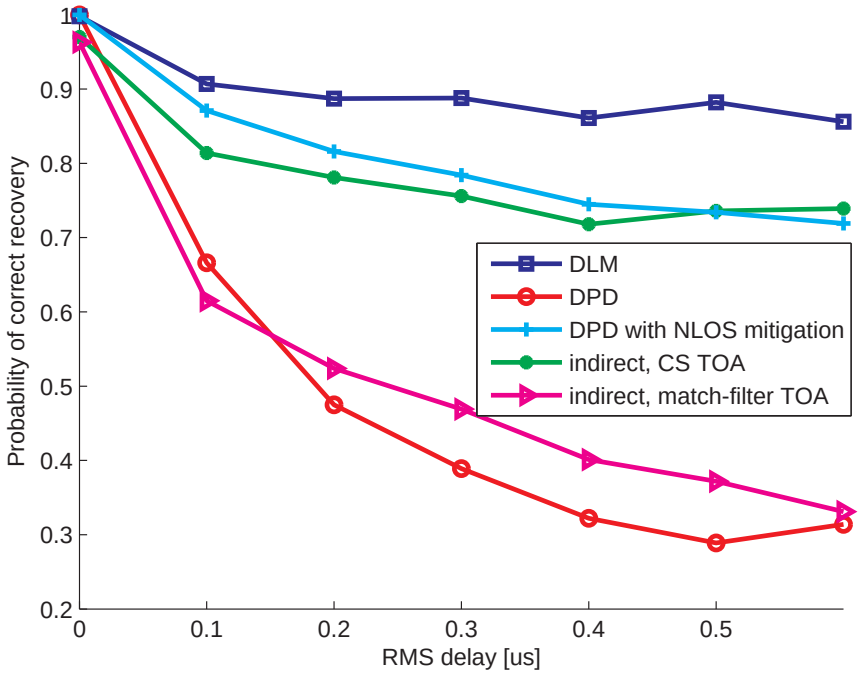

Figure 3.10 Probability of correct recovery vs. rms delay spread for the scenario in Figure 3.4 in a multipath environment for a 30 dB SNR.

delay spread ranging from 0 to 0.6 µs at 30 dB SNR. At high-SNR and at a zero delay spread all localization techniques perform similarly. However, as soon as the rms delay spread increases by a little as 0.2 µs, DPD's performance drops markedly. The techniques specifically designed for multipath channels, such as the indirect technique based on CS TOA estimates and DLM, degrade very slightly as the rms delay spread increases. DLM outperforms all other techniques and is capable of recovering the sources locations with a high probability of correct recovery irrespective of the delay spread.

3.6.4 Probability of Correct Recovery vs. Number of Grid Refinement Steps

The purpose of the grid refinement procedure introduced in Section 3.4.6 is to reduce the computational complexity of DLM, while maintaining the localization accuracy.

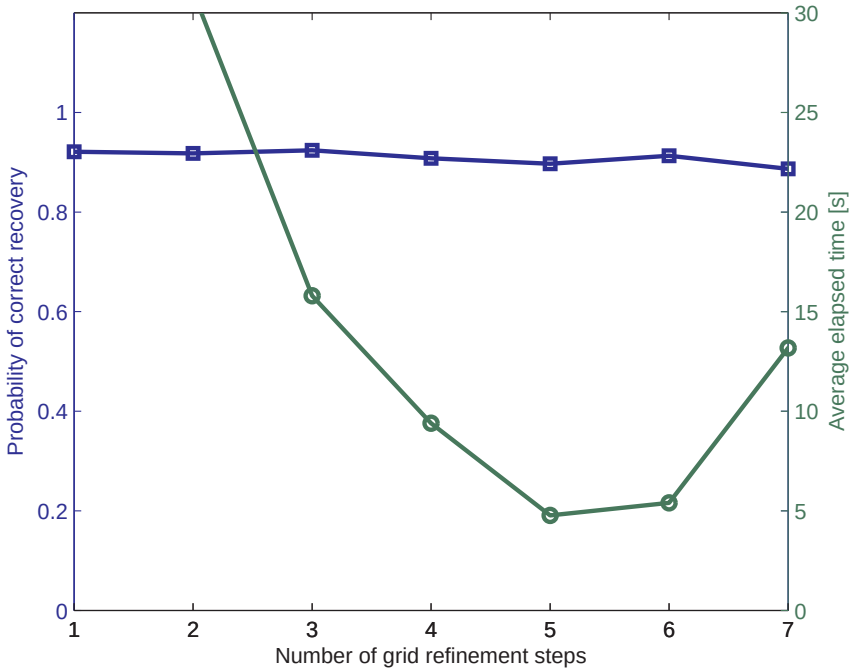

Figure 3.11 The left axis plots the probability of correct recovery and the right axis the mean elapsed time for running DLM's Stage 2, vs. the number of grid refinement steps. The SNR is fixed at 30 dB.

Figure 3.11 plots the probability of correct recovery (square marker) and the DLM's mean elapsed time at Stage 2 (circle marker), versus the number of grid refinement steps. The SNR is fixed at 30 dB. DLM is run on a computer with an Intel Xeon processor at 2.8 GHz with 4 GB of RAM memory. Perhaps surprisingly, the probability of correct recovery remains almost constant irrespective of the number of steps. The lowest computational time is 5 s and is obtained for five grid refinement steps. The number of grid steps that results in the lowest computational time depends on many factors such as number of grid points, efficiency of the conic solver, particular scenario and so forth. Thus, in general, the optimum number of steps must be found by in situ testing.

3.6.5 Multiple Sources

In this example is evaluated the probability of correct recovery of multiple sources emitting different signals overlapping in the time and frequency domain. The SNR is fixed at 30 dB. The definition of the probability of correct recovery defined in (3.63) was for a single source. In the case of multiple sources, we define the average probability of correct recovery

$$P_{\text{av}} = \frac{1}{ZQ} \sum_{z=1}^{Z} \sum_{q=1}^{Q} \mathbb{1} \left(|\mathbf{p}_q - \hat{\mathbf{p}}_q^{(z)}| < \frac{r}{3} \right), \tag{3.65}$$

and the probability of correct recovery of all sources as

$$P_{\text{all}} = \frac{1}{Z} \sum_{z=1}^{Z} \prod_{q=1}^{Q} \mathbb{1} \left(|\mathbf{p}_q - \hat{\mathbf{p}}_q^{(z)}| < \frac{r}{3} \right), \tag{3.66}$$

where $\mathbf{p}_q$ is the true location of the q-th source, $\hat{\mathbf{p}}_q^{(z)}$ is its estimate, and r is the waveform's ranging resolution as defined in (3.62). The latter metric is stricter than the former because an experiment is counted as successful only when all sources are located correctly. For $Q = 1$, both metrics boil down to the probability of correct recovery of a single source (3.63), i.e., $P_{\text{av}} = P_{\text{all}} = P_c$. In Figure 3.12, it is shown how the average probability of correct recovery degrades as the number of sources increases. This is expected because the signals from different sources interfere with each other. Nonetheless, in Figures 3.12 and 3.13, we can observe that DLM outperforms all other localization techniques when localizing multiple sources.

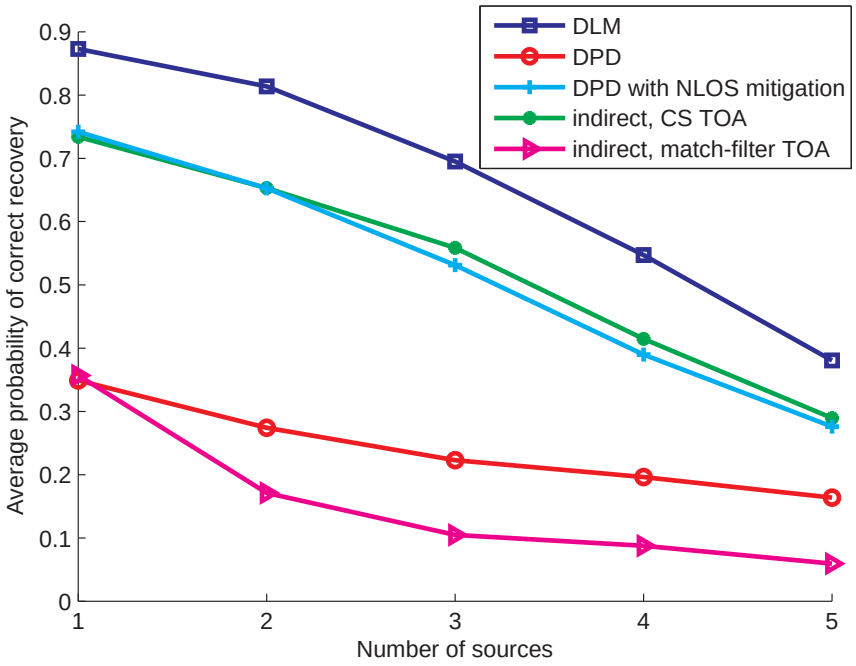

Figure 3.12 Average probability of correct recovery vs. the number of sources for a 30 dB SNR.

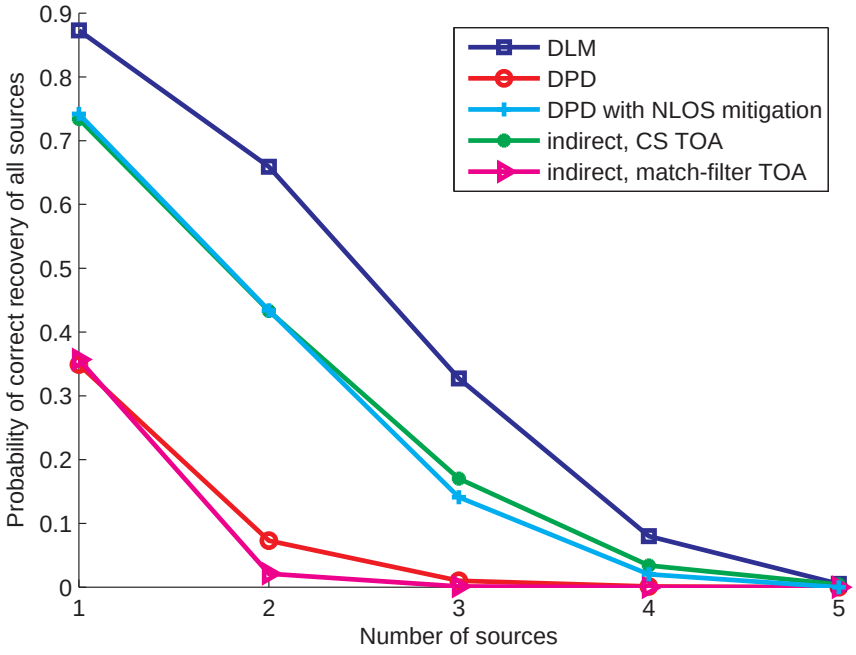

Figure 3.13 Probability of correct recovery of all sources vs. the number of sources for a 30 dB SNR.

CHAPTER 4

CONCLUSIONS AND FUTURE WORK

With the goal of performing high-accuracy active and passive TOA-based localization, this dissertation has addressed two important problems: allocating the limited available power and/or bandwidth among transmitters for optimal localization accuracy and the localization problem itself.

In Chapter 2, strategies for allocating power and/or bandwidth are formulated, given that transmitters access the medium using disjoint bandwidths of the spectrum. Extensive simulations are run on the performance of resource allocation for different SNR's in terms of the theoretical CRLB and tested by a multilateration algorithm. Numerical evidence shows that very rarely more than three transmitters are required for optimal allocation of power and/or bandwidth. For the case of five transmitters, up to 70%, 50% and 10% reduction in localization error in comparison to uniform allocation can be achieved by jointly allocating power and bandwidth, allocating bandwidth only and allocating power only, respectively. Thus, it follows that bandwidth is a more valuable resource than power.

By combining concepts from compressive sensing and direct localization, in Chapter 3, a novel direct passive localization technique, dubbed DLM, was developed for multiple sources in the presence of multipath. DLM assumes the emitted waveforms are known but requires no prior information on the channel. In fact, its localization accuracy is almost constant irrespective of the delay spread of the channel. At the core of this technique lies an optimization problem that recovers the locations of the sources with high accuracy by exploiting properties that are different for LOS and NLOS paths. It is shown theoretically how to set the algorithm's parameters to guarantee successful recovery including a parameter that determines the relative contributions of the LOS and NLOS components to the cost function. Contrary to

indirect techniques, the proposed technique is capable of localizing sources with an accuracy beyond that of the signal resolution, with high probability. In absence of multipath, DLM's accuracy matches that of the maximum likelihood estimator of the sources' locations. In the presence of multipath, DLM's accuracy outperforms indirect and other direct techniques, and can find the sources' location even when some sensors suffer from LOS blockage. The gain in localization accuracy does not come for free, as DLM requires larger computational resources than previous techniques. To this end, a grid refinement procedure is proposed which greatly reduces the computational complexity without affecting its localization accuracy. Nonetheless, this should be less of a burden as computational power keeps increasing and second-order cone program solvers become more efficient. DLM's high accuracy is validated by extensive numerical simulations.

The novel sparse framework introduced in Chapter 3 exploits the fact that LOS paths must originate from the same location to estimate the sources' locations. This framework may be extended to other cases of direct localization in different conditions. For instance, when the signals are unknown, the indirect approach for localizing the sources consists in cross-correlating the signals received at the sensors with that of a reference sensor. The peaks of such cross-correlations can provide estimates of the time-difference-of-arrivals (TDOA's). Then, the sources' locations can be estimated by hyperbolic multilateration from the TDOA measurements. In the case of multipath channels, such approach fails because multiple peaks appear on such cross-correlations and it is virtually impossible to find out which peaks correspond to time-differences between LOS components, a problem known in the literature as the data-association problem. Instead, by employing the novel framework in this work, we expect to estimate the sources' locations directly, and therefore, completely bypass the data-association problem.

A drawback of direct localization is that it requires that the baseband signals acquired at all sensors are relayed to a fusion center. In contrast, indirect techniques only transmit the TOA estimates at all sensors to the fusion center. Therefore, a possible future line of research is to investigate and develop techniques that combine the advantages of both worlds, i.e., techniques that require relaying only a function of the received signals while still achieving high localization accuracy.

APPENDIX A

PROOF OF PROPOSITION 1

The power allocation $\mathbf{p}_{opt}^j$ and the bandwidth allocation $\mathbf{w}_{opt}^j$ as solutions for Problem 3 must satisfy $\mathbf{p}_{opt}^j \leq P$ and $\mathbf{w}_{opt}^j \leq B$, and must be colinear. To prove the latter, we define two colinear allocations $\hat{\mathbf{p}}$ and $\hat{\mathbf{w}}$ whose m-th components are defined as

$$\hat{p}(m) = \frac{P}{\sum_{i=1}^{M} \left(p_{opt}^j(i)\right)^{\frac{1}{3}} \left(w_{opt}^j(i)\right)^{\frac{2}{3}}} \left(p_{opt}^j(m)\right)^{\frac{1}{3}} \left(w_{opt}^j(m)\right)^{\frac{2}{3}} \tag{A.1}$$

$$\hat{w}(m) = \frac{B}{\sum_{i=1}^{M} \left(p_{opt}^j(i)\right)^{\frac{1}{3}} \left(w_{opt}^j(i)\right)^{\frac{2}{3}}} \left(p_{opt}^j(m)\right)^{\frac{1}{3}} \left(w_{opt}^j(m)\right)^{\frac{2}{3}} \tag{A.2}$$

The cost (2.11) associated to these new allocations can be written in terms of the cost function of the previous allocations using (2.3)

$$g(\hat{\mathbf{p}}, \hat{\mathbf{w}}) = \frac{\left[\sum_{i=1}^{M} \left(p_{opt}^j(i)\right)^{\frac{1}{3}} \left(w_{opt}^j(i)\right)^{\frac{2}{3}}\right]^3}{PB^2} g(\mathbf{p}_{opt}^j, \mathbf{w}_{opt}^j) \tag{A.3}$$

By Hölder's inequality [86], and using the fact that $p_{opt}^j(i), w_{opt}^j(i) \geq 0$, the numerator in the above fraction satisfies

$$\left[\sum_{i=1}^{M} \left(p_{opt}^j(i)\right)^{\frac{1}{3}} \left(w_{opt}^j(i)\right)^{\frac{2}{3}}\right]^3 \leq \left[(\mathbf{1}^\top \mathbf{p}_{opt}^j)^{\frac{1}{3}} (\mathbf{1}^\top \mathbf{w}_{opt}^j)^{\frac{2}{3}}\right]^3 \tag{A.4}$$

Since the allocations must satisfy $\mathbf{1}^\top \mathbf{p}_{opt}^j \leq P$ and $\mathbf{w}_{opt}^j \leq B$, it follows easily that $\left[(\mathbf{1}^\top \mathbf{p}_{opt}^j)^{\frac{1}{3}} (\mathbf{1}^\top \mathbf{w}_{opt}^j)^{\frac{2}{3}}\right]^3 \leq PB^2$, and therefore (A.3) reads

$$g(\hat{\mathbf{p}}, \hat{\mathbf{w}}) \leq g(\mathbf{p}_{opt}^j, \mathbf{w}_{opt}^j) \tag{A.5}$$

Thus for any power and bandwidth allocation, it exists always a colinear alternative solution $(\hat{\mathbf{p}}, \hat{\mathbf{w}})$ performing equal or better, and such that $\hat{\mathbf{w}} = \frac{B}{P}\hat{\mathbf{p}}$. Hence, the solution $(\mathbf{p}^j_{opt}, \mathbf{w}^j_{opt})$ must also satisfy this property, i.e. $\mathbf{w}^j_{opt} = \frac{B}{P}\mathbf{p}^j_{opt}$.

APPENDIX B

PROOF OF PROPOSITION 2

The proof of Proposition 2 is by contradiction. Call $\mathbf{y}'$ the solution to problem (2.22). Suppose that problem (2.19) admits a solution $\mathbf{y}^*$ that is better than any scaled copy of $\mathbf{y}'$ satisfying the constraints of problem (2.19); i.e. $\mathbf{y}^*$ better than $\alpha\mathbf{y}'$ for any α such that $0 < \alpha < \frac{D}{\mathbf{1}^\top\mathbf{y}'}$. As a better solution, the objective function evaluated at $\mathbf{y}^*$ must be smaller than evaluated at $\alpha\mathbf{y}'$: $\max_q g_q(\mathbf{y}^*, k) < \max_q g_q(\alpha\mathbf{y}', k)$ for $\alpha \in [0, \frac{D}{\mathbf{1}^\top\mathbf{y}'}]$. For the right side of this inequality, using the definition of $g(\mathbf{y}, k)$ (2.18), we can put the constant α as a factor in front of the max operator: $\max_q g_q(\mathbf{y}^*, k) < \frac{1}{\alpha^{k+1}} \max_q g_q(\mathbf{y}', k)$. The most limiting value of α is $\alpha = \frac{D}{\mathbf{1}^\top\mathbf{y}'}$, thus leading to

$$\max_q g_q(\mathbf{y}^*, k) < \left(\frac{\mathbf{1}^\top\mathbf{y}'}{D}\right)^{k+1} \max_q g_q(\mathbf{y}', k) \leq E\left(\frac{\mathbf{1}^\top\mathbf{y}'}{D}\right)^{k+1} \tag{B.1}$$

where we use the fact that $\mathbf{y}'$ must satisfy the constraints of problem (2.22), i.e. $\max_q g_q(\mathbf{y}', k) \leq E$. The allocation policy $\mathbf{y}'' = \left(\frac{\max_q g_q(\mathbf{y}^*, k)}{E}\right)^{1/k+1} \mathbf{y}^*$ based on $\mathbf{y}^*$, satisfies $g_q(\mathbf{y}'', k) = E$. Computing the sum of $\mathbf{y}''$'s components and making use of (B.1) it is obtained

$$\mathbf{1}^\top\mathbf{y}'' = \left(\frac{\max_q g_q(\mathbf{y}^*, k)}{E}\right)^{1/k+1} \mathbf{1}^\top\mathbf{y}^* < \frac{\mathbf{1}^\top\mathbf{y}'}{D}\mathbf{1}^\top\mathbf{y}^* \tag{B.2}$$

Because $\mathbf{y}^*$ is a solution to problem (2.19) it satisfies $\mathbf{1}^\top\mathbf{y}^* \leq D$, and consequently in (B.2), $\mathbf{1}^\top\mathbf{y}'' < \mathbf{1}^\top\mathbf{y}'$. This indicates that $\mathbf{y}''$, rather than $\mathbf{y}'$, is a solution to problem (2.19) and contradicts the original hypothesis.

APPENDIX C

PROOF OF LEMMA 5

Let an atomic decomposition of $\mathbf{R}$ be (3.23). The goal of the proof is to show that all locations, $\mathbf{p}_q^{(k)}$ for $q = 1, \ldots, Q$ and $k = 1, \ldots, K_q$ are consistent with S_q or more paths if

$$\left\|\mathbf{p}_q^{(k)}\right\|_2 = u_q < \frac{1}{\sqrt{S_q - 1}}. \tag{C.1}$$

From (3.23), the signal at the l-th sensor is

$$\mathbf{r}_l = \sum_{q=1}^{Q} \sum_{\substack{k=1 \\ b_q^{(k)}(l)\neq 0}}^{K_q} c_q^{(k)} b_q^{(k)}(l) \mathbf{s}_q \left(\tau_l\left(\mathbf{p}_q^{(k)}\right)\right) + \sum_{q=1}^{Q} \sum_{k=1}^{K_{ql}} c_{ql}^{(k)} e^{i\phi_{ql}^{(k)}} \mathbf{s}_q\left(\tau_{ql}^{(k)}\right). \tag{C.2}$$

By Assumption 3, $\tau_l(\mathbf{p}_q^{(k)})$ is a true propagation if $b_q^{(k)}(l) \neq 0$. Therefore, if $\mathbf{b}_q^{(k)}$ has S_q or more non-zero entries, according to Definition 2, $\mathbf{p}_q^{(k)}$ is consistent with S_q or more paths. It is left to prove that $\|\mathbf{b}_q^{(k)}\|_0 \geq S_q$. The proof is by contradiction. Let,

$$\left\|\mathbf{b}_1^{(1)}\right\|_0 < S_1. \tag{C.3}$$

and let the atomic decomposition (3.23) in which the atom $\mathbf{L}_1\left(\mathbf{b}_1^{(1)}, \mathbf{p}_1^{(1)}\right)$ is replaced by $\|\mathbf{b}_q^{(k)}\|_0$ NLOS atoms as follows

$$\mathbf{L}_1\left(\mathbf{b}_1^{(1)}, \mathbf{p}_1^{(1)}\right) = \sum_{\substack{l=1 \\ b_1^{(1)}(l)\neq 0}}^{L} \left|b_1^{(1)}(l)\right| \mathbf{N}_{11}\left(\phi\left(b_1^{(1)}(l)\right), \tau_l\left(\mathbf{p}_1^{(1)}\right)\right). \tag{C.4}$$

Consider now the two decompositions (3.23) and the one obtained with (C.4). The costs of the two decompositions differ only in the coefficients of the atoms shown in (C.4). Ignoring the common atoms, the cost of decomposition (3.23) is $c_1^{(1)}$, whereas

the cost of decomposition obtained from combining (C.4) with (3.23) is

$$c_1^{(1)} \sum_{\substack{l=1 \\ b_1^{(1)}(l)\neq 0}}^{L} \left| b_1^{(1)}(l) \right|. \tag{C.5}$$

Normalizing the two costs by $c_1^{(1)}$, and if (3.23), which by (C.3) has a location $\mathbf{p}_1^{(1)}$ with less than S_q paths, is optimal, then

$$1 \leq \sum_{\substack{l=1 \\ b_1^{(1)}(l)\neq 0}}^{L} \left| b_1^{(1)}(l) \right|. \tag{C.6}$$

We show next that inequality (C.6) cannot be satisfied if $\|\mathbf{b}_1^{(1)}\|_2$ satisfies (C.1). Define the vector function $\mathbf{1}(\mathbf{b}_1^{(1)})$ whose l-th entry is one if $b_1^{(1)}(l) \neq 0$, and 0 otherwise, and denote $|\cdot|$ the element-wise absolute value. Then the right hand side of (C.6) is

$$\sum_{\substack{l=1 \\ b_1^{(1)}(l)\neq 0}}^{L} \left| b_1^{(1)}(l) \right| = \left[\mathbf{1}\left(\mathbf{b}_1^{(1)}\right) \right]^T \left| \mathbf{b}_1^{(1)} \right|, \tag{C.7}$$

and by the Cauchy-Schwarz inequality

$$\left[\mathbf{1}\left(\mathbf{b}_1^{(1)}\right) \right]^T \left| \mathbf{b}_1^{(1)} \right| \leq \left\| \mathbf{1}\left(\mathbf{b}_1^{(1)}\right) \right\|_2 \left\| \mathbf{b}_1^{(1)} \right\|_2 = \sqrt{\left\| \mathbf{b}_1^{(1)} \right\|_0} \left\| \mathbf{b}_1^{(1)} \right\|_2. \tag{C.8}$$

However $\|\mathbf{b}_1^{(1)}\|_2 = u_1$, and by equation (C.1), $\|\mathbf{b}_1^{(1)}\|_2 < 1/\sqrt{S_1 - 1}$. Moreover, by assumption (C.3), $\|\mathbf{b}_1^{(1)}\|_0 \leq S_1 - 1$. Therefore, it follows

$$\sqrt{\left\| \mathbf{b}_1^{(1)} \right\|_0} \left\| \mathbf{b}_1^{(1)} \right\|_2 < 1, \tag{C.9}$$

which combined with (C.7) and (C.8) results in

$$\sum_{\substack{l=1 \\ b_1^{(1)}(l)\neq 0}}^{L} \left| b_1^{(1)}(l) \right| < 1, \tag{C.10}$$

which contradicts (C.6).

APPENDIX D

PROOF OF LEMMA 6

Assume the optimal atomic decomposition of $\mathbf{R}$ is (3.23). Then, parameter K_q is the number of locations associated to the optimal atomic decomposition for the q-th source. We aim to prove that if parameter u_q

$$\left\|\mathbf{b}_q^{(k)}\right\|_2 = u_q > \frac{1}{\sqrt{S_q}}, \tag{D.1}$$

then $K_q \geq 1$. The proof is by contradiction. Let $K_1 = 0$, then the optimal atomic decomposition (3.23) simplifies to

$$\mathbf{R} = \sum_{q=2}^{Q}\sum_{k=1}^{K_q} c_q^{(k)}\mathbf{L}_q\left(\mathbf{b}_q^{(k)}, \mathbf{p}_q^{(k)}\right) + \sum_{q=1}^{Q}\sum_{l=1}^{L}\sum_{k=1}^{K_{ql}} c_{ql}^{(k)}\mathbf{N}_{ql}\left(\phi_{ql}^{(k)}, \tau_{ql}^{(k)}\right), \tag{D.2}$$

and the signal at the l-th sensor is

$$\mathbf{r}_l = \sum_{q=2}^{Q}\sum_{\substack{k=1 \\ b_q^{(k)}(l)\neq 0}}^{K_q} c_q^{(k)} b_q^{(k)}(l)\mathbf{s}_q\left(\tau_l\left(\mathbf{p}_q^{(k)}\right)\right) + \sum_{q=1}^{Q}\sum_{k=1}^{K_{ql}} c_{ql}^{(k)} e^{i\phi_{ql}^{(k)}}\mathbf{s}_q\left(\tau_{ql}^{(k)}\right). \tag{D.3}$$

Notice that the first summation begins with $q = 2$ because $K_1 = 0$. By Assumption 3,

$$\left\{\tau_{1l}^{(k)}\right\}_{k=1}^{K_{1l}} \tag{D.4}$$

are the true propagation delays of the paths between source 1 and sensor l. By Assumption 2, there are S_1 LOS paths from source 1. Let

$$\{l_1, \ldots, l_{S_1}\} \subseteq \{1, \ldots, L\} \tag{D.5}$$

be the indexes of the destination sensors of such LOS paths, and let $\tau_{1l}^{(1)}$ in (D.4) be the propagation delay corresponding to the LOS path between source 1 and sensor l, i.e.

$$\tau_{1l}^{(1)} = \tau_l\left(\mathbf{p}_1\right) \text{ for } l \in \{l_1, \ldots, l_{S_1}\}. \tag{D.6}$$

We show next that there exists a decomposition different than (D.2) for which $K_1 \geq 1$ and whose cost is smaller, thus contradicting the assumption that (D.2) is optimal. According to (3.15) and (3.16), the sum of NLOS atoms with delays $\tau_{1l}^{(1)}$ for $l \in \{l_1, \ldots, l_{S_1}\}$ in the presumed optimal atomic decomposition (D.2), i.e., $\sum_{l\in\{l_1,\ldots,l_{S_1}\}} c_{1l}^{(1)} \mathbf{N}_{1l}(\phi_{1l}^{(1)}, \tau_{1l}^{(1)})$, can be expressed for any parameter c as

$$\sum_{l\in\{l_1,\ldots,l_{S_1}\}} c_{1l}^{(1)} \mathbf{N}_{1l}\left(\phi_{1l}^{(1)}, \tau_{1l}^{(1)}\right) = \\ = \frac{\sqrt{S_1}c}{u_1}\mathbf{L}_1\left(\mathbf{b}, \mathbf{p}_1\right) + \sum_{l\in\{l_1,\ldots,l_{S_1}\}} \left(c_{1l}^{(1)} - c\right) \mathbf{N}_{1l}\left(\phi_{1l}^{(1)}, \tau_{1l}^{(1)}\right), \quad \text{(D.7)}$$

where $\mathbf{b}$ is

$$b(l) = \begin{cases} \frac{u_1}{\sqrt{S_1}} e^{i\phi_{1l}^{(1)}} & \text{for } l \in \{l_1, \cdots, l_{S_1}\} \\ 0 & \text{otherwise.} \end{cases} \quad \text{(D.8)}$$

Let $c = c_{\min}$ defined by

$$c_{\min} = \min_{l\in\{l_1,\ldots,l_{S_1}\}} c_{1l}^{(1)}. \quad \text{(D.9)}$$

Next it is shown that the cost of the decomposition obtained by combining (D.7)–(D.9) with (D.2) is lower than the cost of the decomposition (D.2), contradicting the assumption that (D.2) is optimal. Notice the former decomposition includes the LOS atom $\mathbf{L}_1(\mathbf{b}, \mathbf{p}_1)$. The costs of the two decompositions differ only in the coefficients of the atoms shown in (D.7). Ignoring the common atoms, the cost of decomposition (D.2) is

$$\sum_{l\in\{l_1,\ldots,l_{S_1}\}} c_{1l}^{(1)} \quad \text{(D.10)}$$

whereas the cost of decomposition obtained from (D.7) is

$$\frac{\sqrt{S_1}c_{\min}}{u_1} + \sum_{l\in\{l_1,\ldots,l_{S_1}\}} \left(c_{1l}^{(1)} - c_{\min}\right). \quad \text{(D.11)}$$

Since (D.2) is optimal, it means they must satisfy

$$\sum_{l\in\{l_1,\ldots,l_{S_1}\}} c_{1l}^{(1)} \leq \frac{\sqrt{S_1}c_{\min}}{u_1} + \sum_{l\in\{l_1,\ldots,l_{S_1}\}} \left(c_{1l}^{(1)} - c_{\min}\right), \tag{D.12}$$

and after simplification $u_1 \leq 1/\sqrt{S_1}$, which contradicts (D.1).

BIBLIOGRAPHY

[1] B. Hofmann-Wellenhof, H. Lichtenegger, and E. Wasle, *GNSS–global navigation satellite systems: GPS, GLONASS, Galileo, and more*. New York: Springer Science & Business Media, 2007.

[2] P. D. Groves, *Principles of GNSS, inertial, and multisensor integrated navigation systems*. Norwood, MA: Artech House, 2013.

[3] P. Misra and P. Enge, *Global positioning system: signals, measurements and performance*, 2nd ed. Lincoln, MA: Ganga-Jamuna Press, 2006.

[4] B. Hofmann-Wellenhof, H. Lichtenegger, and J. Collins, *Global positioning system: theory and practice*. New York: Springer Science & Business Media, 2012.

[5] P. M. Woodward, *Probability and information theory, with applications to radar*. Oxford, United Kingdom: Pergamon, 1953.

[6] M. A. Richards, J. Scheer, W. A. Holm *et al.*, *Principles of modern radar: basic principles*. Herndon, VA: SciTech Publishing, 2010.

[7] S. Sesia, I. Toufik, and M. Baker, *LTE: the UMTS long term evolution*, 2nd ed. Chippenham, Wiltshire, United Kingdom: Wiley Online Library, 2009.

[8] A. Küpper, *Location-based services: fundamentals and operation*. West Sussex, United Kingdom: John Wiley & Sons, 2005.

[9] E. Fishler, A. Haimovich, R. Blum, D. Chizhik, L. Cimini, and R. Valenzuela, "MIMO radar: an idea whose time has come," in *IEEE Radar Conference*, 2004, pp. 71–78.

[10] A. M. Haimovich, R. S. Blum, and L. J. Cimini, "MIMO radar with widely separated antennas," *IEEE Signal Processing Magazine*, vol. 25, no. 1, pp. 116–129, 2008.

[11] N. H. Lehmann, A. M. Haimovich, R. S. Blum, and L. Cimini, "High resolution capabilities of MIMO radar," in *Signals, Systems and Computers, IEEE 40th Asilomar Conference on*, 2006, pp. 25–30.

[12] N. H. Lehmann, E. Fishler, A. M. Haimovich, R. S. Blum, D. Chizhik, L. J. Cimini, and R. A. Valenzuela, "Evaluation of transmit diversity in MIMO-radar direction finding," *Signal Processing, IEEE Transactions on*, vol. 55, no. 5, pp. 2215–2225, 2007.

[13] E. Fishler, A. Haimovich, R. S. Blum, L. J. Cimini, D. Chizhik, and R. A. Valenzuela, "Spatial diversity in radars-models and detection performance," *Signal Processing, IEEE Transactions on*, vol. 54, no. 3, pp. 823–838, 2006.

[14] Q. He, N. H. Lehmann, R. S. Blum, and A. M. Haimovich, "MIMO radar moving target detection in homogeneous clutter," *Aerospace and Electronic Systems, IEEE Transactions on*, vol. 46, no. 3, pp. 1290–1301, 2010.

[15] G. Mao, B. Fidan, and B. D. Anderson, "Wireless sensor network localization techniques," *Computer networks*, vol. 51, no. 10, pp. 2529–2553, 2007.

[16] A. Beck, P. Stoica, and J. Li, "Exact and approximate solutions of source localization problems," *Signal Processing, IEEE Transactions on*, vol. 56, no. 5, pp. 1770–1778, 2008.

[17] E. Elnahrawy, X. Li, and R. P. Martin, "The limits of localization using signal strength: A comparative study," in *Sensor and Ad Hoc Communications and Networks, 1st Annual IEEE Communications Society Conference on*, 2004, pp. 406–414.

[18] M. Bshara, U. Orguner, F. Gustafsson, and L. Van Biesen, "Fingerprinting localization in wireless networks based on received-signal-strength measurements: A case study on WiMAX networks," *Vehicular Technology, IEEE Transactions on*, vol. 59, no. 1, pp. 283–294, 2010.

[19] X. Li and K. Pahlavan, "Super-resolution TOA estimation with diversity for indoor geolocation," *Wireless Communications, IEEE Transactions on*, vol. 3, no. 1, pp. 224–234, 2004.

[20] H. Saarnisaari, "Tls-esprit in a time delay estimation," in *IEEE 47th.*

[21] J. Caffery and G. L. Stuber, "Subscriber location in cdma cellular networks," *Vehicular Technology, IEEE Transactions on*, vol. 47, no. 2, pp. 406–416, 1998.

[22] C. Knapp and G. C. Carter, "The generalized correlation method for estimation of time delay," *Acoustics, Speech and Signal Processing, IEEE Transactions on*, vol. 24, no. 4, pp. 320–327, 1976.

[23] H. Liu, H. Darabi, P. Banerjee, and J. Liu, "Survey of wireless indoor positioning techniques and systems," *Systems, Man, and Cybernetics, Part C: Applications and Reviews, IEEE Transactions on*, vol. 37, no. 6, pp. 1067–1080, 2007.

[24] E. Fishler, A. Haimovich, R. Blum, R. Cimini, D. Chizhik, and R. Valenzuela, "Performance of MIMO radar systems: advantages of angular diversity," in *Signals, Systems and Computers, IEEE 38th Asilomar Conference on*, vol. 1, 2004, pp. 305–309.

[25] R. L. Mitchell, "Models of extended targets and their coherent radar images," *Proceedings of the IEEE*, vol. 62, no. 6, pp. 754–758, 1974.

[26] Q. He, R. S. Blum, H. Godrich, and A. M. Haimovich, "Target velocity estimation and antenna placement for MIMO radar with widely separated antennas," *Selected Topics in Signal Processing, IEEE Journal of*, vol. 4, no. 1, pp. 79–100, 2010.

[27] Q. He, R. S. Blum, and A. M. Haimovich, "Noncoherent MIMO radar for location and velocity estimation: More antennas means better performance," *Signal Processing, IEEE Transactions on*, vol. 58, no. 7, pp. 3661–3680, 2010.

[28] H. Godrich, A. Haimovich, and R. S. Blum, "Target localisation techniques and tools for multiple-input multiple-output radar," *IET Radar, Sonar & Navigation*, vol. 3, no. 4, pp. 314–327, 2009.

[29] H. Wang and H. Guo, "Hyperbolic localization method for MIMO radar," in *IEEE International Radar Symposium (IRS)*, 2011, pp. 880–885.

[30] O. Bar-Shalom and A. J. Weiss, "Direct positioning of stationary targets using MIMO radar," *Signal Processing*, vol. 91, no. 10, pp. 2345–2358, 2011.

[31] A. Dekker, "A taxonomy of network centric warfare architectures," Defense Technical Information Center (DTIC) Document, Canberra, Australia, Tech. Rep., 2008.

[32] M. E. Nelms and P. J. Collins, "Development and evaluation of a multistatic ultrawideband random noise radar network," in *IEEE Radar Conference*, 2011, pp. 1068–1073.

[33] S. Gezici, Z. Tian, G. B. Giannakis, H. Kobayashi, A. F. Molisch, H. V. Poor, and Z. Sahinoglu, "Localization via ultra-wideband radios: a look at positioning aspects for future sensor networks," *IEEE Signal Processing Magazine*, vol. 22, no. 4, pp. 70–84, 2005.

[34] E. Paolini, A. Giorgetti, M. Chiani, R. Minutolo, and M. Montanari, "Localization capability of cooperative anti-intruder radar systems," *EURASIP Journal on Advances in Signal Processing*, vol. 2008, no. 1, p. 726854, 2008.

[35] C. Tong, M. Inggs, and A. Mishra, "Towards a MIMO radar based on commensal use of fm broadcast transmitters of opportunity," in *Synthetic Aperture Radar, 9th European Conference on*. VDE, 2012, pp. 283–286.

[36] H. Godrich, A. M. Haimovich, and R. S. Blum, "Target localization accuracy gain in MIMO radar-based systems," *Information Theory, IEEE Transactions on*, vol. 56, no. 6, pp. 2783–2803, 2010.

[37] S. K. Sengijpta, "Fundamentals of statistical signal processing: Estimation theory," *Technometrics*, vol. 37, no. 4, pp. 465–466, 1995.

[38] D. Gabor, "Theory of communication. part 1: the analysis of information," *Journal of the Institution of Electrical Engineers — Part III: Radio and Communication Engineering*, vol. 93, no. 26, pp. 429–441, 1946.

[39] H. Godrich, V. M. Chiriac, A. M. Haimovich, and R. S. Blum, "Target tracking in MIMO radar systems: Techniques and performance analysis," in *IEEE Radar Conference*, 2010, pp. 1111–1116.

[40] J. Tabrikian, "Barankin bounds for target localization by MIMO radars," in *Sensor Array and Multichannel Processing, IEEE 4th Workshop on*, 2006, pp. 278–281.

[41] C. Musso and J.-P. Ovarlez, "Improvement of the ziv-zakai lower bound for time delay estimation," in *15th European Signal Processing Conference*, 2007, pp. 960–964.

[42] I. Güvenc and C. C. Chong, "A survey on TOA based wireless localization and NLOS mitigation techniques," *IEEE Communications Surveys & Tutorials*, vol. 11, pp. 107–124, August 2009.

[43] P. C. Chen, "A non-line-of-sight error mitigation algorithm in location estimation," *1999 IEEE Wireless Communications and Networking Conference*, vol. 1, pp. 316–320, September 1999.

[44] M. Wax, T.-J. Shan, and T. Kailath, "Location and the spectral density estimation of multiple sources," Defense Technical Information Center (DTIC) Document, Stanford, CA, Tech. Rep., 1982.

[45] M. Wax and T. Kailath, "Optimum localization of multiple sources by passive arrays," *Acoustics, Speech and Signal Processing, IEEE Transactions on*, vol. 31, no. 5, pp. 1210–1217, 1983.

[46] A. J. Weiss and A. Amar, "Direct position determination of multiple radio signals," *EURASIP Journal on Applied Signal Processing*, vol. 2005, no. 1, pp. 37–49, 2005.

[47] J. S. Picard and A. J. Weiss, "Localization of multiple emitters by spatial sparsity methods in the presence of fading channels," in *Positioning Navigation and Communication (WPNC), IEEE 7th Workshop on*, 2010, pp. 62–67.

[48] O. Bialer, D. Raphaeli, and A. J. Weiss, "Maximum-likelihood direct position estimation in dense multipath," *Vehicular Technology, IEEE Transactions on*, vol. 62, no. 5, pp. 2069–2079, 2013.

[49] K. Papakonstantinou and D. Slock, "Direct location estimation using single-bounce NLOS time-varying channel models," in *IEEE 68th Vehicular Technology Conference*, 2008, pp. 1–5.

[50] K. Chen and R. Duan, "C-RAN: the road towards green RAN," China Mobile Research Institute, White Paper, 2011, version 2.5.

[51] J. Wu, S. Rangan, and H. Zhang, *Green communications: theoretical fundamentals, algorithms and applications*. Boca Raton, FL: CRC Press, 2012.

[52] "FCC Docket No. 07-114. In the Matter of Wireless E911 Location Accuracy Requirements," Federal Communications Commission, Tech. Rep., January 2015.

[53] C. M. De Dominicis, P. Pivato, P. Ferrari, D. Macii, E. Sisinni, and A. Flammini, "Timestamping of ieee 802.15. 4a CSS signals for wireless ranging and time synchronization," *Instrumentation and Measurement, IEEE Transactions on*, vol. 62, no. 8, pp. 2286–2296, 2013.

[54] S. A. Golden and S. S. Bateman, "Sensor measurements for Wi-Fi location with emphasis on time-of-arrival ranging," *Mobile Computing, IEEE Transactions on*, vol. 6, no. 10, pp. 1185–1198, 2007.

[55] M. Ciurana, F. Barcelo-Arroyo, and F. Izquierdo, "A ranging system with ieee 802.11 data frames," in *IEEE Radio and Wireless Symposium*, 2007, pp. 133–136.

[56] A. Hatami and K. Pahlavan, "Hybrid TOA-RSS based localization using neural networks," in *IEEE Global Telecommunications Conference (GLOBECOM'06)*, 2006, pp. 1–5.

[57] G. Li, D. Arnitz, R. Ebelt, U. Muehlmann, K. Witrisal, and M. Vossiek, "Bandwidth dependence of cw ranging to UHF RFID tags in severe multipath environments," in *IEEE International Conference on RFID*, 2011, pp. 19–25.

[58] V. Chandrasekaran, B. Recht, P. A. Parrilo, and A. S. Willsky, "The convex geometry of linear inverse problems," *Foundations of Computational mathematics*, vol. 12, no. 6, pp. 805–849, 2012.

[59] C. Wei, Q. He, and R. S. Blum, "Cramer-rao bound for joint location and velocity estimation in multi-target non-coherent mimo radars," in *Information Sciences and Systems (CISS), IEEE 44th Annual Conference on*, 2010, pp. 1–6.

[60] S. Boyd and L. Vandenberghe, *Convex optimization*. Cambridge, United Kingdom: Cambridge University Press, 2004.

[61] B. R. Marks and G. P. Wright, "Technical notea general inner approximation algorithm for nonconvex mathematical programs," *Operations Research*, vol. 26, no. 4, pp. 681–683, 1978.

[62] A. Beck, A. Ben-Tal, and L. Tetruashvili, "A sequential parametric convex approximation method with applications to nonconvex truss topology design problems," *Journal of Global Optimization*, vol. 47, no. 1, pp. 29–51, 2010.

[63] A. dAspremont and S. Boyd, "Relaxations and randomized methods for nonconvex qcqps," *EE392o Class Notes, Stanford University*, 2003.

[64] J. Bibby, "Axiomatisations of the average and a further generalisation of monotonic sequences," *Glasgow Mathematical Journal*, vol. 15, no. 01, pp. 63–65, 1974.

[65] H. Godrich, A. P. Petropulu, and H. V. Poor, "Power allocation strategies for target localization in distributed multiple-radar architectures," *Signal Processing, IEEE Transactions on*, vol. 59, no. 7, pp. 3226–3240, 2011.

[66] D. P. Bertsekas, *Nonlinear programming*, 2nd ed. Belmont, MA: Athena Scientific, 2003.

[67] J. Li and R. Wu, "An efficient algorithm for time delay estimation," *Signal Processing, IEEE Transactions on*, vol. 46, no. 8, pp. 2231–2235, 1998.

[68] A. V. Oppenheim, R. W. Schafer, J. R. Buck *et al.*, *Discrete-time signal processing*. Englewood Cliffs, NJ: Prentice-Hall, 1989, vol. 2.

[69] D. Koller and N. Friedman, *Probabilistic graphical models: principles and techniques*. Cambridge, Massachusetts: MIT press, 2009.

[70] J.-J. Fuchs, "Multipath time-delay detection and estimation," *Signal Processing, IEEE Transactions on*, vol. 47, no. 1, pp. 237–243, 1999.

[71] M. Elad, *Sparse and redundant representations: from theory to applications in signal and image processing*. New York: Springer Science & Business Media, 2010.

[72] G. Tang, B. N. Bhaskar, P. Shah, and B. Recht, "Compressed sensing off the grid," *Information Theory, IEEE Transactions on*, vol. 59, no. 11, pp. 7465–7490, 2013.

[73] A. L. Swindlehurst, "Time delay and spatial signature estimation using known asynchronous signals," *Signal Processing, IEEE Transactions on*, vol. 46, no. 2, pp. 449–462, 1998.

[74] E. J. Candès and C. Fernandez-Granda, "Towards a mathematical theory of super-resolution," *Communications on Pure and Applied Mathematics*, vol. 67, no. 6, pp. 906–956, 2014.

[75] G. Tang, B. N. Bhaskar, and B. Recht, "Sparse recovery over continuous dictionaries-just discretize," in *Signals, Systems and Computers, IEEE Asilomar Conference on*, 2013, pp. 1043–1047.

[76] D. Malioutov, M. Çetin, and A. S. Willsky, "A sparse signal reconstruction perspective for source localization with sensor arrays," *Signal Processing, IEEE Transactions on*, vol. 53, no. 8, pp. 3010–3022, 2005.

[77] M. M. Hyder and K. Mahata, "Direction-of-arrival estimation using a mixed norm approximation," *Signal Processing, IEEE Transactions on*, vol. 58, no. 9, pp. 4646–4655, 2010.

[78] N. Hu, Z. Ye, D. Xu, and S. Cao, "A sparse recovery algorithm for DOA estimation using weighted subspace fitting," *Signal processing*, vol. 92, no. 10, pp. 2566–2570, 2012.

[79] G. Obozinski, L. Jacob, and J.-P. Vert, "Group lasso with overlaps: the latent group lasso approach," *arXiv preprint arXiv:1110.0413*, 2011.

[80] E. van den Berg and M. P. Friedlander, "Sparse optimization with least-squares constraints," *SIAM Journal on Optimization*, vol. 21, no. 4, pp. 1201–1229, 2011.

[81] E. D. Andersen, C. Roos, and T. Terlaky, "On implementing a primal-dual interior-point method for conic quadratic optimization," *Mathematical Programming*, vol. 95, no. 2, pp. 249–277, 2003.

[82] J.-J. Fuchs and B. Delyon, "Minimal l_1-norm reconstruction function for oversampled signals: applications to time-delay estimation," *Information Theory, IEEE Transactions on*, vol. 46, no. 4, pp. 1666–1673, 2000.

[83] M. S. Lobo, L. Vandenberghe, S. Boyd, and H. Lebret, "Applications of second-order cone programming," *Linear algebra and its applications*, vol. 284, no. 1, pp. 193–228, 1998.

[84] G. L. Turin, F. D. Clapp, T. L. Johnston, S. B. Fine, and D. Lavry, "A statistical model of urban multipath propagation," *Vehicular Technology, IEEE Transactions on*, vol. 21, no. 1, pp. 1–9, 1972.

[85] MOSEK ApS, "The MOSEK optimization toolbox for MATLAB manual, version 7.1 (revision 24)," http://mosek.com, (accessed on March 20, 2015).

[86] G. H. Hardy, J. E. Littlewood, and G. Pólya, *Inequalities*, 2nd ed. Cambridge, United Kingdom: Cambridge University Press, 1934.